Resilient Vertical Forest Renovation of Reinforced Concrete Structures in Seismic Prone Areas
(H.F.R.I. Project Number 015376)

Assessment of the performance of tested as built structure

Deliverable D2.5 Work package 2

Funding source

"Hellenic Foundation for Research & Innovation (H.F.R.I.)
Greece 2.0
Basic Research Financing Action"

Host Organization

Democritus University of Thrace (DUTH)

Collaborating Organizations
Aristotle University of Thessaloniki (AUTH)

May 2025

Funded by the European Union
NextGenerationEU

The research project is implemented in the framework of H.F.R.I call “Basic research Financing (Horizontal support of all Sciences)” under the National Recovery and Resilience Plan “Greece 2.0” funded by the European Union – NextGenerationEU (H.F.R.I. Project Number: 015376)

Version	Date	Comments-Modifications
1	May 2025	Final Version

Suggested citation:

Rousakis T., Voutetaki M., Kellis S., Zapris A., Lappa M., Xynopoulos I., Sapidis G., Papadopoulos N., Mallinis G., Stefanidou M., Theodoridou I., Karampini M., Kytinou V., Chalioris C., 2025. Assessment of the performance of tested as-built structure. Greenergy-Resilient Vertical Forest Renovation of Reinforced Concrete Structures in Seismic Prone Areas (H.F.R.I. Project Number 015376). Deliverable D2.5 Democritus University of Thrace, Xanthi.

Project Title	Resilient Vertical Forest Renovation of Reinforced Concrete Structures in Seismic Prone Areas
Acronym	GREENERGY
HFRI Project Number	015376
Call identifier	Basic Research Financing (Horizontal support for all Sciences), National Recovery and Resilience Plan (Greece 2.0) / Sub-action 2. Funding Projects in Leading-Edge Sectors – RRFQ: Basic Research Financing (Horizontal support for all Sciences)
Thematic area	ThA1. Physical Sciences, Engineering Sciences and Technology, Environment and Energy
Thematic Field	1.16 Smart Cities
Host Organization	Democritus University of Thrace
Collaborating Institutions	Aristotle University of Thessaloniki
Project starting date	13/3/2024
Project Principal Investigator	**Dr. Theodoros Rousakis**
Affiliation	**Democritus University of Thrace / Department of Civil Engineering**
Email	**trousak@civil.duth.gr**
Telephone	25410 79645, 461 / 6977421569
Deliverable number and title	*D2.5 Assessment of the performance of tested as-built structure.*
Related work package	**WP2** – Experimental dynamic assessment of physical model structure towards holistic renovation
Authors	Theodoros Rousakis, Maristella Voutetaki, Stefanos Kellis, Adamantis Zapris, Martha Lappa, Ioannis Xynopoulos, Georgios Sapidis, Nikolaos Papadopoulos (DUTh), Martha Karampini, Kytinou Violetta, Chalioris Constantine. Georgios Mallinis, Maria Stefanidou, Ifigeneia Theodoridou (AUTh)

Τίτλος Έργου	Ανθεκτική Αντισεισμική Ανακαίνιση Κατασκευών από Ωπλισμένο Σκυρόδεμα σε Κάθετο Δάσος
Ακρωνύμιο	GREENERGY
Αριθμός Έργου ΕΛΙΔΕΚ	015376
Δράση	Χρηματοδότηση Βασικής Έρευνας (Οριζόντια υποστήριξη όλων των Επιστημών), Εθνικό Σχέδιο Ανάκαμψης και Ανθεκτικότητας (Ελλάδα 2.0)
Θεματική Περιοχή	ΘΠ1. Φυσικές Επιστήμες, Επιστήμες Μηχανικού και Τεχνολογίας, Περιβάλλον και Ενέργεια
Θεματικό Πεδίο	1.16 Έξυπνες Πόλεις
Φορέας Υποδοχής	Δημοκρίτειο Πανεπιστήμιο Θράκης
Συνεργαζόμενος Φορέας	Αριστοτέλειο Πανεπιστήμιο Θεσσαλονίκης
Ημερομηνία έναρξης Έργου	13/3/2024
Επιστημονικά Υπεύθυνος Έργου	**Δρ. Θεόδωρος Ρουσάκης**
Ίδρυμα / Τμήμα	**Δημοκρίτειο Πανεπιστήμιο Θράκης / Πολιτικών Μηχανικών**
Email	**trousak@civil.duth.gr**
Τηλέφωνα	25410 79645, 461 / 6977421569
Αριθμός και Τίτλος Παραδοτέου	***Π2.5 Αποτίμηση της επιτελεστικότητας από πειραματικές δοκιμές στην υφιστάμενη κατασκευή***
Σχετική Ενότητα Εργασίας	**ΕΕ2** – Πειραματική δυναμική αποτίμηση του φυσικού προσομοιώματος της κατασκευής προς την ολιστική ανακαίνιση
Συγγραφείς	Θεόδωρος Ρουσάκης, Μαριστέλλα Βουτετάκη, Στέφανος Κέλλης, Αδαμάντης Ζάπρης, Μάρθα Λάππα, Ιωάννης Ξυνόπουλος, Γεώργιος Σαπίδης, Νικόλαος Παπαδόπουλος (ΔΠΘ), Μάρθα Καραμπίνη, Βιολέττα Κυτίνου, Κωνσταντίνος Χαλιορής Γιώργος Μαλλίνης, Μαρία Στεφανίδου, Ιφιγένεια Θεοδωρίδου (ΑΠΘ)

Acknowledgements

This project is carried out within the framework of the National Recovery and Resilience Plan Greece 2.0, funded by the European Union – NextGenerationEU (Implementation body: HFRI).

Περιεχόμενα

LIST OF TABLES

LIST OF FIGURES

LIST OF ACRONYMS

VF	Vertical Forest
RC	Reinforced Concrete
PZT	Piezoelectric sensors or piezoelectric transducers
3D	3 Dimensions
etc	et cetera
D25	Deliverable 25
e.g.	for example
SHM	Structural Health Monitoring
EMI	Electromechanical Impedance
DUTH	Democritus University of Thrace
NTUA	National Technical University of Athens
SAs	Smart aggregates
AUTH	Aristotle University of Thessaloniki

Abstract

GREENERGY aims to assess the dynamic performance of old type deficient structures. The project involves a series of shaking table tests on a one-storey brick wall infilled reinforced concrete building. The as-built structure is subjected to five main different levels of shaking intensity. The earthquake excitations are based on Thessaloniki, 1978 recording with maximum acceleration adjusted to 0,1g or 0,2g or 0,5g or 0,8g or 1,1g accordingly. Also, before and after each earthquake shaking, the structure was excited through the whole range of frequencies of the structure under low acceleration intensity in order to investigate changes in eigen periods of the structure. This assessment focuses on and evaluates the damage caused by shaking table excitations. Regarding damages, after excitations, the structure presented debonding of the full Infill wall between columns 1-2 and 3-4 from the top slab and the adjacent columns' surfaces. Also, the structure presented debonding of the partial infill walls from column 1 or 2 and from the top slab. The full and partial infill revealed cracking of the horizontal bed joints. The report gathers all maximum and minimum values of bottom foundation and top slab accelerations, column displacement drifts and steel rebar strains. Further, PZT recordings before and after main excitations are thoroughly elaborated.

Keywords: damages, infills, seismic table, assessment, structural health monitoring, PZT

ΠΕΡΙΛΗΨΗ

Το έργο GREENERGY στοχεύει να διερευνήσει την δυναμική συμπεριφορά και επιτελεστικότητα παλαιού τύπου ανεπαρκών κατασκευών. Το έργο περιλαμβάνει μια σειρά δοκιμών, στην σεισμική τράπεζα σε ένα μονώροφο κτίριο από οπλισμένο σκυρόδεμα με τοιχοπληρώσεις από τούβλα. Η κατασκευή υπόκειται σε πέντε κύρια διαφορετικά επίπεδα έντασης σεισμού. Οι σεισμικές διεγέρσεις περιλαμβάνουν ιστορικό βασισμένο στον σεισμό της Θεσσαλονίκης 1978 με σταδιακά αυξανόμενη ένταση και επιτάχυνση προσαρμοσμένη σε 0,1g ή 0,2g ή 0,5g ή 0,8g ή 1,1g αντίστοιχα. Επίσης, πριν και μετά από κάθε κύρια σεισμική διέγερση, η κατασκευή διεγέρθηκε σε όλο το εύρος συχνοτήτων, υπό χαμηλή ένταση, προκειμένου να διερευνηθούν οι αλλαγές στις ιδιοπεριόδους της κατασκευής. Αυτή η αξιολόγηση, εστιάζει στις βλάβες που προκλήθηκαν από τις σεισμικές διεγέρσεις. Όσον αφορά τις βλάβες, μετά τις διεγέρσεις, η κατασκευή παρουσίασε αποκόλληση της πλήρους τοιχοπλήρωσης μεταξύ των υποστυλωμάτων 1-2 και 3-4 από την άνω πλάκα και τις επιφάνειες των παρακείμενων υποστυλωμάτων. Επίσης, η κατασκευή παρουσίασε αποκόλληση των μερικών τοιχοπληρώσεων από τα υποστυλώματα 1 ή 2 και από την άνω πλάκα. Στην πλήρη και μερική τοιχοπλήρωση προέκυψαν οριζόντιες ρωγμές. Η αξιολόγηση συγκεντρώνει όλες τις μέγιστες και ελάχιστες τιμές των επιταχύνσεων της θεμελίωσης και της άνω πλάκας, των μετατοπίσεων των υποστυλωμάτων και των παραμορφώσεων των χαλύβδινων οπλισμών. Επιπλέον, οι καταγραφές PZT πριν και μετά από κύριες διεγέρσεις αξιολογούνται διεξοδικά.

Λέξεις κλειδιά: βλάβες, τοιχοπληρώσεις, σεισμική τράπεζα, αξιολόγηση, παρακολούθηση δομικής υγείας SHM, PZT

1 Test set up and instrumentation

Below are cited again the diagrams with the location of the measuring instruments (for more details see D2.3), as well as the relevant table that allow as to further assess the recordings of different mechanical response parameters of the structure (Chalioris et al. 2015, 2016, 2020, 2021, Naoum et al. 2023,2024, Rousakis et al. 2020, 2021, Hojdys et al. 2023, Sam-Daliri et al. 2018, 2021, Thomoglou et al. 2024, Voutetaki et al. 2022).

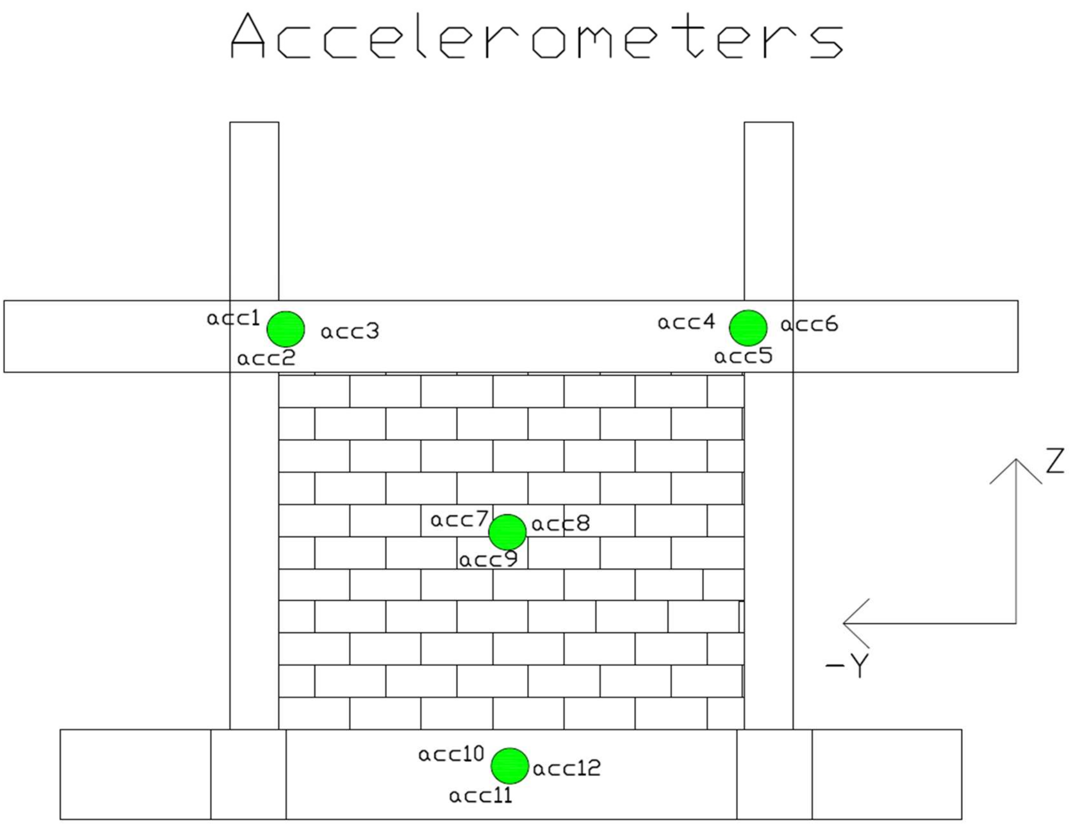

Figure 1.1 Position of accelerometers (specimen's view perpendicular to the direction of the seismic table movement)

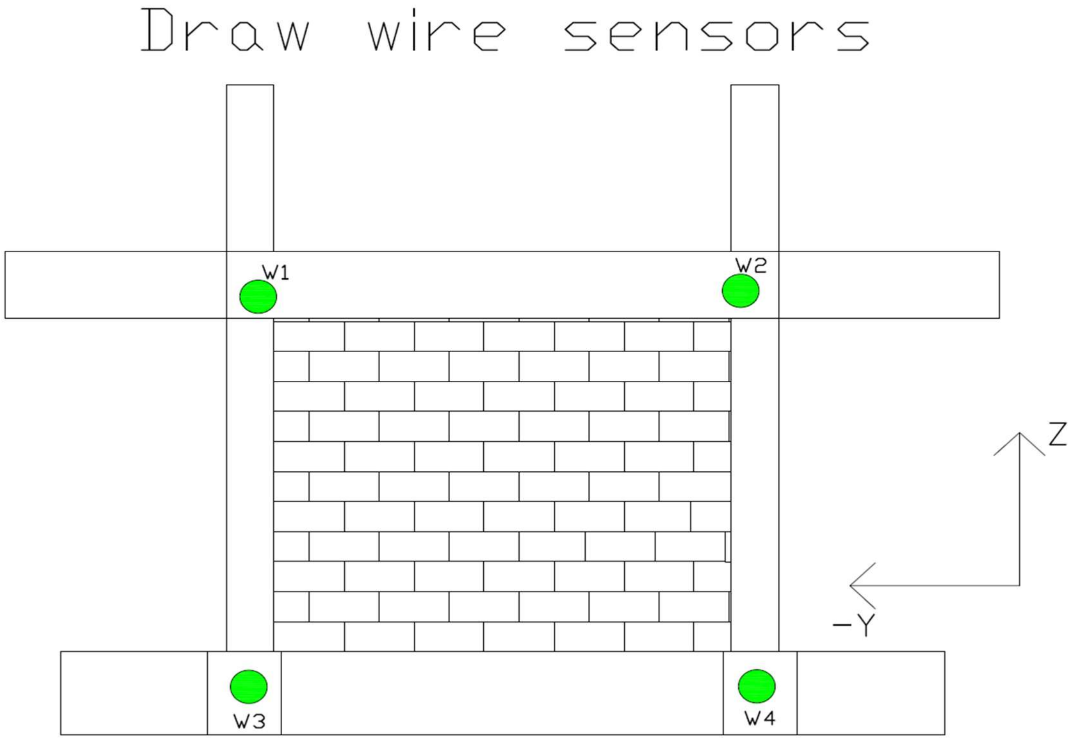

Figure 1.2 Position of the draw wire sensors on the concrete structure slab and foundation beams (specimen's view parallel to the direction of the seismic table movement)

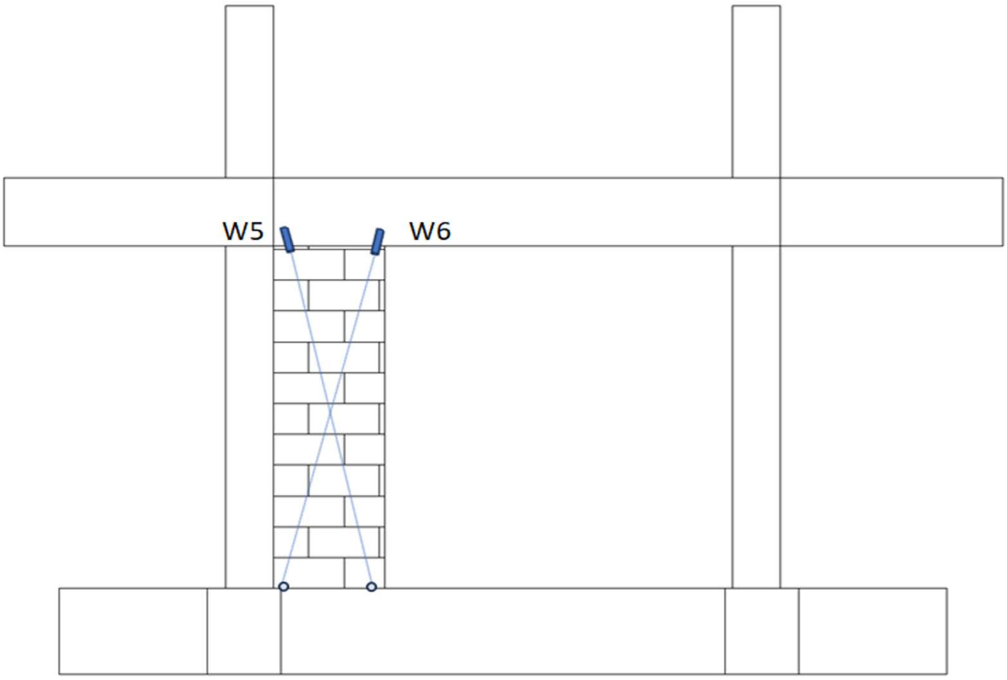

Figure 1.3 Position of the diagonal draw wire sensors, along the diagonals of the partial infill (specimen's view parallel to the direction of the seismic table movement)

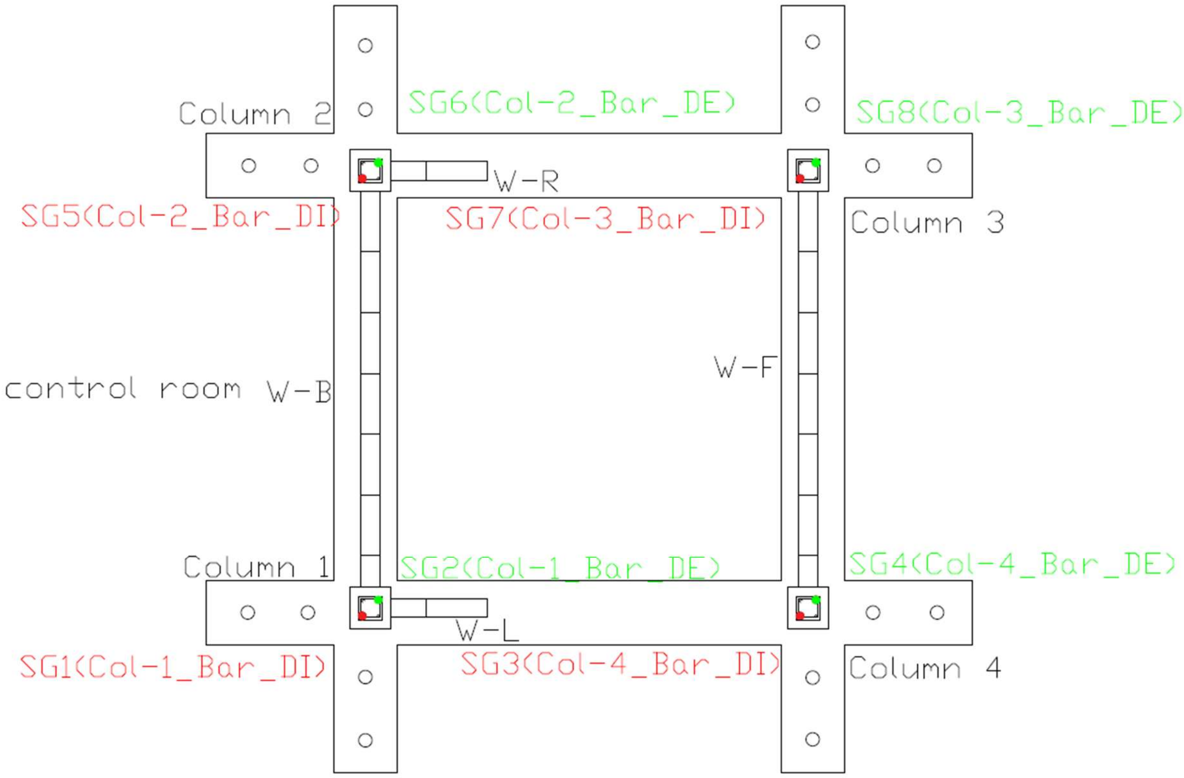

Figure 1.4 Floor plan with strain gauges at the bottom of the columns (DE)

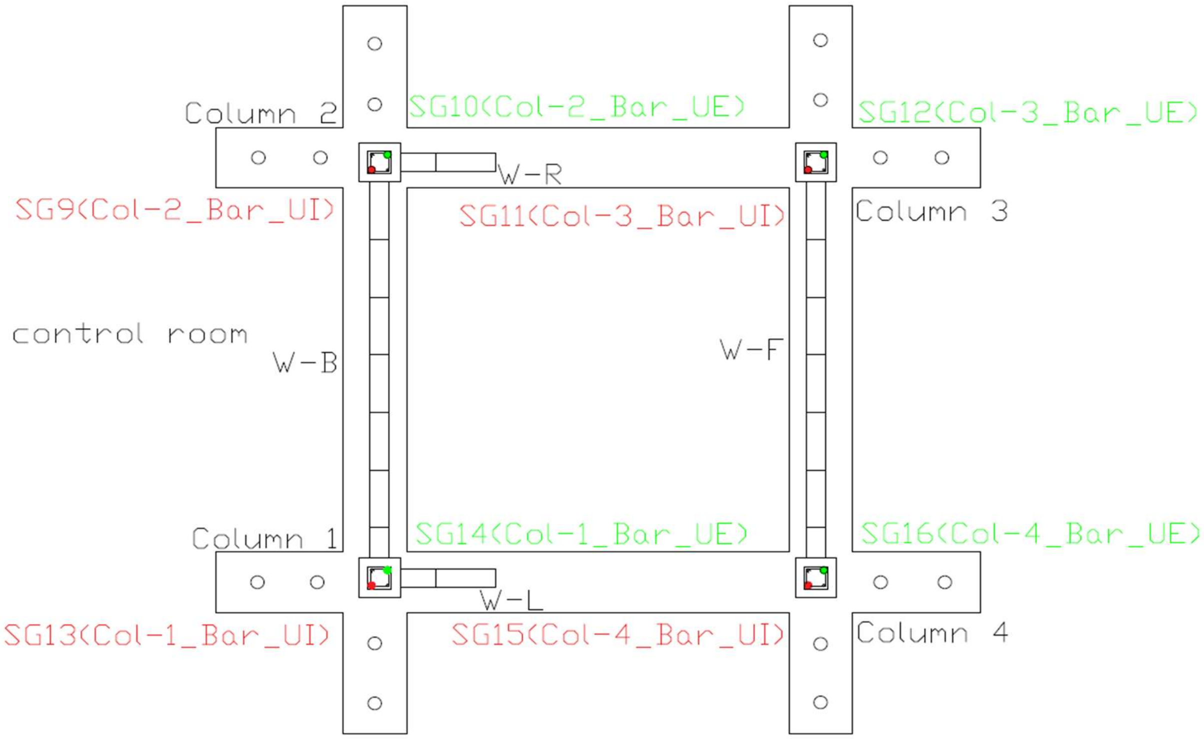

Figure 1.5 Floor plan with strain gauges at the top of the columns (UE)

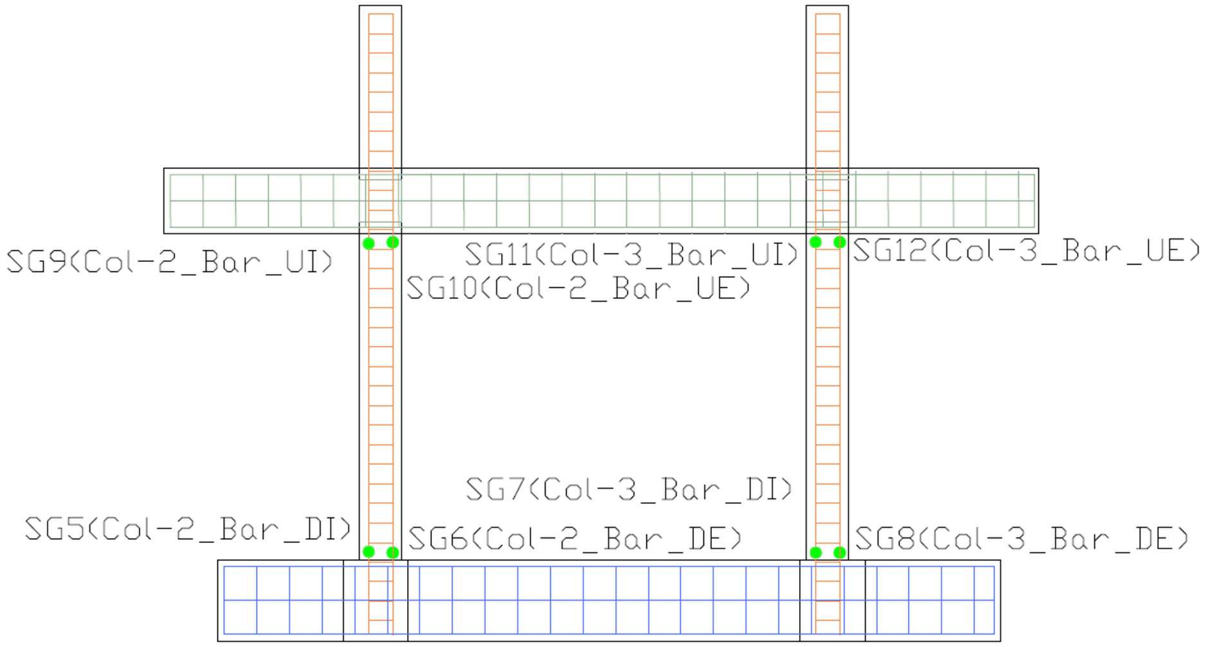

Figure 1.6 View of the structure with strain gauges in frame of Columns 2-3

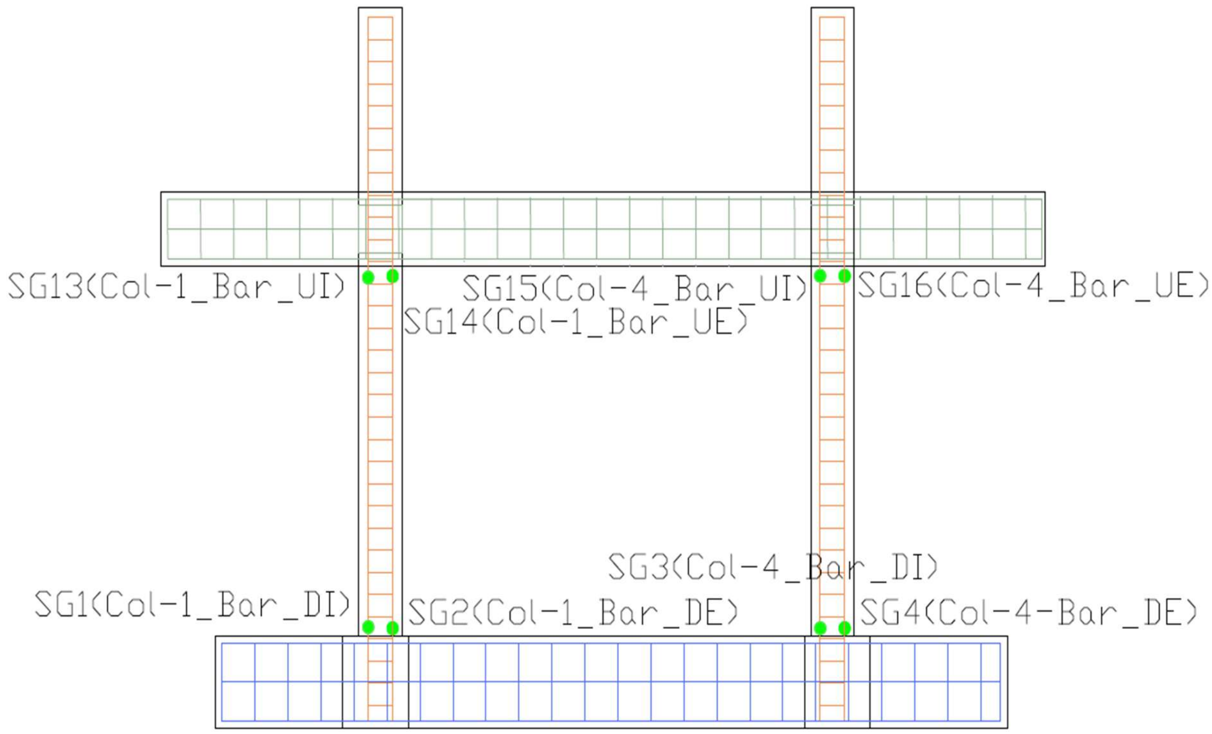

Figure 1.7 View of the structure with strain gauges in frame of columns 1-4

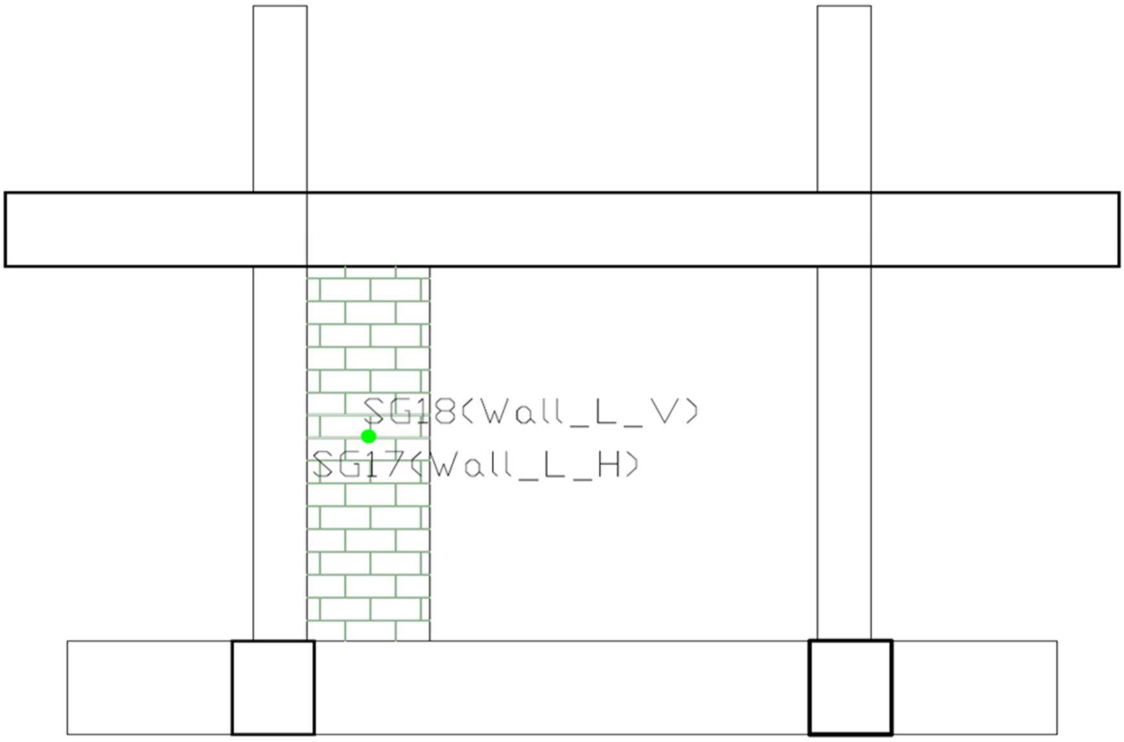

Figure 1.8 View of the infill wall with strain gauges in frame 1-4

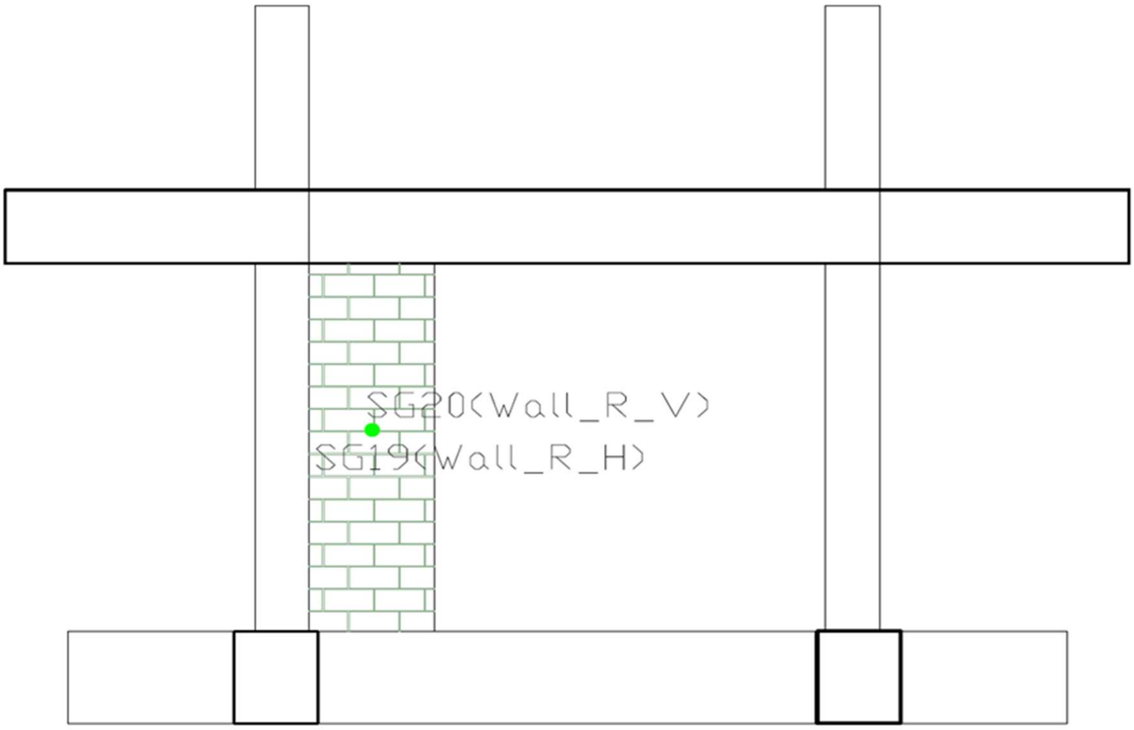

Figure 1.9 View of the infill wall with strain gauges in frame 2-3

Table 1.1: Detailed list of accelerometers, draw wire meters and strain gauges placed inside and on the structure

Ch No.	Channel name	Type of instrument	Measured quantity (units)	Position
1	ACC 1	Accelerometer	Acceleration (g)	On the slab, on the left corner, dir. (x)
2	ACC 2			On the slab, on the left corner, dir. (y)
3	ACC 3			On the slab, on the left corner, dir. (z)
4	ACC 4			On the slab, on the right corner, dir. (x)
5	ACC 5			On the slab, on the right corner, dir. (y)
6	ACC 6			On the slab, on the right corner, dir. (z)
7	ACC 7			On the infill, on the center, dir (x)
8	ACC 8			On the infill, on the center, dir (y)
9	ACC 9			On the infill, on the center, dir (x)
10	ACC 10			On the foundation, on the center, dir (x)
11	ACC 11			On the foundation, on the center, dir (y)
12	ACC 12			On the foundation, on the center, dir (z)
13	W 1	Draw wire sensors	Length (mm)	On the slab, on the left side
14	W 2			On the slab, on the right side
15	W 3			On the foundation, on the left side
16	W 4			On the foundation, on the right side
17	W 5			along the partial masonry infill diagonal
18	W 6			along the partial masonry infill diagonal
19	W 7			along the partial masonry infill diagonal
20	W 8			along the partial masonry infill diagonal
21	S1	Strain gauges	Strain	In the longitudinal reinforcement, on the underside
22	S2			
23	S3			
24	S4			
25	S5			
26	S6			
27	S7			
28	S8			
29	S9			In the longitudinal reinforcement, on the upper side
30	S10			
31	S11			
32	S12			
33	S13			
34	S14			
35	S15			
36	S16			

37	S17			On the centre of partial masonry 1 along direction x
38	S18			On the centre of partial masonry 1 along direction z
39	S19			On the centre of partial masonry 2 along direction x
40	S20			On the centre of partial masonry 2 along direction z

2 Position of smart PZT sensors for the vertical forest (VF) structure

Below are the diagrams with the location of the PZTs. (for more details see D2.3)

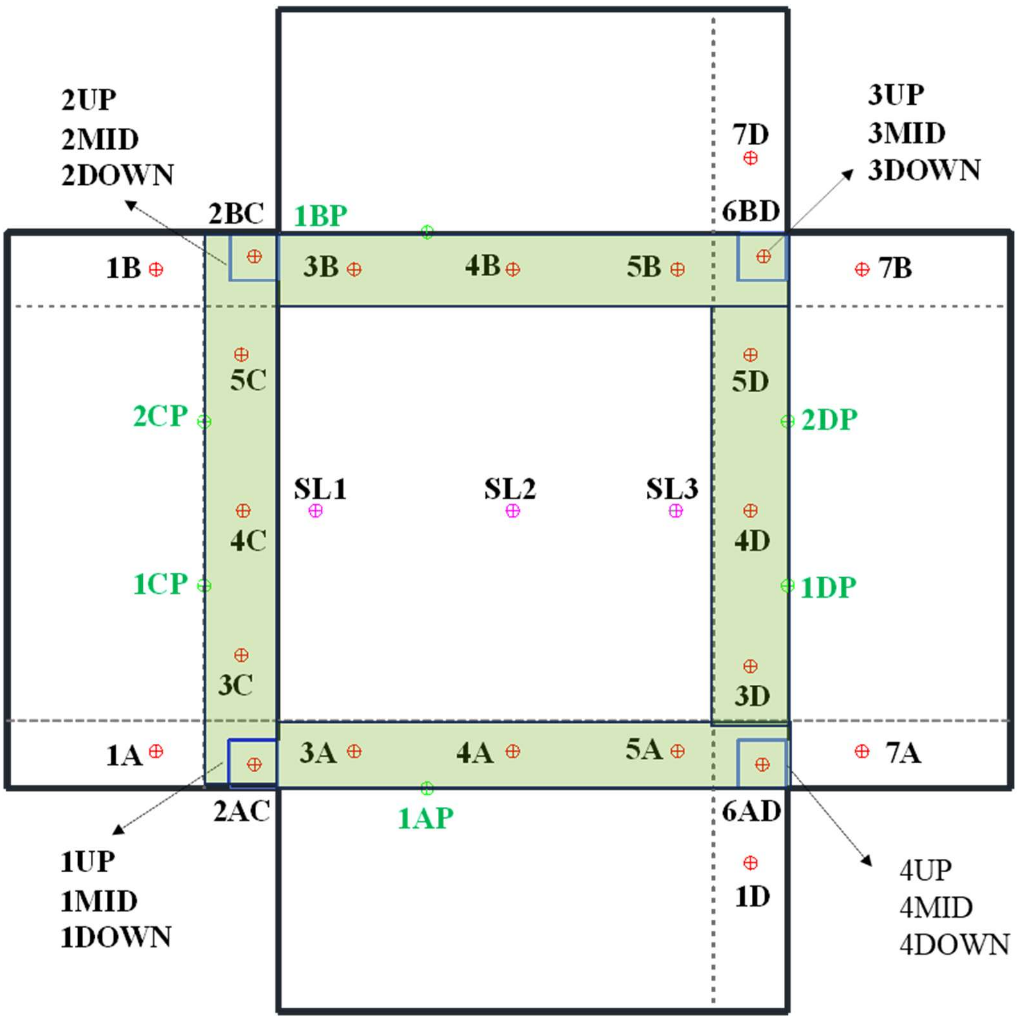

Figure 2.1 Location of the PZT sensors inside the beams

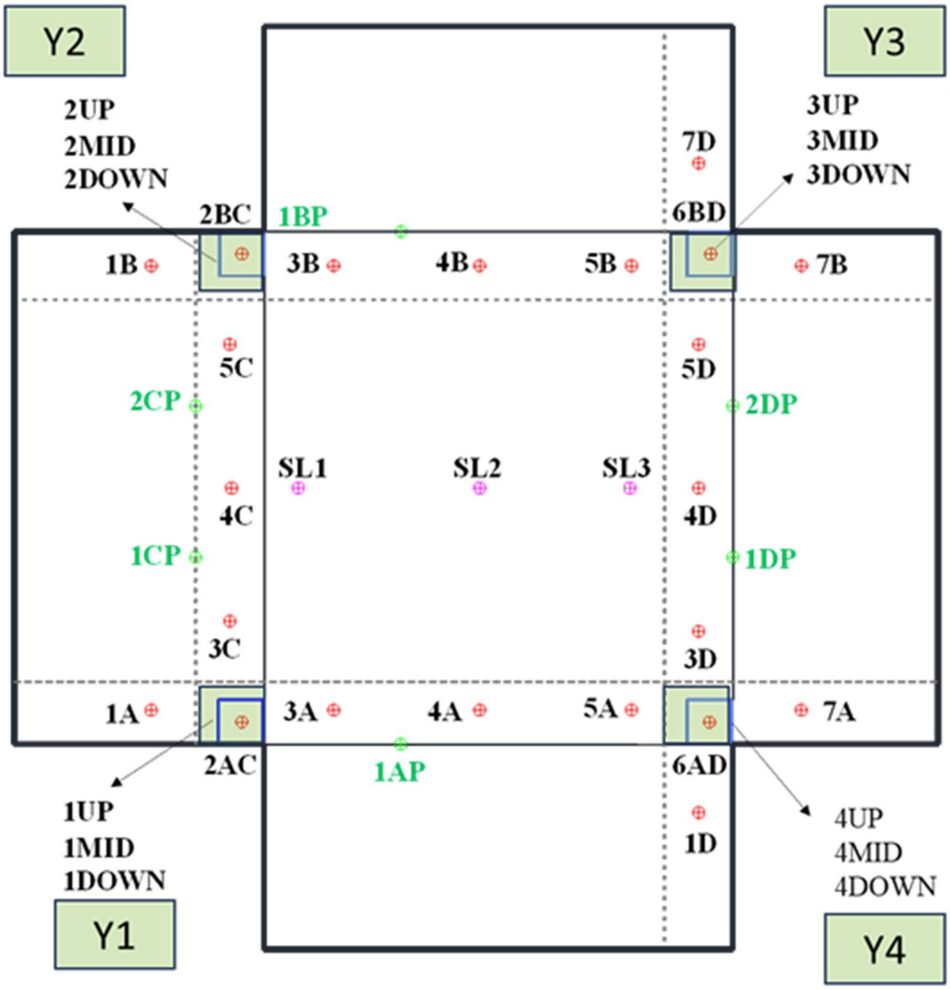

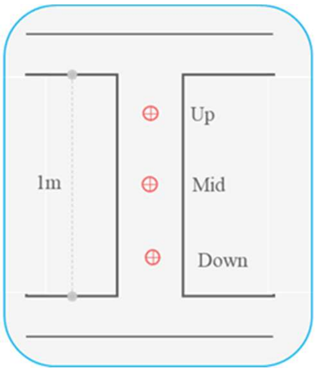

Figure 2.2 Location of the PZTs inside the columns

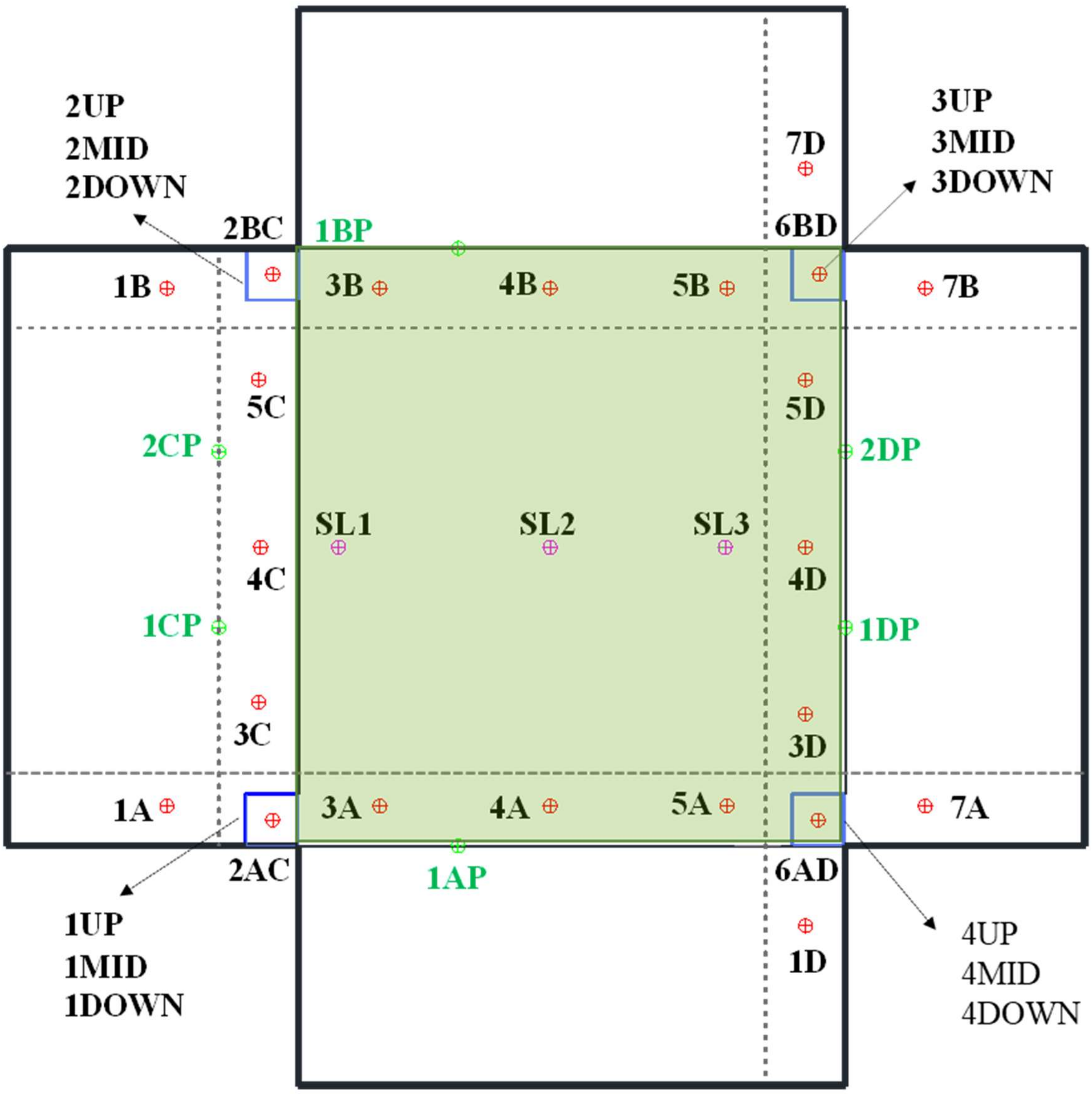

Figure 2.3 Location of PZT sensors inside the slab

3 Assessment of the performance of tested as built structure.

Below are the excitations applied to the seismic table, as shown in table 3.1. (for more details see D2.3)

Table 3.1: Testing sequence

Shake table tests			
Test No.	**Name**	**Type of excitation**	**Intensity (g)**
Phase A			
ST1	WNb0,1g	White noise	0,08
ST2	EQ0,1g	Earthquake	0,10
ST3	WNb0,2g	White noise	0,08
ST4	EQ0,2g	Earthquake	0,20
ST5	WNb0,5g	White noise	0,08
ST6	EQ0,5g	Earthquake	0,50
ST7	WNb0,8g	White noise	0,08
ST8	EQ0,8g	Earthquake	0,80
ST9	WNb1,1g	White noise	0,08
ST10	EQ1,1g	Earthquake	1,10
ST11	WNa1,1g	White noise	0,08

3.1 Assessment of the performance of tested as built structure.

Figure 3.12.1 displays the acceleration time -histories for the one-storey rc building at five different levels of earthquake intensity. That is the dynamic shake table tests comprised of gradually increasing maximum input intensity level (peak acceleration of the excitation of the seismic table) from 0,1g to 1,1g (0,1g, 0,2g, 0,5g, 0,8g, 1,1g) based on the adopted earthquake Thessaloniki 1978. Before and after each earthquake excitation, the structure was excited through the whole range of frequencies of the structure (white noise excitation, Figure 3.12.2) under low acceleration intensity in order to investigate changes in eigen periods of the structure. The peak acceleration of each one of the six white noise excitations of the seismic table was 0,08g. The direction of excitation was parallel to partial infills (W-L, W-R in plane) and vertical to full infills plane (W-B, W-F out of plane).

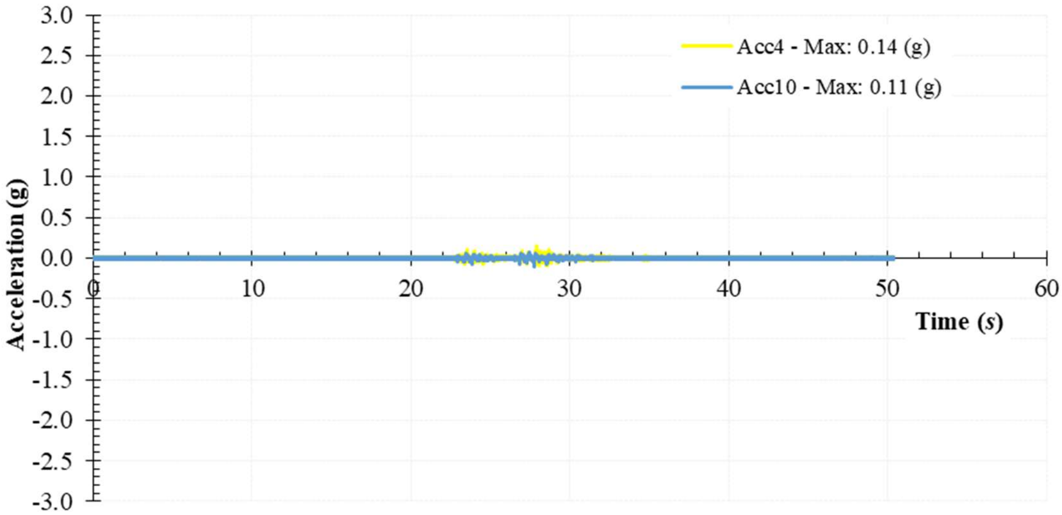

(a)

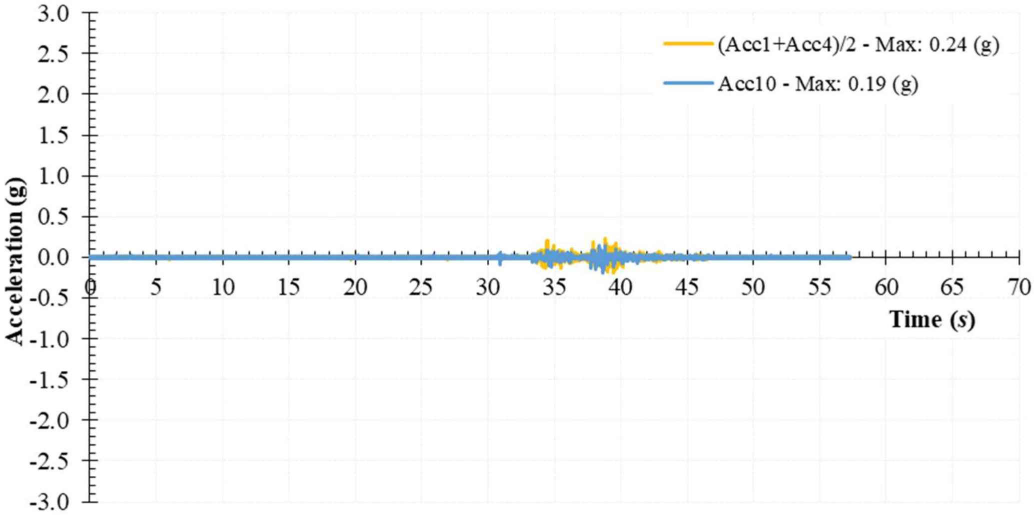
(Acc1+Acc4)/2 - Max: 0.24 (g)
Acc10 - Max: 0.19 (g)
Acceleration (g)
Time (s)

(b)

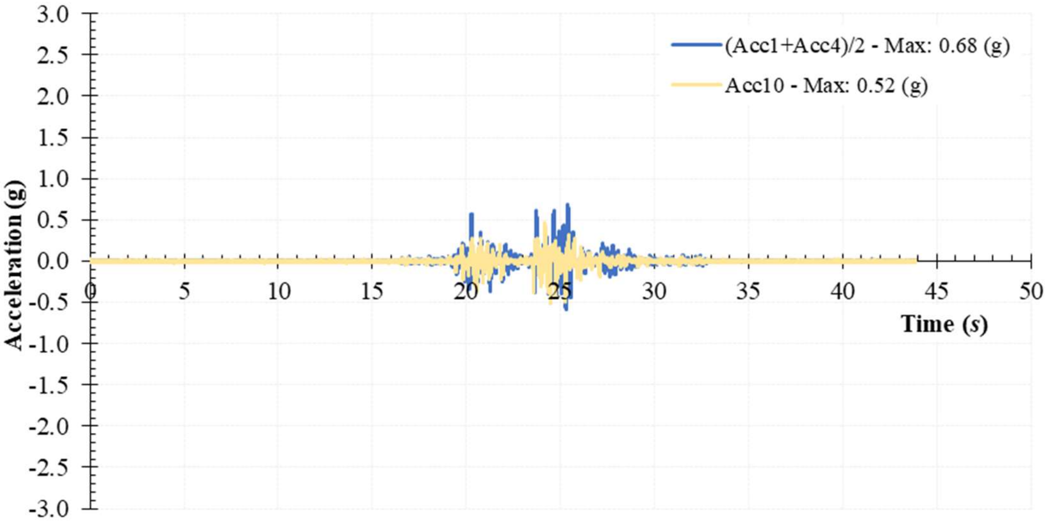
(Acc1+Acc4)/2 - Max: 0.68 (g)
Acc10 - Max: 0.52 (g)
Acceleration (g)
Time (s)

(c)

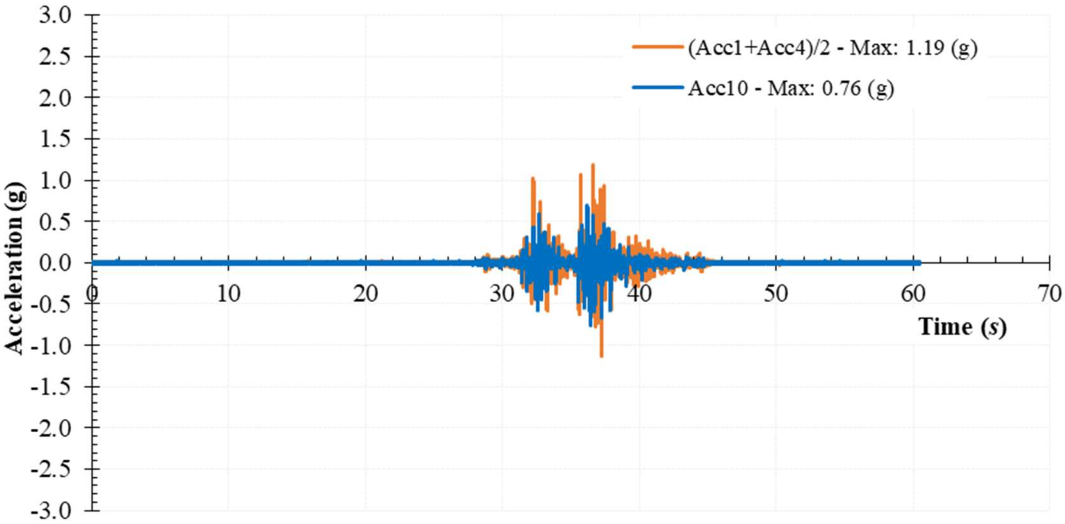

(d)

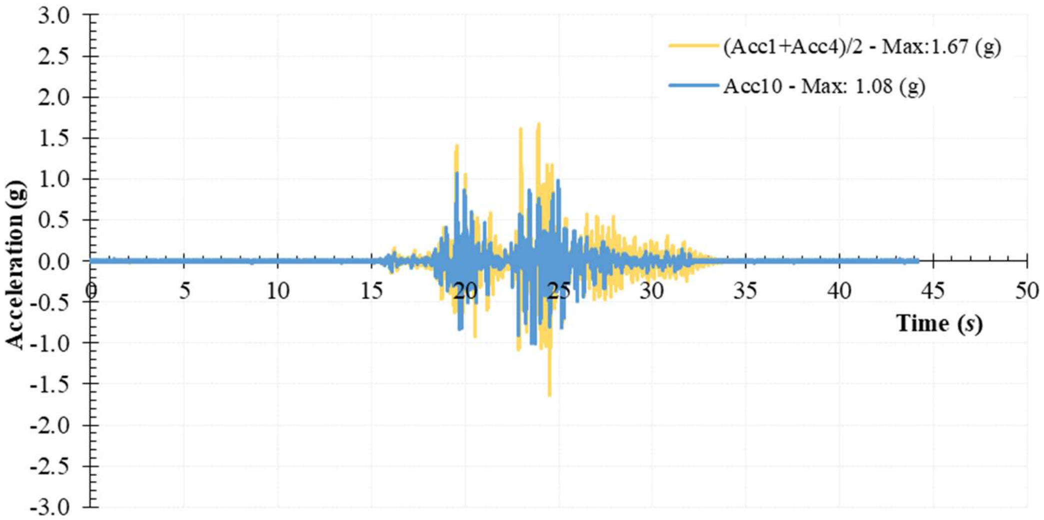

(e)

Figure 3.1.1 Bottom and slab acceleration time-histories for the five levels of earthquake intensity (a) 0.1g, (b) 0.2g, (c) 0.5g, (d) 0.8g and (e) 1.1g

Regarding excitation EQ0.1g, the peak acceleration at the bottom (PGA) level was 0.11g and the peak acceleration at the top (PFA) level was 0.14g. At 0.1g excitation, the top slab acceleration is 1.27 times the ground acceleration. Peak top acceleration of 0.14g occurred 0.17 sec after peak shake table acceleration. At excitation with intensity 0.2g the peak acceleration at the ground (PGA) level was 0.19g and the peak acceleration at the floor (PFA) level was 0.24g. Peak top acceleration of 0.24g occurred 0.16 sec after peak shake table acceleration. As we can see, at 0.2g, the floor acceleration is 1.26 times the bottom acceleration. At excitation with intensity 0.5g the peak acceleration at the bottom (PGA) level was 0.52g and the peak acceleration at the floor (PFA) level was 0.68g. At 0.5g, the floor acceleration is 1.31 times the ground acceleration. Peak top acceleration of 0.68g occurred 0.93 sec after peak shake table acceleration. Regarding excitation EQ0.8g, the peak acceleration at the ground (PGA) level was 0.76g and the peak acceleration at the floor (PFA) level was 1.19g. At 0.8g excitation, the floor acceleration is 1.57 times the ground acceleration. Peak top acceleration of 1.19 g occurred 0.18 sec after peak shake table acceleration. Regarding excitation 1.1g, the peak acceleration at the ground (PGA) level was 1.08g and the peak acceleration at the top (PFA) level was 1.67g. At 1.1g excitation, the floor acceleration is 1.55 as much as the ground acceleration. Peak top acceleration of 1.67 g occurred 4.35 sec after peak shake table acceleration.

Below are the comparative acceleration-time diagrams at the top and bottom of the structure, for the six white noise excitations.

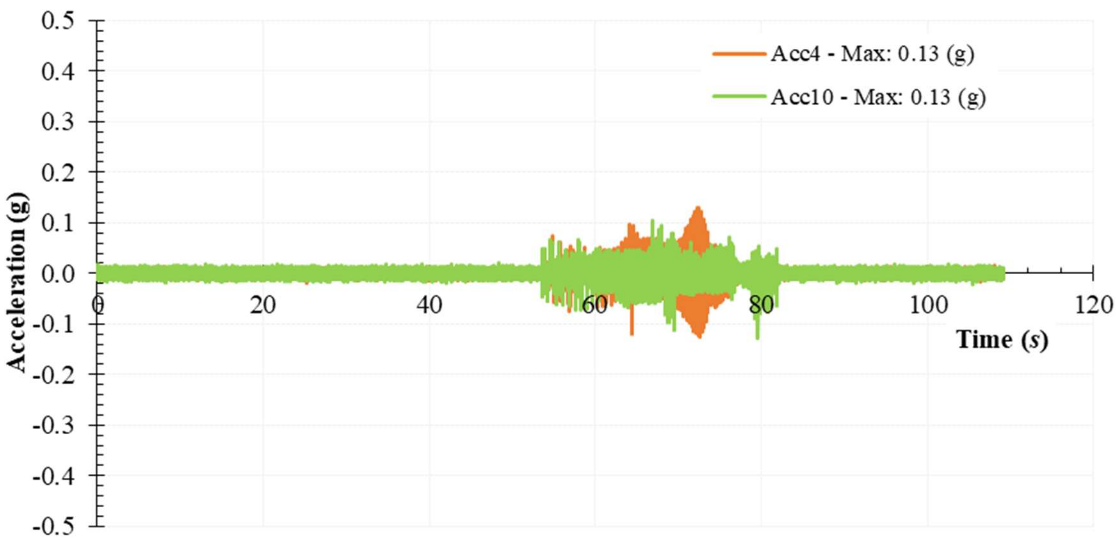

(a)

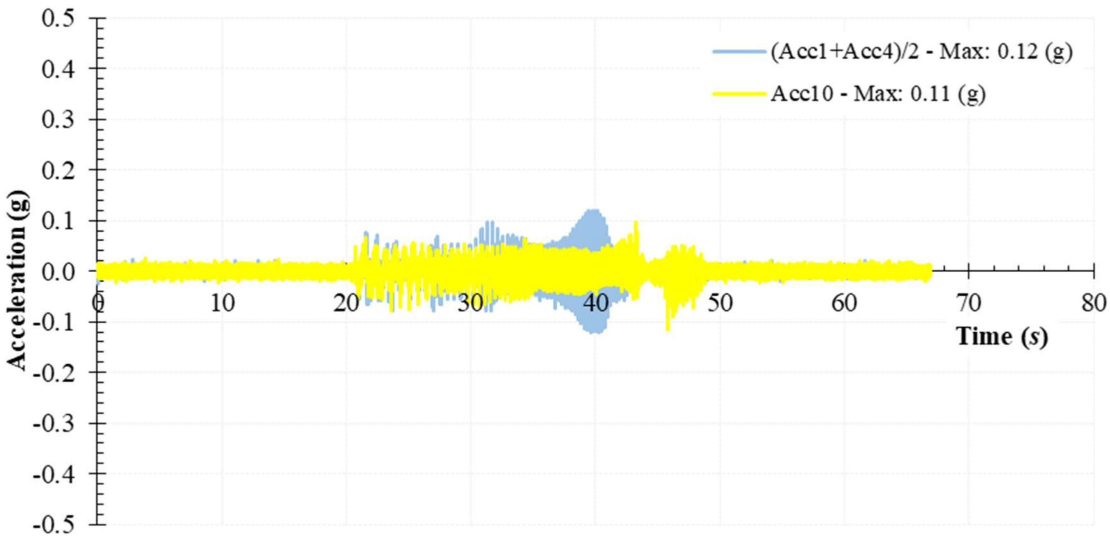
(Acc1+Acc4)/2 - Max: 0.12 (g)
Acc10 - Max: 0.11 (g)
Acceleration (g)
Time (s)

(b)

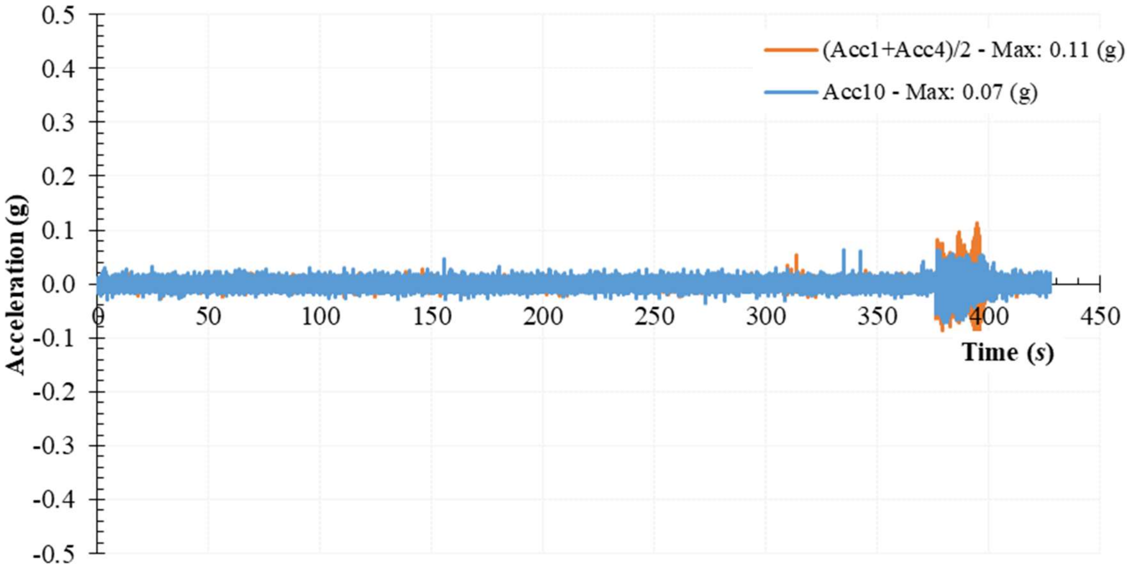
(Acc1+Acc4)/2 - Max: 0.11 (g)
Acc10 - Max: 0.07 (g)
Acceleration (g)
Time (s)

(c)

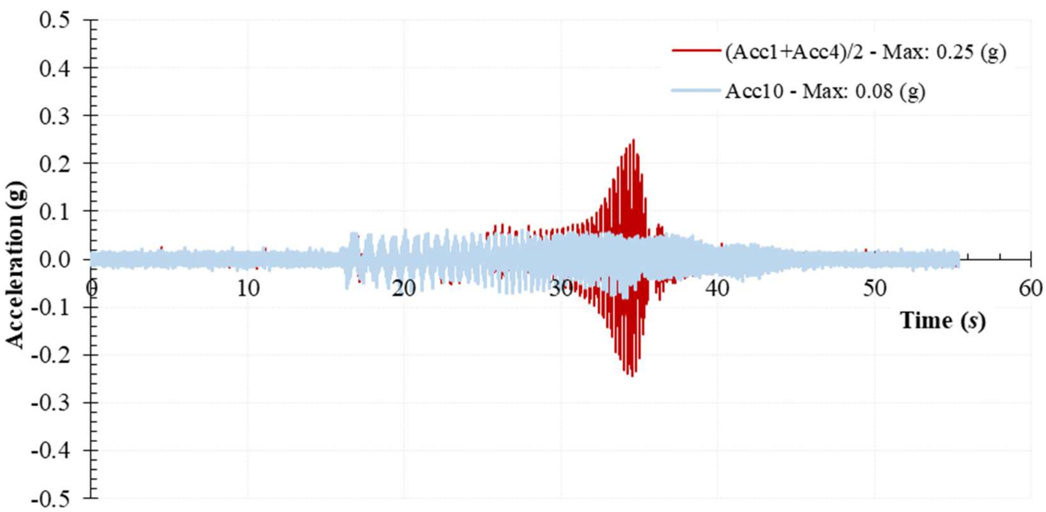
(Acc1+Acc4)/2 - Max: 0.25 (g)
Acc10 - Max: 0.08 (g)
Acceleration (g)
Time (s)

(d)

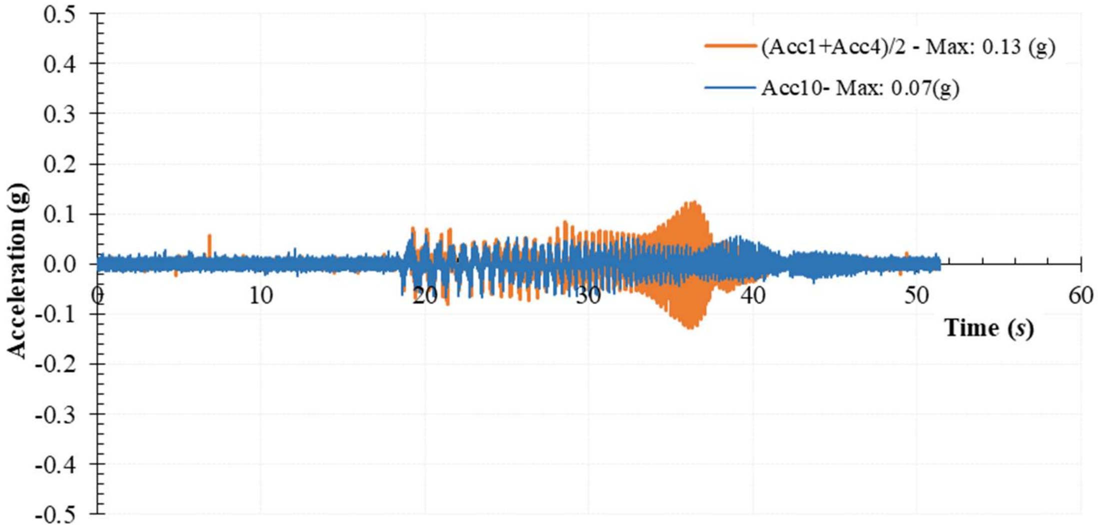

(e)

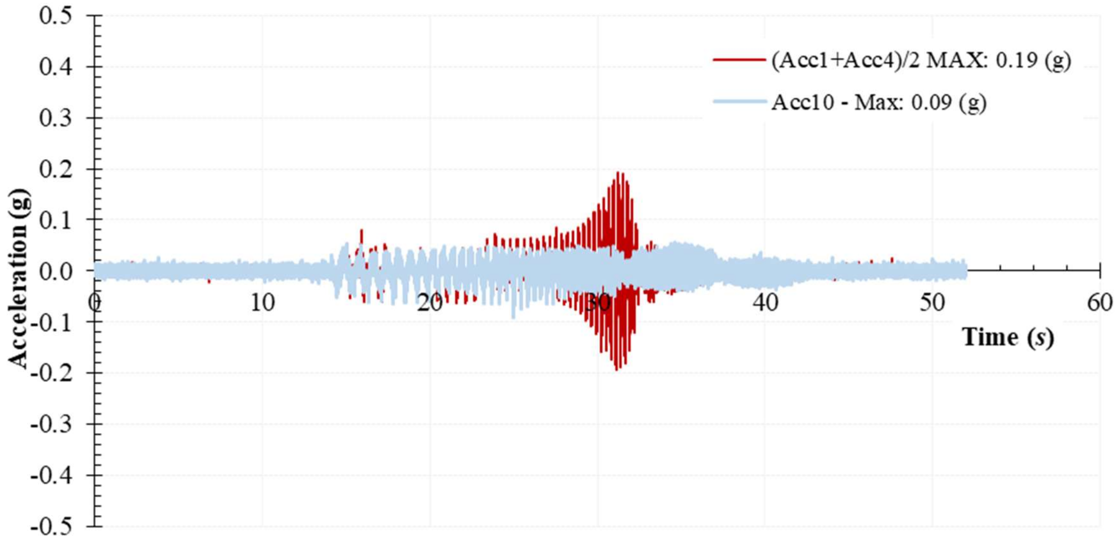

(f)

Figure 3.1.2 Ground and slab acceleration time-histories for the six levels of white noise before intensity (a) 0.1g, (b) 0.2g, (c) 0.5g, (d) 0.8g, (e) 1.1g and (f) after 0.1g

Regarding excitation white noise before EQ0.1g, that is WNb0,1g, the peak acceleration at the bottom (PGA) level was 0.13g and the top acceleration at the floor (PFA) level was 0.13g. Peak top acceleration of 0.13g occurred 7.1 sec before peak shake table acceleration. At excitation white noise before EQ0.2g with intensity 0.08g the peak acceleration at the bottom (PGA) level was 0.11g and the peak acceleration at the floor (PFA) level was 0.12g. Peak top acceleration of 0.12g occurred 5.5 sec before peak shake table acceleration. At WNb0.2g excitation, the floor acceleration is 1.09 times the ground acceleration. At excitation white noise before EQ0.5g the peak acceleration at the ground (PGA) level was 0.07g and the peak acceleration at the floor (PFA) level was 0.12g. At WNb 0.5g, the floor acceleration is 1.57 times the ground acceleration. Regarding excitation white noise before EQ0.8g, the peak acceleration at the ground (PGA) level was 0.08g and the peak acceleration at the floor (PFA) level was 0.25g. At WNb0.8g, the floor acceleration is 3.13 times the ground acceleration. Peak top acceleration of 0.25g occurred 0.42 sec after peak shake table acceleration. Regarding excitation white noise before WNb1.1g, the peak acceleration at the bottom (PGA) level was 0.07g and the peak acceleration at the top (PFA) level was 0.13 (g). At WNb1.1g excitation, the floor acceleration is 1.86 times the ground acceleration. Peak top acceleration of 0.13g occurred 12.61 sec after peak shake table acceleration. Regarding excitation white noise after 1.1g, the peak acceleration at the ground (PGA) level was 0.09g and the peak acceleration at the floor (PFA) level was 0.19g. At WNa1.1g excitation, the floor acceleration is 2.11 times the ground acceleration. Peak top acceleration of 0.19g occurred 6.09 sec after peak shake table acceleration.

Below are the tables with the summary of results for accelerometers, draw wires and strain gauges.

Table 3.1.1a Summary of results

		Intensity (g)	max Acc1 (g)	max Acc4 (g)	max Acc7 (g)	max Acc10 (g)
ST1	**WNb 0.1g**	0.08	-	0.13	0.22	0.13
ST2	**EQ 0.1g**	0.1	-	0.14	0.12	0.11
ST3	**WNb 0.2g**	0.08	0.12	0.13	0.12	0.11
ST4	**EQ 0.2g**	0.2	0.25	0.23	0.37	0.19
ST5	**WNb 0.5g**	0.08	0.12	0.12	0.10	0.07
ST6	**EQ 0.5 g**	0.5	0.64	0.74	1.72	0.52
ST7	**WNb 0.8g**	0.08	0.27	0.27	0.41	0.08
ST8	**EQ 0.8g**	0.8	1.23	1.41	1.26	0.76
ST9	**WNb 1.1g**	0.08	0.13	0.13	0.14	0.07
ST10	**EQ 1.1g**	1.1	1.7	1.75	2.19	1.08
ST11	**WNa 1.1g**	0.08	0.2	0.2	0.19	0.09

Table 3.1.1b Summary of results (continued)

		Intensity (g)	max W1 (mm)	min W1 (mm)	max W2 (mm)	min W2 (mm)	max W3 (mm)	min W3 (mm)	max W4 (mm)	min W4 (mm)
ST1	**WNb 0.1g**	0.08	14.38	-13.17	14.63	-13.02	14.24	-13.24	14.62	-13.1
ST2	**EQ 0.1g**	0.1	3.45	-2.47	3.55	-2.61	1.98	-1.71	2.13	-1.85
ST3	**WNb 0.2g**	0.08	14.26	-13.43	14.41	-13.31	14.07	-13.37	14.45	-13.26
ST4	**EQ 0.2g**	0.2	6.72	-5.64	6.81	-5.5	4.16	-3.84	4.52	-3.82
ST5	**WNb 0.5g**	0.08	14.75	-12.88	14.94	-12.9	-14.49	-12.86	14.83	-0.29
ST6	**EQ 0.5 g**	0.5	16.75	-14.6	16.33	-14.6	10.4	-9.76	10.58	-9.82
ST7	**WNb 0.8g**	0.08	14.22	-13.54	14.3	-13.72	14.04	-13.51	14.41	-13.61
ST8	**EQ 0.8g**	0.8	26.29	-25.16	25.94	-25.25	16.39	-15.84	16.65	-15.8
ST9	**WNb 1.1g**	0.08	14.63	-13.02	14.76	-12.97	14.23	-13.07	14.6	-13.06
ST10	**EQ 1.1g**	1.1	36.69	-34.67	36.31	-34.33	22.9	-21.67	22.97	-21.71
ST11	**WNa 1.1g**	0.08	14.32	-13.26	14.56	-13.35	14.21	-13.32	14.41	-13.31

Table 3.1.1c Summary of results (continued)

		Intensity (g)	max W5 (mm)	min W5 (mm)	max W6 (mm)	min W6 (mm)	max W7 (mm)	min W7 (mm)	max W8 (mm)	min W8 (mm)
ST1	**WNb 0.1g**	0.08	1.17	-0.5	0.31	-0.56	0.96	-0.67	0.72	-0.69
ST2	**EQ 0.1g**	0.1	1.09	-0.12	0.48	-0.39	1.01	-0.5	0.69	-0.4
ST3	**WNb 0.2g**	0.08	1.15	-0.6	0.3	-0.44	0.13	-0.66	0.18	-0.8
ST4	**EQ 0.2g**	0.2	0.92	-0.71	0.7	-0.52	0.5	-0.68	0.44	-0.68
ST5	**WNb 0.5g**	0.08	1.21	-0.97	0.32	-0.49	0.84	-0.55	0.56	-0.55
ST6	**EQ 0.5 g**	0.5	2.24	-1.78	1.91	-1.18	2.01	-1.41	1.71	-1.39
ST7	**WNb 0.8g**	0.08	1.1	-0.77	0.72	-0.61	0.83	-0.75	0.74	-0.71
ST8	**EQ 0.8g**	0.8	4.11	-2.62	3.1	-1.99	3.68	-2.26	2.92	-1.86
ST9	**WNb 1.1g**	0.08	1.11	-0.7	0.51	-0.43	0.72	-0.85	0.15	-0.82
ST10	**EQ 1.1g**	1.1	5.17	-3.69	4.44	-2.83	4.55	-3.32	4.43	-2.39
ST11	**WNa 1.1g**	0.08	0.95	-0.95	0.79	-0.83	0.76	-0.66	0.79	-0.68

Table 3.1.1d Summary of results (continued)

		Intensity (g)	max (W1+W2)/2	min (W1+W2)/2	max (W3+W4)/2	min (W3+W4)/2	max drift (‰)	min drift (‰)	Residual drift (mm)	Residual drift (‰)
ST1	**WNb 0.1g**	0.08	14.5	-13.09	14.41	-13.17	0.04	-0.07	-0.04	-0.033
ST2	**EQ 0.1g**	0.1	3.49	-2.54	2.06	-1.77	1.2	-0.84	-0.02	-0.016
ST3	**WNb 0.2g**	0.08	14.33	-13.36	14.26	-13.3	1.08	-0.96	-0.02	-0.016
ST4	**EQ 0.2g**	0.2	6.76	-5.56	4.34	-3.83	1.99	-1.75	-0.04	-0.033
ST5	**WNb 0.5g**	0.08	14.83	-12.89	14.66	-12.86	1.01	-0.88	0	0
ST6	**EQ 0.5 g**	0.5	16.33	-14.6	10.49	-9.78	5.06	-5.14	0.01	0.008
ST7	**WNb 0.8g**	0.08	14.04	-13.51	14.22	-13.54	2.29	-2.32	-0.06	-0.049
ST8	**EQ 0.8g**	0.8	26.11	-25.19	16.52	-15.816	8.04	-8.22	-0.03	-0.024
ST9	**WNb 1.1g**	0.08	14.69	-12.99	14.41	-13.07	1.32	-1.29	-0.03	-0.024
ST10	**EQ 1.1g**	1.1	36.5	-34.48	22.93	-21.67	11.37	-10.97	0.25	0.204
ST11	**WNa 1.1g**	0.08	14.43	-13.29	14.3	-13.31	2.3	-2.31	0.04	0.033

Table 3.1.1e Summary of results (continued)

		Intensity (g)	max SG1 rain)	min SG1 (ustrain)	Residual	max SG2 rain)	min SG2 rain)	Residual SG2	max SG3 rain)	min SG3 rain)	Residual SG3
ST1	**WNb 0.1g**	0.08	122.07	-137.33	0	76.3	-45.78	-30.52	76.3	-45.78	-15.26
ST2	**EQ 0.1g**	0.1	91.56	-152.59	15.26	61.04	-61.04	15.26	61.04	-76.3	-15.26
ST3	**WNb 0.2g**	0.08	122.07	-91.56	0	45.78	-76.3	15.26	61.04	-91.56	-76.3
ST4	**EQ 0.2g**	0.2	152.29	-183.11	-15.26	76.3	-61.04	-15.26	76.3	-45.78	15.26
ST5	**WNb 0.5g**	0.08	91.56	-106.81	0	106.81	-91.56	15.26	122.07	-106.81	0
ST6	**EQ 0.5 g**	0.5	457.78	-320.44	-45.78	183.11	-61.04	-15.26	152.59	-76.3	0
ST7	**WNb 0.8g**	0.08	244.15	-183.11	0	61.04	-91.56	-30.52	106.81	-30.52	45.78
ST8	**EQ 0.8g**	0.8	839.26	-320.44	-15.26	488.3	-45.78	15.26	381.48	-91.56	-15.26
ST9	**WNb 1.1g**	0.08	1.37	-1.35	0	0.76	-0.61	0	0.76	-0.61	0
ST10	**EQ 1.1g**	1.1	1190.22	-335.7	-15.26	808.74	-91.56	-15.26	701.93	-91.56	30.52
ST11	**WNa 1.1g**	0.08	213.63	-198.37	-30.52	45.78	-91.56	15.26	91.56	-45.78	15.26

Table 3.1.1f Summary of results (continued)

		Intensity (g)	max SG4 (ustrain)	min SG4 (ustrain)	Residual SG4	max SG5 (ustrain)	min SG5 (ustrain)	Residual SG5	max SG6 (ustrain)	min SG6 (ustrain)	Residual SG6
ST1	**WNb 0.1g**	0.08	61.04	-76.3	-30.52	221.24	-279.14	-39.87	83.23	-65.29	0.82
ST2	**EQ 0.1g**	0.1	122.07	-106.81	-15.26	167.6	-271.86	-11.39	62.84	-55.5	26.12
ST3	**WNb 0.2g**	0.08	106.81	-106.81	-30.52	166.66	-170.78	-16.26	50.54	-28.53	6.52
ST4	**EQ 0.2g**	0.2	198.37	-137.33	-30.52	357.67	-315.62	2.44	76.63	-48.92	-1.63
ST5	**WNb 0.5g**	0.08	91.56	-91.56	-30.52						
ST6	**EQ 0.5 g**	0.5	534.07	-228.89	15.26						
ST7	**WNb 0.8g**	0.08	228.89	-45.78	-0.15	467.52	-380.05	-1.63	96.13	-56.22	0
ST8	**EQ 0.8g**	0.8	839.26	-274.67	0	2015.62	-680.56	11.39	1003.52	-61.11	-4.89
ST9	**WNb 1.1g**	0.08	1.53	-0.92	15.26	241.36	-235.79	-11.38	55.19	-39.78	8.12
ST10	**EQ 1.1g**	1.1	1205.48	-427.26	-76.3	2334.67	-1136.19	-411.52	1763.86	-73.87	-49.52
ST11	**WNa 1.1g**	0.08	183.11	-198.37	-15.26	432.74	-344.35	1.63	80.38	-28.42	2.44

Table 3.1.1g Summary of results (continued)

		Intensity (g)	max SG7 (ustrain)	min SG7 (ustrain)	Residual SG7	max SG8 (ustrain)	min SG8 (ustrain)	Residual SG8	max SG9 (ustrain)	min SG9 (ustrain)	Residual SG9
ST1	**WNb 0.1g**	0.08	61.04	-76.3	15.26	45.78	-91.56	30.52	96.83	-70.8	-22.79
ST2	**EQ 0.1g**	0.1	61.04	-76.3	30.52	122.07	-152.59	-15.26	133.47	-38.26	13.84
ST3	**WNb 0.2g**	0.08	61.04	-76.3	0	106.81	-152.59	-15.26	43.91	-18.71	-9.76
ST4	**EQ 0.2g**	0.2	61.04	-61.04	0	228.89	-183.11	0	76.63	-9.76	-3.25
ST5	**WNb 0.5g**	0.08	106.81	-106.81	-30.52	106.81	-106.81	15.26			
ST6	**EQ 0.5 g**	0.5	198.37	-45.78	-15.26	610.37	-305.19	-15.26			
ST7	**WNb 0.8g**	0.08	106.81	-45.78	15.26	305.19	-183.11	0.46	216.24	-6.51	0
ST8	**EQ 0.8g**	0.8	412	-76.3	-15.26	946.07	-320.44	0	1322.93	-15.46	-12.21
ST9	**WNb 1.1g**	0.08	0.31	-0.92	-30.52	1.37	-1.53	0	62.61	-11.39	0
ST10	**EQ 1.1g**	1.1	701.93	-45.78	-83.15	1129.18	-445.52	-91.56	1979.4	-56.12	-46.36
ST11	**WNa 1.1g**	0.08	76.3	-76.3	0	183.11	-198.37	-45.78	258.59	-7.32	717.39

Table 3.1.1h Summary of results (continued)

		Intensity (g)	max SG10 (ustrain)	min SG10 (ustrain)	Residual SG10	max SG11 (ustrain)	min SG11 (ustrain)	Residual SG11	max SG12 (ustrain)	min SG12 (ustrain)	Residual SG12
ST1	**WNb 0.1g**	0.08	187.74	-209.05	-61.23	61.04	-76.3	15.26	106.81	-30.52	0
ST2	**EQ 0.1g**	0.1	144.52	-191.94	-4.9	137.33	-106.81	-15.26	61.04	-76.3	-30.52
ST3	**WNb 0.2g**	0.08	122.44	-131.46	-14.7	106.81	-122.07	0	30.52	-106.81	-30.52
ST4	**EQ 0.2g**	0.2	255.48	-207.43	-2.45	213.63	-106.81	30.52	91.56	-45.78	0
ST5	**WNb 0.5g**	0.08				106.81	-106.81	30.52	91.56	-106.81	0
ST6	**EQ 0.5 g**	0.5				503.56	-167.85	0	213.63	-106.81	-61.04
ST7	**WNb 0.8g**	0.08	351.97	-218.17	-0.82	213.63	-137.33	0	106.81	-91.56	-30.52
ST8	**EQ 0.8g**	0.8	1521.18	-250.05	-3.27	824	-183.11	15.26	549.33	-61.04	0.15
ST9	**WNb 1.1g**	0.08	165.67	-158.38	-13.88	1.22	-1.22	-30.52	0.76	-0.76	-15.26
ST10	**EQ 1.1g**	1.1	1961.66	-269.46	-53.88	1068.15	-198.37	-30.52	854.52	-76.3	-0.64
ST11	**WNa 1.1g**	0.08	314.26	-172.32	2.44	152.59	-152.59	-30.52	106.81	-76.3	-15.26

Table 3.1.1i Summary of results (continued)

		Intensity (g)	max SG13 (ustrain)	min SG13 (ustrain)	Residual SG13	max SG14 (ustrain)	min SG14 (ustrain)	Residual SG14	max SG15 (ustrain)	min SG15 (ustrain)	Residual SG15
ST1	**WNb 0.1g**	0.08	91.56	-45.78	-15.26	91.56	-76.3	0	61.04	-76.3	0
ST2	**EQ 0.1g**	0.1	61.04	-61.04	15.26	106.81	-122.07	15.26	122.07	-106.81	-30.52
ST3	**WNb 0.2g**	0.08	76.3	-61.04	0	106.81	-106.81	0	122.07	-106.81	15.26
ST4	**EQ 0.2g**	0.2	133.33	-76.3	-15.26	152.59	-152.59	-15.26	213.63	-122.07	15.26
ST5	**WNb 0.5g**	0.08	106.81	-106.81	-45.78	122.07	-91.56	15.26	91.56	-106.81	-45.78
ST6	**EQ 0.5 g**	0.5	381.48	-45.78	30.52	412	213.63	0	30.52	-213.63	-15.26
ST7	**WNb 0.8g**	0.08	137.33	-61.04	30.52	198.37	-137.33	0.15	213.63	-167.85	-15.26
ST8	**EQ 0.8g**	0.8	701.93	-45.78	15.26	747.7	-213.63	15.26	900.3	-228.89	-15.26
ST9	**WNb 1.1g**	0.08	0.61	-0.61	-30.52	1.22	-1.22	0	1.37	-1.07	15.26
ST10	**EQ 1.1g**	1.1	1007.11	-91.56	0	1083.41	-198.37	-0.15	1174.96	-259.41	0
ST11	**WNa 1.1g**	0.08	122.07	-76.3	-15.26	183.11	-152.59	30.52	183.11	-152.59	-15.26

Table 3.1.1j Summary of results (continued)

		Intensity (g)	max SG16 (ustrain)	min SG16 (ustrain)	Residual SG16	max SG17 (ustrain)	min SG17 (ustrain)	Residual SG17	max SG18 (ustrain)	min SG18 (ustrain)	Residual SG18
ST1	**WNb 0.1g**	0.08	76.3	-61.04	15.26	76.3	-45.78	15.26	61.04	-76.3	0
ST2	**EQ 0.1g**	0.1	106.81	-106.81	0	91.56	-76.3	0	91.56	-45.78	30.52
ST3	**WNb 0.2g**	0.08	76.3	-76.3	-15.26	61.04	-76.3	0	45.78	-91.56	-30.52
ST4	**EQ 0.2g**	0.2	137.33	-106.81	-30.52	45.78	-91.56	0	45.78	-76.3	-15.26
ST5	**WNb 0.5g**	0.08	106.81	-106.81	-15.26	122.07	-122.07	0	106.81	-91.56	30.52
ST6	**EQ 0.5 g**	0.5	366.22	-122.07	0	30.52	-91.56	0	45.78	-76.3	-30.52
ST7	**WNb 0.8g**	0.08	244.15	-61.04	30.52	45.78	-76.3	-0.15	91.56	-45.78	15.26
ST8	**EQ 0.8g**	0.8	610.37	-152.59	-30.52	61.04	-76.3	15.26	91.56	-76.3	45.78
ST9	**WNb 1.1g**	0.08	1.22	-0.76	0	0.61	-0.76	-15.26	0.61	-0.76	-15.26
ST10	**EQ 1.1g**	1.1	839.26	-137.33	0.15	76.3	-61.04	0	61.04	-91.56	23.27
ST11	**WNa 1.1g**	0.08	213.63	-76.3	15.26	30.52	-106.81	-61.04	76.3	-61.04	45.78

Table 3.1.1k Summary of results (continued)

		Intensity (g)	max SG19 (ustrain)	min SG19 (ustrain)	Residual SG19	max SG20 (ustrain)	min SG20 (ustrain)	Residual SG20
ST1	**WNb 0.1g**	0.08	27.59	-51.94	-22.72	37.42	-51.25	-21.97
ST2	**EQ 0.1g**	0.1	30.03	-38.96	-7.31	51.25	-94.39	-6.51
ST3	**WNb 0.2g**	0.08	3.24	-0.81	0	17.07	-5.69	9.76
ST4	**EQ 0.2g**	0.2	1.62	-2.43	0.81	13.82	-22.77	3.25
ST5	**WNb 0.5g**	0.08						
ST6	**EQ 0.5 g**	0.5						
ST7	**WNb 0.8g**	0.08	1.62	-2.43	0.81	5.69	-20.33	0.81
ST8	**EQ 0.8g**	0.8	2.43	-2.43	5.69	9.76	-78.89	0
ST9	**WNb 1.1g**	0.08	2.43	-3.24	-0.81	2.44	-4.88	-0.81
ST10	**EQ 1.1g**	1.1	4.87	-3.24	1.62	16.25	-71.52	12.19
ST11	**WNa 1.1g**	0.08	3.24	-1.62	2.45	4.06	-0.81	2.44

Table 3.1.1l. Summary of results (continued)

		Intensity (g)	max (acc1+acc4)/2	min (acc1+acc4)/2	max (acc1+acc4)/2-acc10	min (acc1+acc4)/2-acc10	Δt(t14-t10) (sec)
ST1	**WNb 0.1g**	0.08	0.13	-0.13	0.14	-0.11	-7.1
ST2	**EQ 0.1g**	0.1	0.14	-0.09	0.09	-0.07	0.17
ST3	**WNb 0.2g**	0.08	0.12	-0.12	0.14	-0.15	-5.5
ST4	**EQ 0.2g**	0.2	0.24	-0.2	0.2	-0.23	0.16
ST5	**WNb 0.5g**	0.08	0.12	-0.13	0.11	-0.11	
ST6	**EQ 0.5 g**	0.5	0.68	-0.59	0.6	-0.55	0.93
ST7	**WNb 0.8g**	0.08	0.25	-0.24	0.25	-0.28	0.42
ST8	**EQ 0.8g**	0.8	1.19	-1.13	1.15	-1.39	0.18
ST9	**WNb 1.1g**	0.08	0.12	-0.13	0.13	-0.13	12.61
ST10	**EQ 1.1g**	1.1	1.67	-1.62	1.59	-1.58	4.35
ST11	**WNa 1.1g**	0.08	0.21	-0.2	0.21	-0.2	6.09

Table 3.1.2 Summary of results

Test	WNb 0.1g	0.1g	WNb 0.2g	0.2g	WNb 0.5g	0.5g
PGA (g)	+0.13/-0.13	+0.07/-0.11	+0.1/-0.11	+0.15/-0.19	+0.06/-0.07	+0.47/-0.52
PFA (g)	+0.11/-0.13	+0.14/-0.09	+0.12/-0.12	+0.24/-0.2	+0.11/-0.11	+0.68/-0.59
FAF	1	1.27	1.09	1.26	1.57	1.31
drift (‰)	+0.04/-0.07	+1.20/-0.84	+1.08/-0.96	+1.99/-1.75	+0.15/-0.15	+5.06/-5.14
Test	**WNb 0.8g**	**0.8g**	**WNb 1.1g**	**1.1g**	**WNa 1.1g**	
PGA (g)	+0.06/-0.08	+0.69/-0.76	+0.06/-0.07	+1.08/-1	+0.06/-0.09	
PFA (g)	+0.25/-0.24	+1.19/-1.13	+0.12/-0.13	+1.67/-1.62	+0.19/-0.19	
FAF	3.13	1.57	1.86	1.55	2.11	
drift (‰)	+2.29/-2.32	+8.04/-8.22	1.32/-1.29	+11.37/-10.97	+2.30/-2.31	

3.2 Concluding assessment remarks

In table 3.1.1 the maximum accelerations for each excitation are sited. Accelerometer Acc1 is located at the left corner of the slab along the direction x (direction of excitation). Accelerometer Acc4 is located at the right corner of the slab along direction x. Accelerometer Acc7 is located at the center of full infill along x direction. Acc10 is located at the center of foundation along x direction. The ratio between peak top slab and peak foundation acceleration fluctuates 1 at white noise before 0,1g to 3.13 at white noise before 0.8g. The ratio between peak top slab and peak foundation seismic acceleration fluctuates 1.26 during ST2 and ST4 that is EQ0.1g and EQ0.2g to 1.57 during ST8 and ST10 that is EQ0.8 and EQ1.1g. Table 3.1.1c, d provides the values from Draw wire displacement sensors (W1, W2,,W3,W4,W5,W6,W7,W8). The max drift ‰ occurs during 1,1g excitation, with value 11,37‰ (13.93mm). The minimum peak drift is 0.07 ‰ at white noise before 0,1g. The max residual drift is 0,25 mm at 1,1g excitation (Table 3.1.1e).

During ST6 excitation of EQ0.5g, infill wall 3-4 starts to significantly accelerate. In table 3.1.1f the values of the strain gauges are gathered. During ST6 excitation of EQ0.5g, SG1, 4, 8, 11, 14 present 2 to 4 times higher strains of the rebars than during previous excitations.

During ST7 excitation of WNb0.8g, infill wall 3-4 presents the highest out of plane white noise acceleration at its center point. This infill wall presented serious debonding at both sides and at the top.

During ST8 excitation of EQ0.8g, several strain gauges show more than 2 times higher strains of the rebars than during ST6. Additional cracks occur inside the bed joints of the infill wall between the bricks as well as at the concrete-to-concrete joints at the interfaces between columns and to slab or bottom beams. During ST9 excitation WNb1.1g, the damages in the infills remain unchanged.

During ST10 excitation EQ1.1g, infill wall 3-4 presents the highest out of plane earthquake excitation. During ST10, the columns developed maximum steel strain as high as 2000-2350μstrain, well below the yield strain of the B500C steel (2890 μstrain, see section 4.1). Strain gauge SG5 reveals that the steel rebar at the external face of column 2, at the bottom, suffers the highest tensile strain of 2334.67 μstrain. Strain gauge SG5 reveals that the steel rebar at the external face of column 2, at the bottom, suffers the highest compressive strain of 1136.19 μstrain. Strain gauge SG6 reveals that the steel rebar at the internal face of column 2, at the bottom, suffers the tensile of 1763.86 μstrain. Strain gauge SG9, reveals that the steel rebar at the external face of column 2, at the top, suffers the tensile of 1979.4 μstrain. Finally, strain gauge SG10, reveals that the steel rebar at the internal face of column 2, develops the tensile strain of 1961.66 μstrain. At 1.1g excitation, we have the highest values for all strain gauges. The maximum value of -717,39 μstrain of residual strain is measured with SG9, during 1.1g excitation.

Table 3.1.13 shows the values of time (t14), at which (Acc1+Acc4)/2 receive maximum. Therefore, the time difference of the accelerometers between the top slab and the foundation is given as Δt(t14-t10). At white noise before WNb0.5g, observed the maximum difference Δt.

3.3 Damage assessment

In this section the observed damage at the different stages of the shaking table tests is described in detail. During the tests, an increasing level of damage was observed.

During ST6 excitation of EQ0.5g, infill wall 3-4 starts to accumulate damage. During ST7 excitation of WNb0.8g, infill wall 3-4 presents the highest out of plane white noise acceleration at its center point. This infill wall presented serious debonding at both sides and at the top.

During ST8 excitation of EQ0.8g, additional cracks occur inside the bed joints of the infill wall between the bricks as well as at the concrete-to-concrete joints at the interfaces between columns and to slab or bottom beams.

After the 1.1g excitation, cracks with separation between bricks were noticed and debonding of the wall from the frame at each side. As shown in Figure 3.3.1a, the wall infill 3-4 vertical to the direction of movement of the seismic table, presents thin horizontal cracks extending between first and second row of bricks and between fourth and fifth row of bricks. Also, thin horizontal cracks extend between sixth and seventh bricks row. Two horizontal cracks occurred under the latest row of bricks. Wall infill 3-4 is seriously debonded from columns 3,4 and top slab (Figure 3.3.2a). At Figure 3.3.1c, the opposite wall infill 1-2 revealed slight stair-stepped diagonal cracks at the center of wall. One horizontal crack occurred between eighth and ninth rows of bricks. Wall infill 1-2 is seriously debonded from columns 1, 2 and top slab (Figure 3.3.3a). Partial infill wall 2-3 (Figure 3.3.1b), parallel to the direction of movement of the seismic table has two cracks between fourth- fifth row of bricks, between sixth-seventh row of bricks and between seventh- eighth row. Also, there is a diagonal cracking at the top row of bricks. A slight stair-stepped diagonal crack occurred at the first row of bricks. Wall infill 2-3 is seriously debonded from column 2 and top slab (Figure 3.3.3b). The remaining partial infill wall 1-4 (Figure 3.3.1d) has two horizontal cracks between third-fourth row and sixth-seventh row of bricks. A small stair-stepped diagonal crack occurred at the bottom on the right side. Wall infill 1-4 is seriously debonded from column 1 and top slab (Figure 3.3.3b). The bottom infill-tie beam interface seems intact for wall infills 1-2, 3-4 excited out of plane.

Further, concrete columns 3 and 4 suffered minor cracking at the edge of the section at the bottom and at the top respectively. The longitudinal bars of the B500C steel of the columns did not suffered yielding (maximum steel strain as high as 2000-2350μstrain as the strain in all cases was below 2890 μstrain.

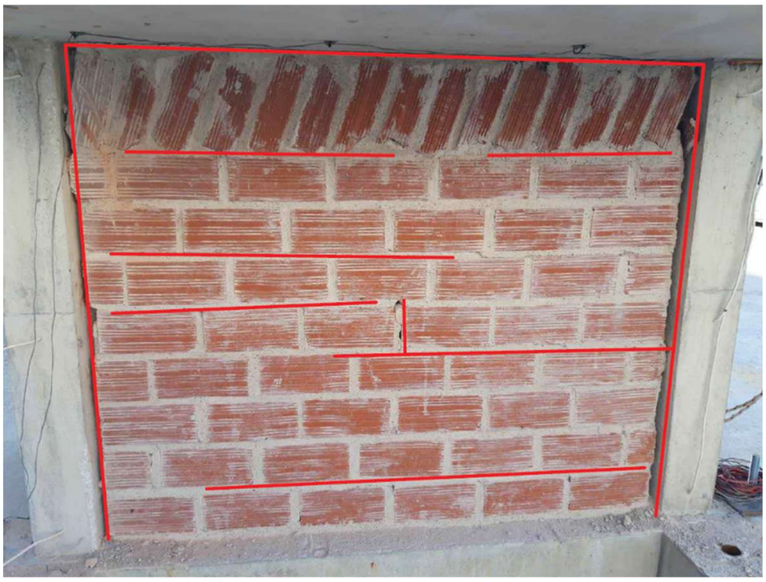
(a)


(b)


(c)

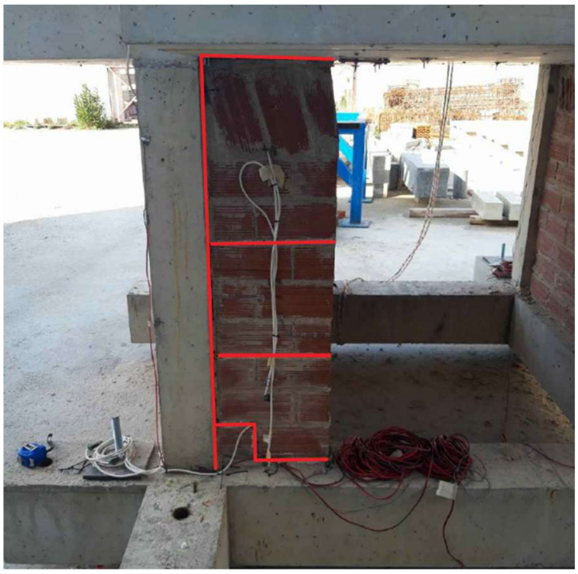
(d)

Figure 3.3.1 Observed damage after 1.1g test: (a) exterior side of wall infill 3-4 vertical to the direction of movement of seismic table (b) wall infill 2-3 parallel to the direction of movement of seismic table (c) Exterior side of wall infill 1-2, transverse to the direction of movement of the seismic table (d) wall infill 1-4 column parallel to the direction of movement of seismic table

Sketch of damages on the infills

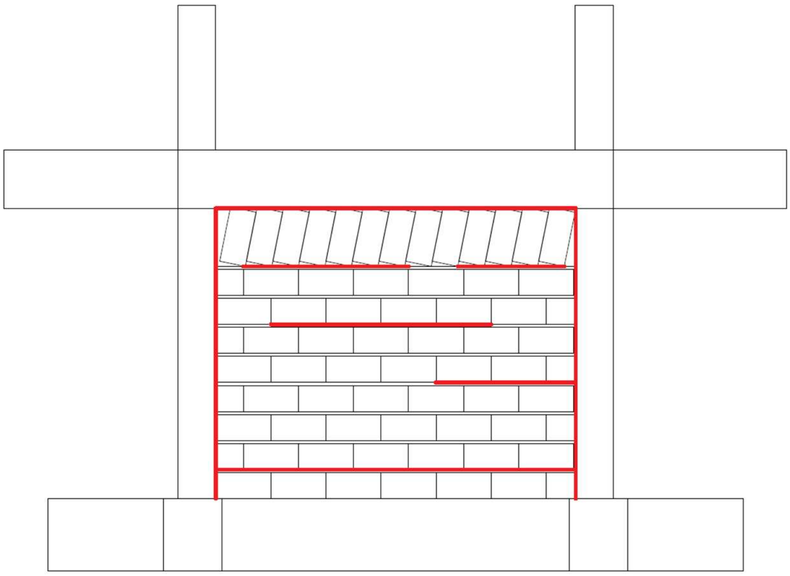

(a)

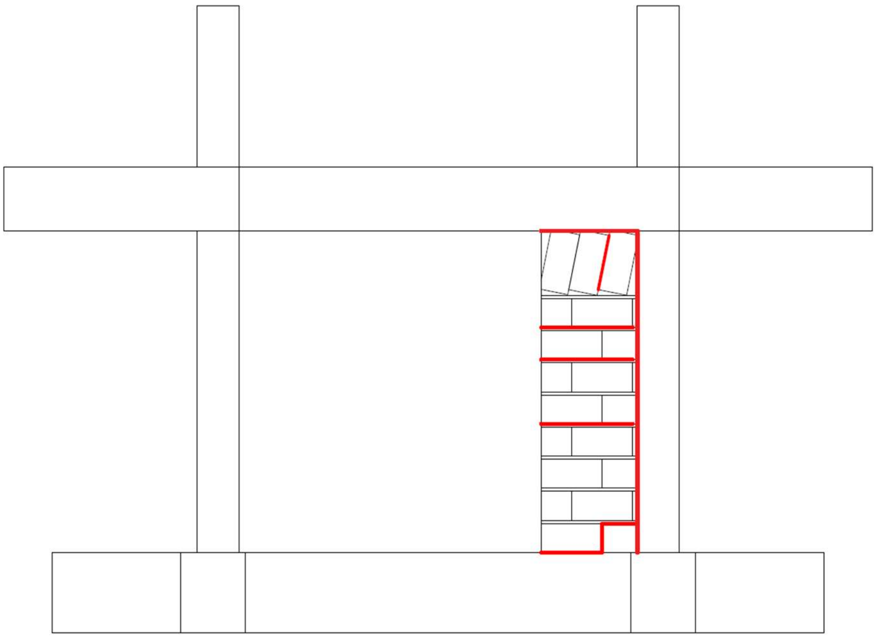

(b)

Figure 3.3.2 Damage and crack patterns after 1.1g test for (a) exterior side of wall infill 3-4, (b) wall infill 2-3

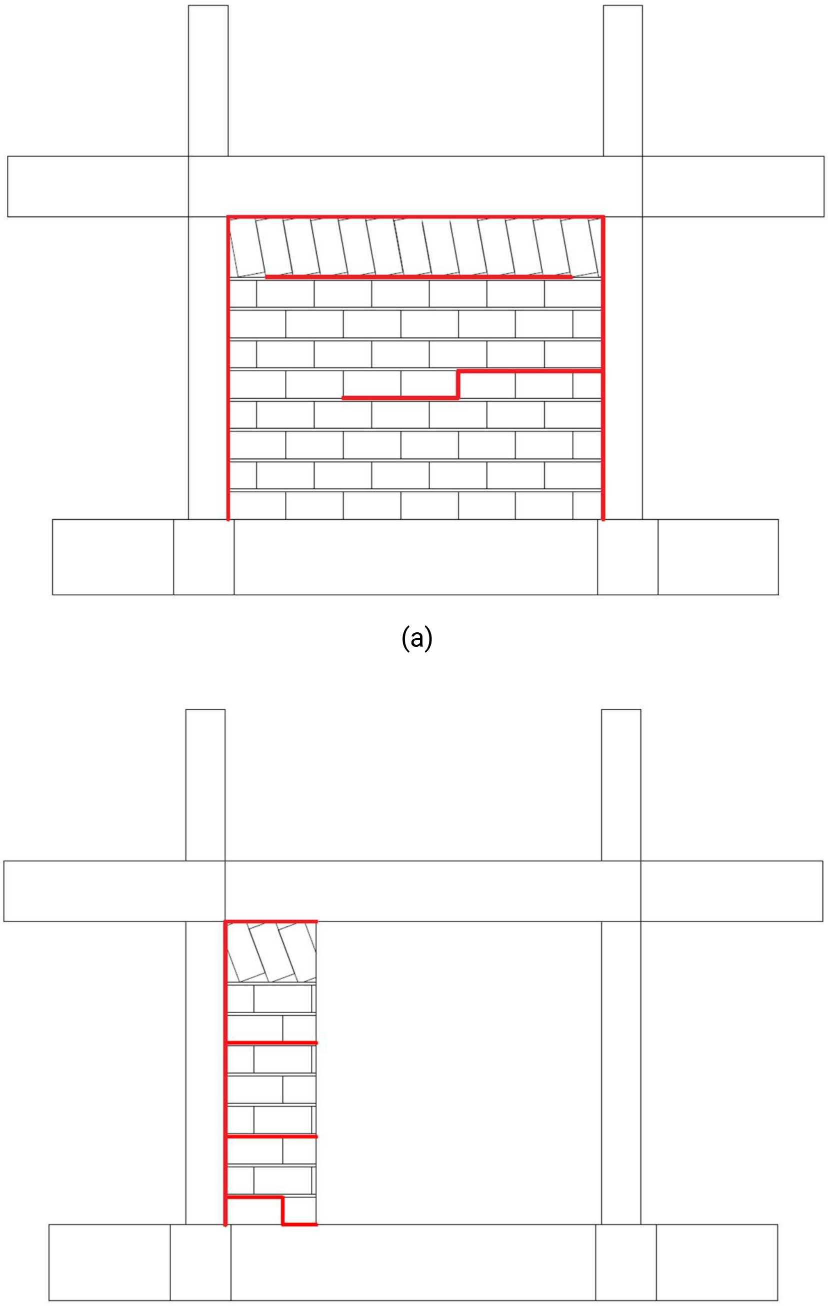

(a)

(b)

Figure 3.3.3 Damage and crack patterns after 1.1g test for (a) exterior side of wall infill 1-2, (b) wall infill 1-4

3.4 Assessment of the performance of tested as-built structure using PZT sensors

The proposed methodology for real-time damage assessment in reinforced concrete (RC) structures using piezoelectric (PZT) sensors offers significant potential for early detection of damage and the provision of critical failure warnings prior to the appearance of visible signs. The system employs a total of 48 PZT sensors installed both internally and externally on the structure. Figures 3.4.1 and 3.4.2, 2.1 to 2.3 illustrate the sensor locations and code names of the PZTs.

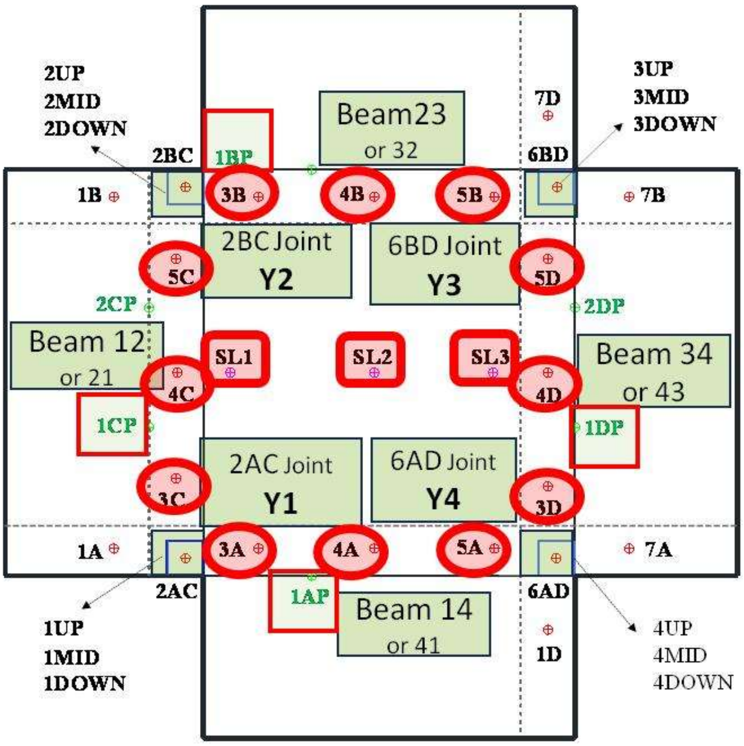

Figure 3.4.1 Location of PZT sensors and code names

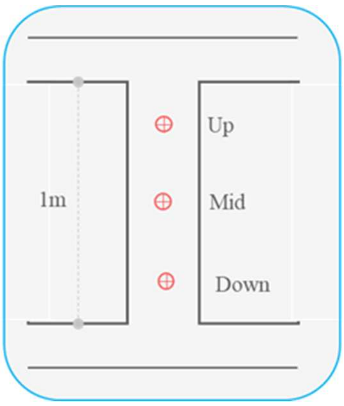

Figure 3.4.2 Location of the PZTs inside the columns and code names

Every acquired measurement through the EMI method constitutes an electromechanical signal of the particular PZT patch. The data analysis of the electromechanical signals should be examined through damage index metrics. Therefore, the elaboration of the EMI signatures through statistical analysis could be a valuable tool in converting the variations of the EMI signatures between the healthy condition and any subsequent one to damage index metrics. In order to quantify damage assessment in vertical forest (VF) structure, the known statistically index of the Root Mean Square Deviation (RMSD) is employed. The signal of every PZT has been installed in the structure at the healthy state corresponds to the baseline measurement used in the adopted statistical analysis with RMSD. Thus, variations in growth trend for the PZT output frequency response signals due to damage at different damage states could be effectively evaluated by integrating the RMSD index. Higher RMSD values indicate detection of increased structural damage.

With the application of statistical tools, the variations of the EMI signatures can be converted to numerical indices. Some of the most common indices in the literature are RMSD (Root Mean Square Deviation). This damage index was regarded as one of the most useful and reliable indices in several fields of SHM (Voutetaki et al. 2016, Chalioris et al. 2020, Chalioris et al. 2021, Na and Baek, 2018). The damage index of RMSD was applied for the statistical analysis of the EMI responses:

$$\mathrm{RMSD} = \sqrt{\frac{\Sigma_1^M \left(\left|V_p(f_r)\right|_D - \left|V_p(f_r)\right|_0\right)^2}{\Sigma_1^M \left(\left|V_p(f_r)\right|_0\right)^2}}$$

Where $\left|V_p(f_r)\right|_0$ is the absolute value of the voltage output signal as extracted from the PZT at the healthy pristine state of the specimen, $\left|V_p(f_r)\right|_D$ is the absolute value of the corresponding voltage output signal as measured from the same PZT at any damage level, and M is the number of measurements in the frequency band. Each SHM device captures the EMI response of a PZT sensor in a predefined frequency range, which was set to 10–240 kHz with a resolution of 1 kHz.

The absolute values of the voltage output response as extracted from the slab PZTs (SL1, SL2 and SL3) versus frequency at the healthy pristine state and the other two loading stages 0.8g and 1.1g are showed in the Tables 3.4.1, 3.4.2 and 3.4.3. Subsequently, Figures 3.4.3a, b and c illustrate the voltage frequency responses of the PZT sensor SL1, SL2 and SL3. The values of RMSD are computed from the absolute values of the voltage output responses and used to evaluate the effectiveness of the SHM method for damage diagnosis and assessment. For this purpose, Figures 3.4.4 up to 3.4.22, 3.4.24, 3.4.26, 3.4.28 illustrate the range of the RMSD values that have been calculated based on the PZT voltage output signals from the total of 48 PZT sensors inside and on the structure.

Slab

Table 3.4.1 Voltage output response of PZT SL1 versus Frequency

SL1	Healthy	EQ0.8g	EQ1.1g
Frequency (kHz)	Voltage (mV)	Voltage (mV)	Voltage (mV)
10	1791.23	1812.65	1815.13
11	1731.46	1752.19	1754.60
12	1673.45	1693.49	1695.84
13	1617.19	1636.57	1638.84
14	1562.69	1581.42	1583.61

SL1	Healthy	EQ0.8g	EQ1.1g
Frequency (kHz)	Voltage (mV)	Voltage (mV)	Voltage (mV)
15	1509.94	1528.03	1530.15
16	1458.96	1476.41	1478.46
17	1409.72	1426.56	1428.54
18	1362.25	1378.48	1380.38
19	1316.53	1332.17	1334.00
20	1272.57	1287.63	1289.38
21	1230.36	1244.85	1246.53
22	1189.91	1203.85	1205.44
23	1151.22	1164.61	1166.13
24	1115.59	1128.38	1129.80
25	1081.81	1094.03	1095.35
26	1049.62	1061.34	1062.56
27	1018.98	1030.17	1031.29
28	989.73	1000.43	1001.48
29	961.78	972.04	973.01
30	935.05	944.89	945.78
31	909.47	918.90	919.73
32	884.94	894.00	894.77
33	861.46	870.12	870.84
34	838.93	847.23	847.89
35	817.32	825.29	825.89
36	796.53	804.14	804.70
37	776.55	783.84	784.35
38	757.30	764.35	764.82
39	738.82	745.62	746.07
40	721.09	727.59	727.98
41	703.96	710.22	710.57
42	687.43	693.45	693.79
43	671.47	677.29	677.61
44	656.10	661.73	662.01
45	641.29	646.75	647.01
46	627.02	632.32	632.56
47	613.20	618.40	618.61
48	599.82	604.94	605.12
49	586.88	591.95	592.12
50	574.42	579.40	579.55
51	562.31	567.25	567.38
52	550.55	555.50	555.60
53	539.15	544.08	544.17
54	528.10	532.97	533.05
55	517.35	522.15	522.21
56	506.86	511.59	511.63
57	496.65	501.36	501.39

SL1	Healthy	EQ0.8g	EQ1.1g
Frequency (kHz)	Voltage (mV)	Voltage (mV)	Voltage (mV)
58	486.79	491.37	491.37
59	477.19	481.62	481.61
60	467.80	472.22	472.18
61	458.77	463.03	462.98
62	449.87	453.98	453.91
63	441.25	445.30	445.23
64	432.90	436.80	436.71
65	424.81	428.54	428.43
66	417.00	420.52	420.40
67	409.34	412.69	412.55
68	401.87	405.15	404.99
69	394.64	397.73	397.57
70	387.54	390.60	390.41
71	380.67	383.59	383.39
72	373.89	376.79	376.57
73	367.36	370.14	369.91
74	360.93	363.69	363.44
75	354.74	357.41	357.15
76	348.62	351.30	351.02
77	342.65	345.26	344.98
78	336.75	339.40	339.10
79	331.05	333.55	333.26
80	325.46	327.88	327.57
81	319.90	322.25	321.93
82	314.51	316.86	316.52
83	309.21	311.51	311.16
84	304.10	306.28	305.92
85	298.91	301.15	300.76
86	293.93	296.14	295.75
87	289.05	291.23	290.79
88	284.24	286.36	285.93
89	279.54	281.72	281.28
90	274.90	277.00	276.56
91	270.35	272.44	272.00
92	265.72	267.89	267.41
93	261.20	263.30	262.82
94	256.77	258.89	258.41
95	252.31	254.39	253.88
96	247.86	249.99	249.49
97	243.63	245.67	245.15
98	239.31	241.39	240.81
99	235.19	237.14	236.55
100	231.04	233.06	232.49

SL1	Healthy	EQ0.8g	EQ1.1g
Frequency (kHz)	Voltage (mV)	Voltage (mV)	Voltage (mV)
101	226.99	228.96	228.41
102	222.95	224.90	224.33
103	219.16	220.97	220.35
104	215.17	217.17	216.61
105	211.58	213.38	212.82
106	208.07	209.81	209.34
107	204.44	206.23	205.82
108	201.10	202.74	202.41
109	197.63	199.26	199.02
110	194.51	195.96	195.77
111	191.29	192.66	192.33
112	188.37	189.49	189.27
113	185.39	186.44	186.27
114	182.40	183.34	183.22
115	179.32	180.23	180.15
116	176.37	177.15	177.11
117	173.41	174.19	174.13
118	170.33	171.11	171.01
119	167.48	168.07	168.00
120	164.49	165.14	165.01
121	161.10	162.13	161.89
122	158.18	159.11	158.45
123	155.31	156.15	155.55
124	151.96	153.09	152.39
125	148.82	150.20	149.70
126	146.18	147.40	147.04
127	143.23	144.52	143.85
128	140.45	141.77	141.38
129	138.30	139.24	139.10
130	135.57	136.72	136.73
131	133.85	134.16	133.97
132	132.00	131.67	132.09
133	129.99	129.29	129.68
134	128.10	126.87	127.69
135	125.98	124.47	125.64
136	124.02	121.90	122.99
137	121.93	119.47	121.10
138	119.90	117.37	118.85
139	117.62	115.23	117.11
140	115.28	113.00	115.22
141	112.85	110.56	113.34
142	110.62	108.35	110.69
143	108.22	106.44	108.61

SL1	Healthy	EQ0.8g	EQ1.1g
Frequency (kHz)	Voltage (mV)	Voltage (mV)	Voltage (mV)
144	105.38	104.05	105.99
145	102.08	102.14	104.42
146	99.63	99.93	102.66
147	97.36	97.77	99.81
148	94.95	95.85	97.31
149	92.73	93.91	95.83
150	89.86	91.99	94.46
151	88.11	89.77	92.36
152	85.92	87.62	91.14
153	83.76	85.74	89.81
154	82.69	84.25	87.95
155	80.73	82.84	86.30
156	79.13	81.28	85.06
157	77.84	79.18	83.82
158	76.97	77.75	82.92
159	76.49	76.24	80.56
160	75.75	74.44	79.21
161	73.65	72.48	76.03
162	73.04	70.50	73.81
163	72.23	68.36	71.85
164	71.14	66.72	70.45
165	68.74	64.39	69.54
166	67.60	62.46	67.36
167	66.13	60.42	64.44
168	64.67	58.71	62.62
169	62.67	56.88	61.47
170	60.61	54.88	59.77
171	58.97	53.49	58.95
172	58.40	52.11	57.20
173	57.34	51.35	55.73
174	56.13	50.90	55.68
175	55.55	50.43	55.93
176	54.76	50.31	56.22
177	54.96	50.61	56.31
178	55.14	52.07	58.20
179	56.44	54.12	59.41
180	58.05	56.64	60.82
181	59.64	59.51	63.97
182	63.18	62.90	67.41
183	66.96	66.87	70.77
184	72.21	72.19	74.66
185	77.63	77.56	78.94
186	110.62	108.35	110.69

SL1	Healthy	EQ0.8g	EQ1.1g
Frequency (kHz)	**Voltage (mV)**	**Voltage (mV)**	**Voltage (mV)**
187	108.22	106.44	108.61
188	105.38	104.05	105.99
189	102.08	102.14	104.42
190	99.63	99.93	102.66
191	97.36	97.77	99.81
192	94.95	95.85	97.31
193	92.73	93.91	95.83
194	89.86	91.99	94.46
195	88.11	89.77	92.36
196	85.92	87.62	91.14
197	83.76	85.74	89.81
198	82.69	84.25	87.95
199	80.73	82.84	86.30
200	79.13	81.28	85.06
201	77.84	79.18	83.82
202	76.97	77.75	82.92
203	76.49	76.24	80.56
204	75.75	74.44	79.21
205	73.65	72.48	76.03
206	73.04	70.50	73.81
207	72.23	68.36	71.85
208	71.14	66.72	70.45
209	68.74	64.39	69.54
210	67.60	62.46	67.36
211	66.13	60.42	64.44
212	64.67	58.71	62.62
213	62.67	56.88	61.47
214	60.61	54.88	59.77
215	58.97	53.49	58.95
216	58.40	52.11	57.20
217	57.34	51.35	55.73
218	56.13	50.90	55.68
219	55.55	50.43	55.93
220	54.76	50.31	56.22
221	54.96	50.61	56.31
222	55.14	52.07	58.20
223	56.44	54.12	59.41
224	58.05	56.64	60.82
225	59.64	59.51	63.97
226	63.18	62.90	67.41
227	66.96	66.87	70.77
228	72.21	72.19	74.66
229	77.63	77.56	78.94

SL1	Healthy	EQ0.8g	EQ1.1g
Frequency (kHz)	Voltage (mV)	Voltage (mV)	Voltage (mV)
230	116.50	118.29	117.93
231	114.30	116.05	115.69
232	112.18	113.97	113.61
233	110.04	111.91	111.54
234	108.11	109.95	109.58
235	106.34	108.21	107.83
236	104.65	106.58	106.18
237	103.12	105.04	104.63
238	101.75	103.63	103.23
239	100.51	102.34	101.95
240	99.41	101.18	100.79

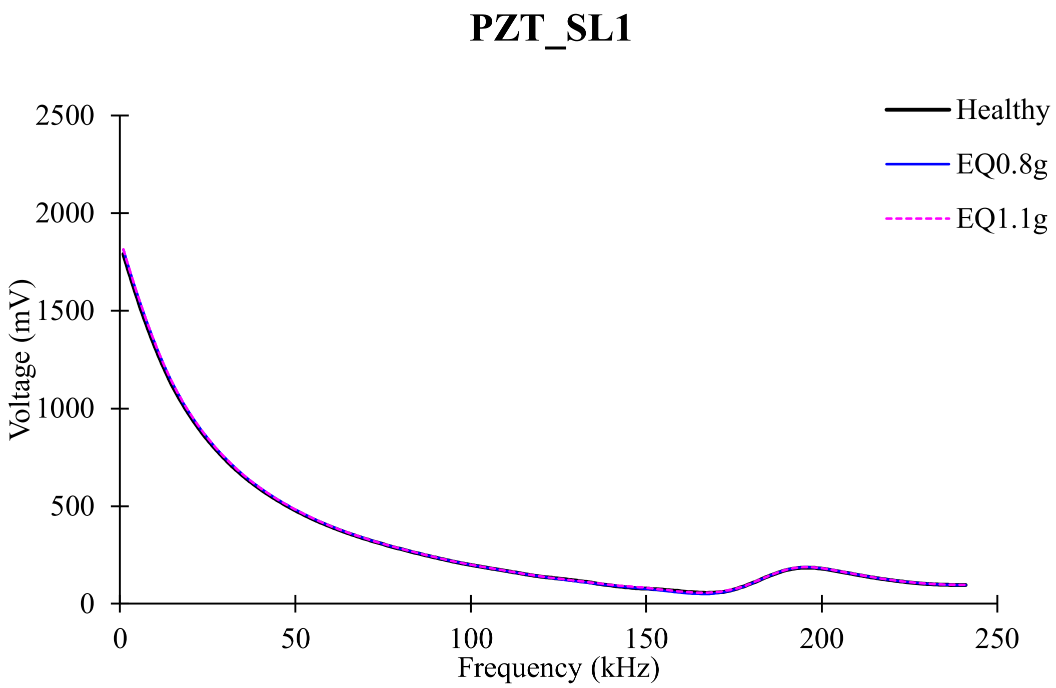

Figure 3.4.3 a Voltage frequency responses of the PZT sensor SL1.

Table 3.4.2 Voltage output response of PZT SL2 versus Frequency

SL2	Healthy	EQ0.8g	EQ1.1g
Frequency (kHz)	Voltage (mV)	Voltage (mV)	Voltage (mV)
10	2017.87	2041.89	2032.16
11	1943.79	1967.31	1958.05
12	1872.17	1895.22	1886.41
13	1803.03	1825.62	1817.22
14	1736.35	1758.50	1750.50
15	1672.13	1693.86	1686.23
16	1610.39	1631.71	1624.43
17	1551.11	1572.04	1565.08
18	1494.29	1514.85	1508.20
19	1439.95	1460.15	1453.77
20	1388.07	1407.93	1401.81
21	1338.65	1358.20	1352.30
22	1291.71	1310.95	1305.26
23	1247.23	1266.18	1260.67
24	1208.33	1226.84	1221.56
25	1171.49	1189.64	1184.77
26	1136.69	1154.43	1149.82
27	1103.60	1121.30	1116.95
28	1072.55	1090.28	1085.77
29	1042.95	1060.73	1055.98
30	1014.73	1032.61	1027.71
31	987.94	1005.80	1000.77
32	962.49	980.41	975.02
33	938.30	955.78	950.46
34	915.21	932.30	927.14
35	893.08	909.91	904.80
36	871.91	888.50	883.46
37	851.73	868.60	863.10
38	832.42	849.17	843.54
39	813.96	830.40	825.01
40	796.14	812.42	807.07
41	778.84	795.04	789.97
42	762.24	778.21	773.30
43	746.31	762.24	757.27
44	730.89	746.72	741.93
45	716.06	731.80	727.04
46	702.04	717.33	712.73
47	688.44	703.27	699.10
48	675.27	690.20	685.98
49	662.70	677.50	673.43
50	650.67	665.06	661.21
51	638.92	653.21	649.50

SL2	Healthy	EQ0.8g	EQ1.1g
Frequency (kHz)	Voltage (mV)	Voltage (mV)	Voltage (mV)
52	627.69	641.66	638.27
53	616.88	630.66	627.44
54	606.42	620.09	616.86
55	596.17	609.87	606.69
56	586.25	599.96	596.84
57	576.63	590.31	587.19
58	567.46	580.73	577.90
59	558.47	571.73	568.77
60	549.72	563.10	560.05
61	541.21	554.71	551.46
62	533.02	546.47	543.13
63	524.98	538.59	534.96
64	517.07	530.72	526.91
65	509.40	523.15	519.01
66	501.85	515.69	511.27
67	494.50	508.30	503.77
68	487.40	501.10	496.48
69	480.36	494.15	489.32
70	473.48	487.29	482.28
71	466.85	480.59	475.59
72	460.37	474.03	469.06
73	454.11	467.65	462.91
74	447.94	461.55	456.87
75	442.00	455.55	450.94
76	436.22	449.66	445.17
77	430.50	443.97	439.73
78	424.97	438.29	434.31
79	419.52	432.88	428.95
80	414.12	427.46	423.71
81	408.83	422.25	418.52
82	403.69	417.03	413.43
83	398.64	412.00	408.52
84	393.68	407.13	403.67
85	388.86	402.61	398.89
86	384.21	398.13	394.32
87	379.62	393.63	389.75
88	375.07	389.19	385.22
89	370.66	384.88	380.83
90	366.34	380.70	376.46
91	362.12	376.50	372.17
92	357.95	372.29	367.91
93	353.86	368.11	363.72
94	349.77	364.04	359.57

SL2	Healthy	EQ0.8g	EQ1.1g
Frequency (kHz)	Voltage (mV)	Voltage (mV)	Voltage (mV)
95	345.74	360.00	355.46
96	341.70	355.97	351.42
97	337.69	352.06	347.45
98	333.74	348.02	343.46
99	329.86	344.07	339.49
100	326.00	340.17	335.54
101	322.21	336.26	331.64
102	318.45	332.43	327.84
103	314.73	328.58	324.08
104	311.10	324.77	320.33
105	307.55	321.06	316.71
106	304.07	317.43	313.13
107	300.65	313.84	309.63
108	297.33	310.43	306.33
109	294.07	307.20	303.12
110	290.89	303.98	299.95
111	287.86	300.86	296.99
112	284.88	297.84	294.11
113	281.98	294.82	291.30
114	279.16	291.96	288.54
115	276.42	289.17	285.87
116	273.73	286.45	283.24
117	271.04	283.75	280.62
118	268.42	281.12	278.09
119	265.80	278.52	275.58
120	263.23	275.99	273.06
121	260.72	273.48	270.64
122	258.20	271.01	268.23
123	255.74	268.53	265.81
124	253.29	266.10	263.50
125	250.89	263.66	261.07
126	248.52	261.31	258.76
127	246.17	258.94	256.48
128	243.81	256.63	254.15
129	241.49	254.24	251.87
130	239.20	251.94	249.52
131	236.90	249.65	247.19
132	234.55	247.32	244.91
133	232.24	245.05	242.67
134	229.93	242.80	240.38
135	227.62	240.46	238.14
136	225.37	238.32	235.91
137	223.19	236.15	233.72

SL2	Healthy	EQ0.8g	EQ1.1g
Frequency (kHz)	**Voltage (mV)**	**Voltage (mV)**	**Voltage (mV)**
138	220.96	233.36	231.52
139	218.72	231.48	229.30
140	216.48	228.76	227.04
141	214.21	225.22	224.73
142	211.98	224.15	222.49
143	209.72	221.61	220.23
144	207.17	220.01	217.96
145	205.07	218.64	215.64
146	202.99	217.89	213.37
147	200.95	218.09	211.18
148	198.84	218.46	208.93
149	196.76	218.68	206.68
150	194.70	218.51	204.54
151	192.69	218.22	202.33
152	190.71	217.57	200.27
153	188.77	216.80	198.22
154	186.85	216.03	196.17
155	185.01	214.86	193.96
156	183.17	213.30	192.06
157	181.35	211.62	190.27
158	179.54	209.96	188.57
159	177.89	208.71	186.92
160	176.24	207.67	185.32
161	174.74	206.85	183.88
162	173.31	206.20	182.50
163	171.96	205.46	181.11
164	170.75	204.77	180.11
165	169.55	204.71	179.13
166	168.59	203.92	178.27
167	167.84	204.29	177.57
168	167.36	206.34	177.15
169	167.03	206.67	176.89
170	166.95	209.06	176.89
171	167.56	211.59	177.11
172	168.07	214.72	177.58
173	168.84	218.07	178.32
174	169.86	220.81	179.43
175	171.15	223.11	180.71
176	172.62	225.38	182.26
177	174.37	227.72	184.02
178	176.33	229.83	186.03
179	178.60	232.06	188.34
180	181.22	234.27	190.94

SL2	Healthy	EQ0.8g	EQ1.1g
Frequency (kHz)	Voltage (mV)	Voltage (mV)	Voltage (mV)
181	184.19	236.44	193.92
182	187.39	238.89	197.50
183	190.83	241.84	201.06
184	194.56	245.34	204.96
185	198.73	249.47	209.27
186	203.21	254.05	213.95
187	208.09	258.95	218.95
188	213.22	264.11	224.25
189	218.66	269.54	229.82
190	224.38	275.17	235.81
191	230.23	280.83	241.78
192	236.34	286.68	247.89
193	242.39	292.46	254.00
194	248.35	298.15	259.99
195	254.14	303.76	265.85
196	259.72	309.08	271.46
197	264.94	314.08	276.66
198	269.70	318.59	281.41
199	273.95	322.55	285.64
200	277.58	325.85	289.22
201	280.50	328.56	292.05
202	282.71	330.78	294.22
203	284.29	331.99	295.72
204	285.19	332.57	296.58
205	285.53	332.54	296.80
206	285.26	332.04	296.40
207	284.33	331.02	295.40
208	282.82	329.45	293.80
209	280.85	327.49	291.74
210	278.61	325.28	289.46
211	276.12	322.82	286.90
212	273.39	320.27	284.11
213	270.48	317.57	281.10
214	267.41	314.69	277.98
215	264.27	311.76	274.81
216	261.12	308.72	271.62
217	257.93	305.68	268.47
218	254.75	302.65	265.30
219	251.58	299.72	262.15
220	248.53	296.91	259.14
221	245.59	294.02	256.27
222	242.75	291.26	253.49
223	240.00	288.60	250.78

SL2	Healthy	EQ0.8g	EQ1.1g
Frequency (kHz)	Voltage (mV)	Voltage (mV)	Voltage (mV)
224	237.35	285.92	248.11
225	234.80	283.37	245.56
226	232.33	280.86	243.11
227	229.97	278.49	240.80
228	227.76	276.17	238.61
229	225.66	273.82	236.58
230	223.68	271.78	234.66
231	221.83	269.83	232.84
232	220.10	268.01	231.13
233	218.46	266.35	229.52
234	216.94	264.84	228.05
235	215.56	263.45	226.69
236	214.27	262.07	225.43
237	213.09	260.83	224.25
238	211.84	259.53	223.01
239	210.67	258.30	221.85
240	209.57	257.15	220.76

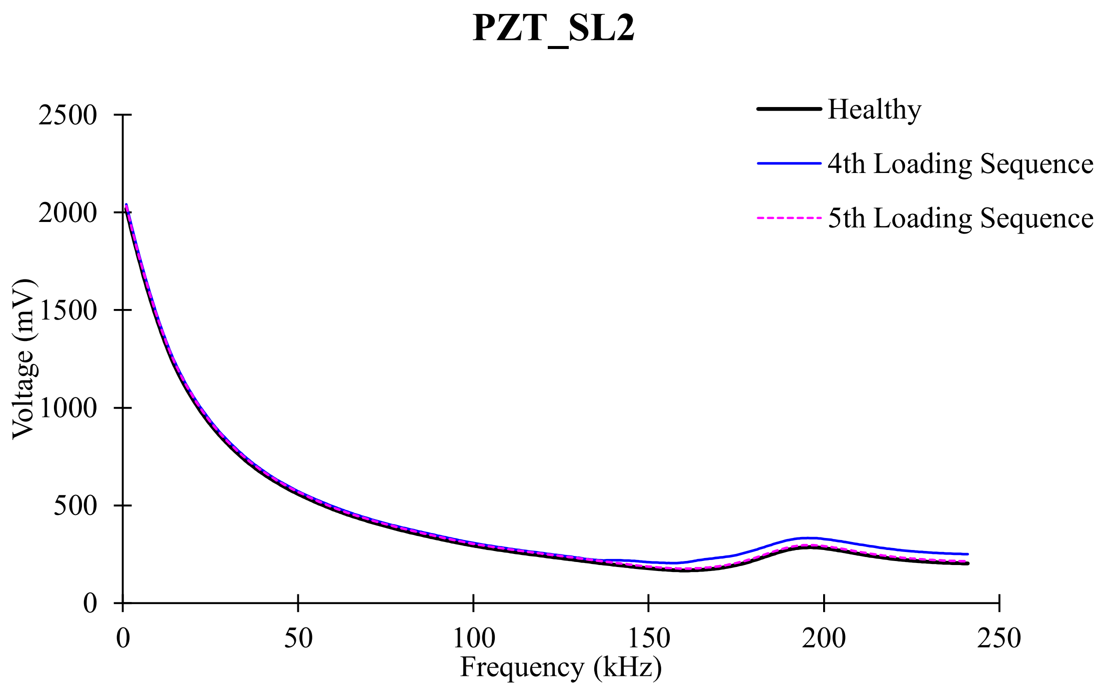

Figure 3.4.3b Voltage frequency responses of the PZT sensor SL2.

Table 3.4.3 Voltage output response of PZT SL3 versus Frequency

SL3	Healthy	EQ0.8g	EQ1.1g
Frequency (kHz)	Voltage (mV)	Voltage (mV)	Voltage (mV)
10	2356.07	2351.19	2350.22
11	2269.23	2264.36	2263.16
12	2185.19	2180.29	2178.90
13	2103.93	2098.95	2097.44
14	2025.46	2020.36	2018.79
15	1949.78	1944.52	1942.93
16	1876.88	1871.42	1869.88
17	1806.78	1801.06	1799.63
18	1739.47	1733.45	1732.18
19	1674.95	1668.58	1667.53
20	1613.21	1606.46	1605.68
21	1554.27	1547.08	1546.63
22	1498.11	1490.45	1490.39
23	1444.74	1436.56	1436.95
24	1396.96	1387.74	1389.04
25	1351.45	1341.91	1343.27
26	1308.55	1297.83	1300.04
27	1267.86	1256.68	1259.77
28	1230.39	1217.98	1221.71
29	1194.09	1180.90	1184.44
30	1158.89	1146.07	1150.57
31	1126.07	1112.80	1118.21
32	1094.58	1081.82	1087.64
33	1064.46	1052.25	1058.42
34	1036.01	1023.40	1031.09
35	1009.19	996.71	1005.37
36	983.37	971.14	980.06
37	958.99	946.26	955.49
38	935.11	923.29	932.74
39	912.01	900.96	910.17
40	889.87	880.11	888.71
41	869.63	859.86	868.83
42	849.74	839.51	848.77
43	829.47	820.18	830.54
44	810.87	801.71	812.72
45	793.52	784.05	794.14
46	776.16	767.08	776.04
47	759.34	750.55	758.54
48	743.65	734.34	741.58
49	728.26	719.56	725.66
50	713.47	703.84	710.27
51	698.27	689.67	694.47

SL3	Healthy	EQ0.8g	EQ1.1g
Frequency (kHz)	Voltage (mV)	Voltage (mV)	Voltage (mV)
52	684.09	674.88	679.36
53	670.87	661.42	665.55
54	658.31	648.34	651.74
55	644.40	634.83	638.12
56	632.10	622.43	626.21
57	620.13	609.77	613.12
58	609.27	597.78	601.12
59	598.70	585.52	589.94
60	588.43	574.04	579.58
61	577.97	564.00	569.97
62	567.97	552.57	559.80
63	557.69	542.81	550.29
64	547.62	533.59	540.89
65	537.80	524.02	532.80
66	529.46	515.02	524.18
67	520.17	506.19	515.28
68	511.25	497.27	506.80
69	503.28	489.34	499.19
70	496.37	482.04	491.08
71	489.39	474.86	482.88
72	480.87	467.79	475.00
73	473.02	461.40	467.60
74	465.55	454.53	460.73
75	458.07	447.79	453.84
76	450.79	440.20	446.01
77	443.25	433.34	437.99
78	435.76	426.00	431.30
79	429.32	419.73	425.00
80	422.51	412.68	418.23
81	415.68	406.02	410.62
82	410.04	399.03	403.59
83	403.52	392.86	397.38
84	397.13	386.53	391.93
85	390.76	380.14	384.94
86	383.40	375.13	379.55
87	376.96	369.58	373.80
88	370.71	363.51	367.25
89	364.05	358.81	360.64
90	357.79	353.39	354.29
91	351.36	347.69	348.30
92	345.18	341.93	341.94
93	339.32	336.27	335.82
94	334.39	330.68	330.65

SL3	Healthy	EQ0.8g	EQ1.1g
Frequency (kHz)	Voltage (mV)	Voltage (mV)	Voltage (mV)
95	329.20	325.97	325.87
96	324.42	321.04	320.39
97	318.72	315.82	315.35
98	312.56	310.21	309.90
99	307.75	305.58	304.83
100	302.65	300.16	299.44
101	297.76	294.95	294.51
102	292.48	289.67	289.19
103	287.86	284.73	285.30
104	283.37	279.56	280.96
105	280.22	275.11	275.79
106	275.87	270.06	270.90
107	271.75	265.63	265.63
108	267.32	261.20	260.87
109	262.54	257.94	257.27
110	258.09	253.66	252.91
111	253.90	249.45	248.66
112	248.90	245.92	245.82
113	245.44	241.79	242.03
114	241.89	237.47	238.10
115	237.30	233.28	234.58
116	233.14	229.44	231.23
117	228.97	225.27	227.49
118	224.82	221.10	224.49
119	221.93	217.24	220.55
120	217.83	213.62	216.91
121	214.05	209.80	213.68
122	209.97	205.88	209.93
123	206.09	202.46	206.59
124	202.38	198.72	202.98
125	199.52	195.41	198.77
126	196.37	191.20	194.65
127	193.43	187.62	191.39
128	190.31	183.91	187.79
129	187.69	180.52	184.23
130	184.44	177.23	179.56
131	181.55	173.78	175.28
132	177.92	170.33	171.83
133	174.50	166.96	168.02
134	171.60	164.05	164.90
135	168.56	160.92	162.20
136	165.45	157.82	158.65
137	162.32	154.41	156.22

SL3	Healthy	EQ0.8g	EQ1.1g
Frequency (kHz)	Voltage (mV)	Voltage (mV)	Voltage (mV)
138	159.39	151.96	153.41
139	156.62	148.92	150.63
140	153.66	145.40	147.56
141	149.35	142.18	144.73
142	145.75	139.51	141.75
143	142.46	136.23	138.23
144	139.78	133.09	135.75
145	137.34	130.25	132.72
146	134.72	127.29	130.36
147	132.19	124.44	128.13
148	130.26	122.23	125.67
149	128.53	119.97	123.12
150	126.93	117.86	120.93
151	125.33	115.94	118.86
152	123.85	114.63	117.42
153	122.26	113.52	116.35
154	120.72	112.67	114.85
155	119.84	112.40	113.45
156	119.11	111.46	112.31
157	119.07	111.07	111.90
158	119.02	111.42	111.83
159	119.22	111.87	111.79
160	119.62	112.90	112.28
161	119.58	113.82	112.63
162	119.81	115.24	113.13
163	120.71	116.33	114.84
164	121.38	117.66	116.19
165	122.00	118.57	117.62
166	123.14	119.72	119.40
167	124.48	121.42	121.32
168	126.61	123.37	123.33
169	129.25	125.29	125.66
170	132.03	127.91	128.93
171	134.96	130.62	131.41
172	138.24	133.49	134.51
173	141.19	136.40	137.87
174	144.96	139.93	141.39
175	148.28	143.45	145.15
176	152.10	147.36	149.36
177	156.06	151.35	153.67
178	160.13	155.63	157.69
179	164.01	159.55	161.56
180	167.94	163.75	165.15

SL3	Healthy	EQ0.8g	EQ1.1g
Frequency (kHz)	Voltage (mV)	Voltage (mV)	Voltage (mV)
181	172.16	167.65	169.01
182	175.93	171.01	172.70
183	179.43	174.81	176.44
184	182.63	178.06	179.72
185	185.39	181.23	182.65
186	187.59	184.01	185.17
187	189.40	186.28	187.07
188	191.20	188.12	188.89
189	192.54	189.39	190.31
190	192.94	190.22	191.22
191	193.28	190.53	191.42
192	193.45	190.55	191.47
193	193.25	190.37	191.17
194	192.57	189.80	190.51
195	191.64	188.91	189.68
196	190.41	187.63	188.12
197	188.83	186.18	186.38
198	186.79	184.45	184.76
199	184.99	182.60	183.02
200	183.15	180.73	181.04
201	181.04	178.63	178.98
202	178.73	176.67	176.95
203	176.39	174.44	174.75
204	174.03	172.01	172.39
205	171.56	169.40	169.80
206	169.27	166.85	167.24
207	167.02	164.33	164.53
208	164.70	161.93	162.11
209	162.45	159.69	159.93
210	160.40	157.65	157.81
211	158.16	155.72	155.71
212	156.23	153.78	153.73
213	154.49	151.97	151.89
214	152.92	150.33	150.25
215	151.44	148.89	148.85
216	150.18	147.81	147.47
217	149.13	146.69	146.29
218	148.25	145.75	145.44
219	147.63	145.09	144.75
220	146.94	144.57	143.93
221	146.44	144.11	143.37
222	145.85	143.75	142.98
223	145.40	143.60	142.75

SL3	Healthy	EQ0.8g	EQ1.1g
Frequency (kHz)	Voltage (mV)	Voltage (mV)	Voltage (mV)
224	145.03	143.46	142.57
225	144.93	143.26	142.42
226	144.60	143.12	142.12
227	144.23	142.91	141.88
228	143.71	142.62	141.62
229	143.13	142.05	141.24
230	142.62	141.41	140.68
231	141.90	140.79	139.92
232	141.18	140.10	139.14
233	140.15	139.33	138.18
234	139.15	138.37	137.24
235	137.95	137.27	136.28
236	136.64	136.04	135.07
237	135.15	134.66	133.77
238	133.87	133.41	132.56
239	132.54	132.10	131.27
240	131.14	130.72	129.93

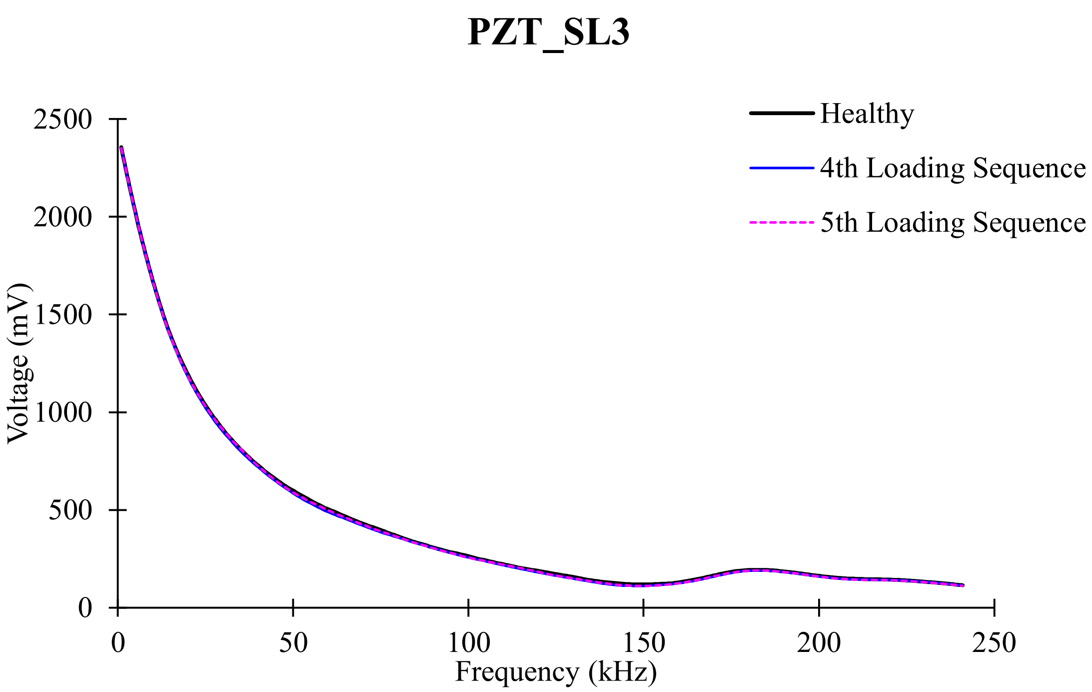

Figure 3.4.3c Voltage frequency responses of the PZT sensor SL3.

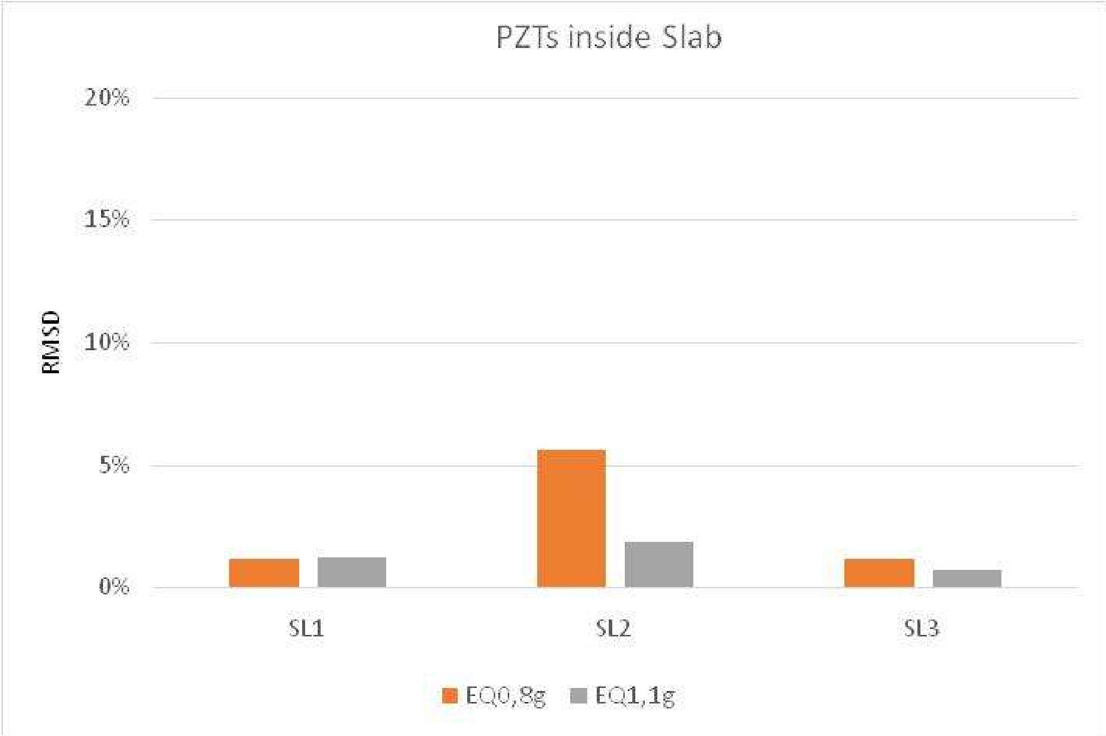

Figure 3.4.4 RMSD Damage Index Values of PZT sensors inside the slab for each PZT Location

Figure 3.4.5 RMSD Damage Index Values of PZT sensors inside the slab for performed tests EQ0,8g and EQ1,1g

Columns

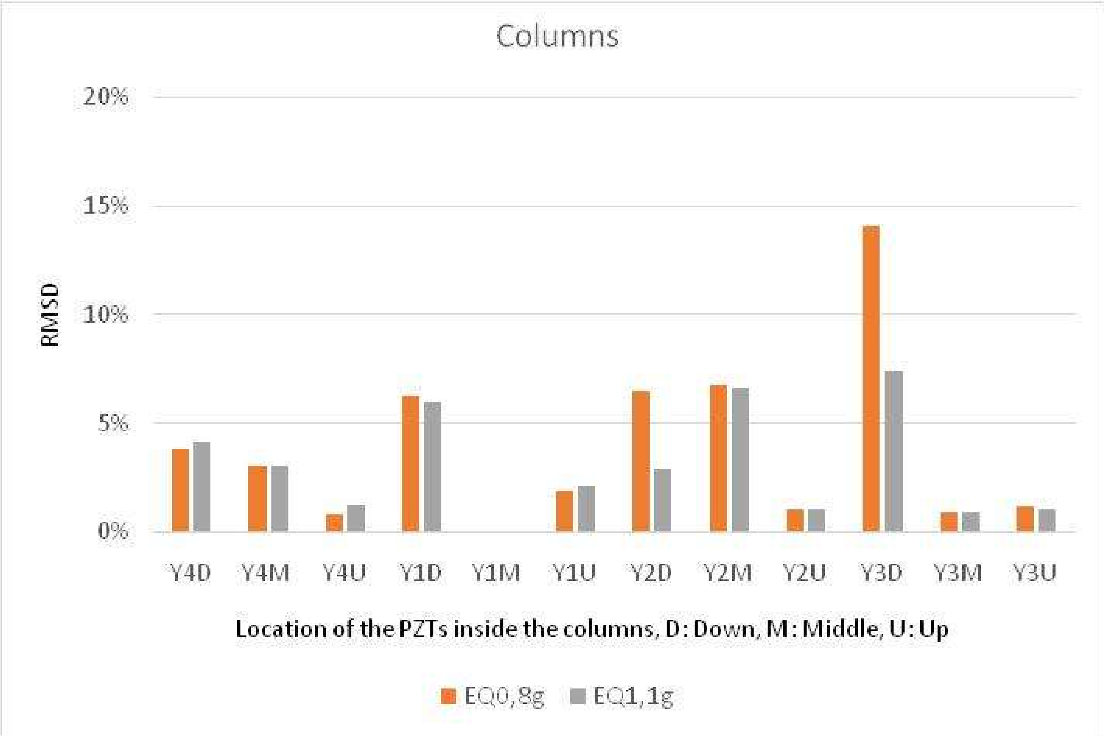

Figure 3.4.6 RMSD Damage Index Values of PZT sensors inside the columns

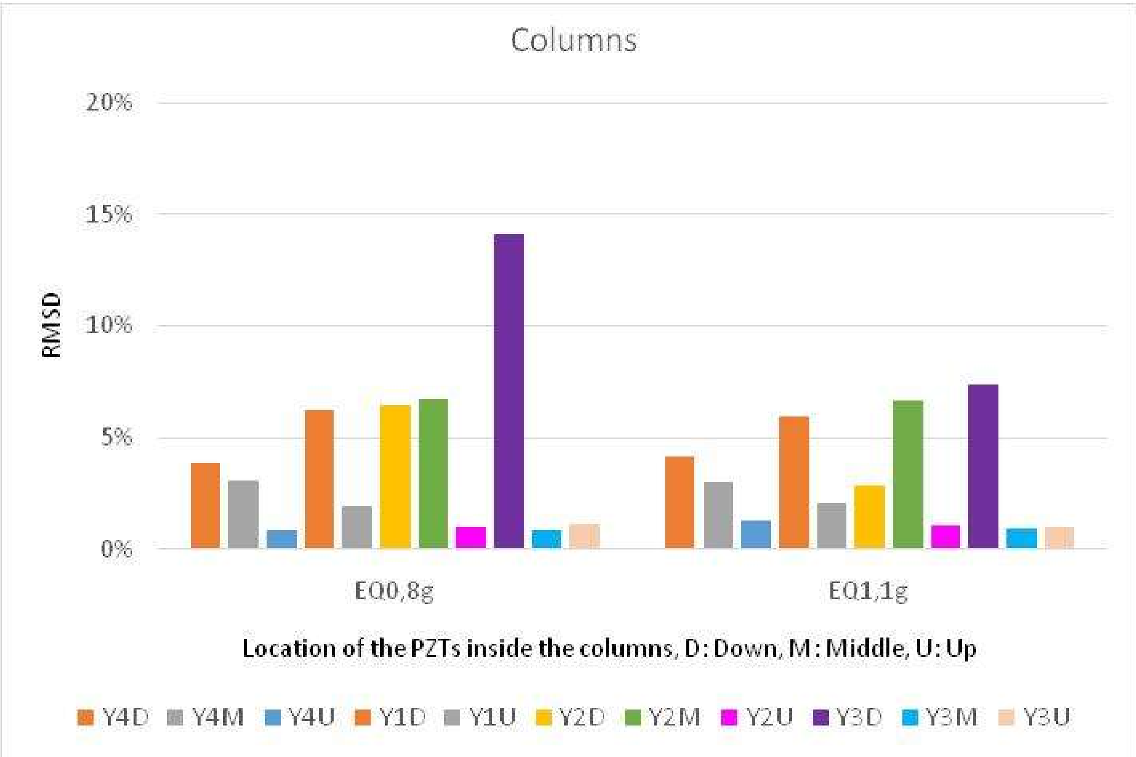

Figure 3.4.7 RMSD Damage Index Values of PZT sensors inside the columns

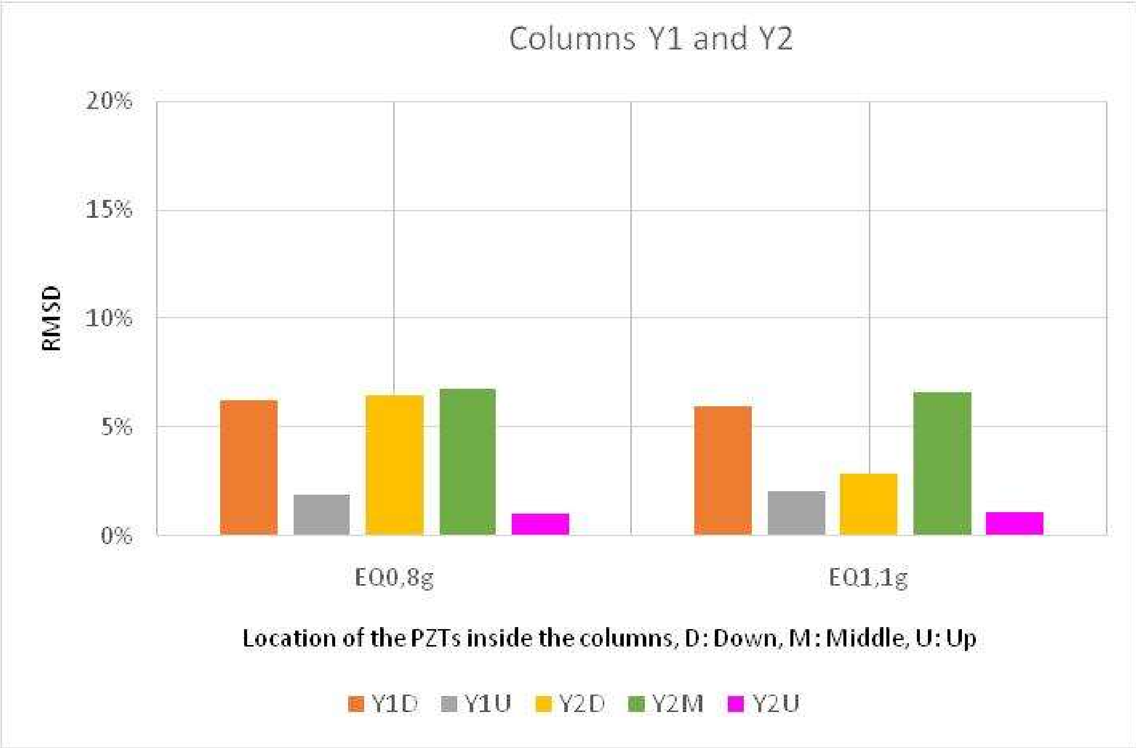

Figure 3.4.8 RMSD Damage Index Values of PZT sensors inside the columns 1 and 2

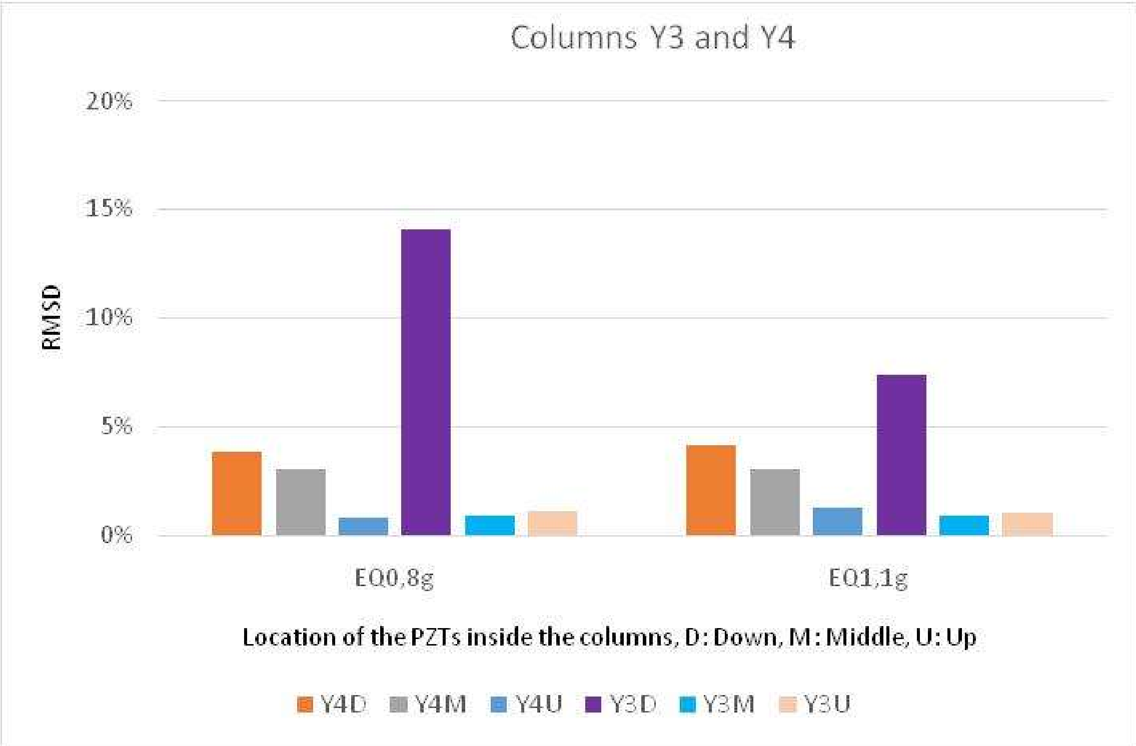

Figure 3.4.9 RMSD Damage Index Values of PZT sensors inside the columns 3 and 4

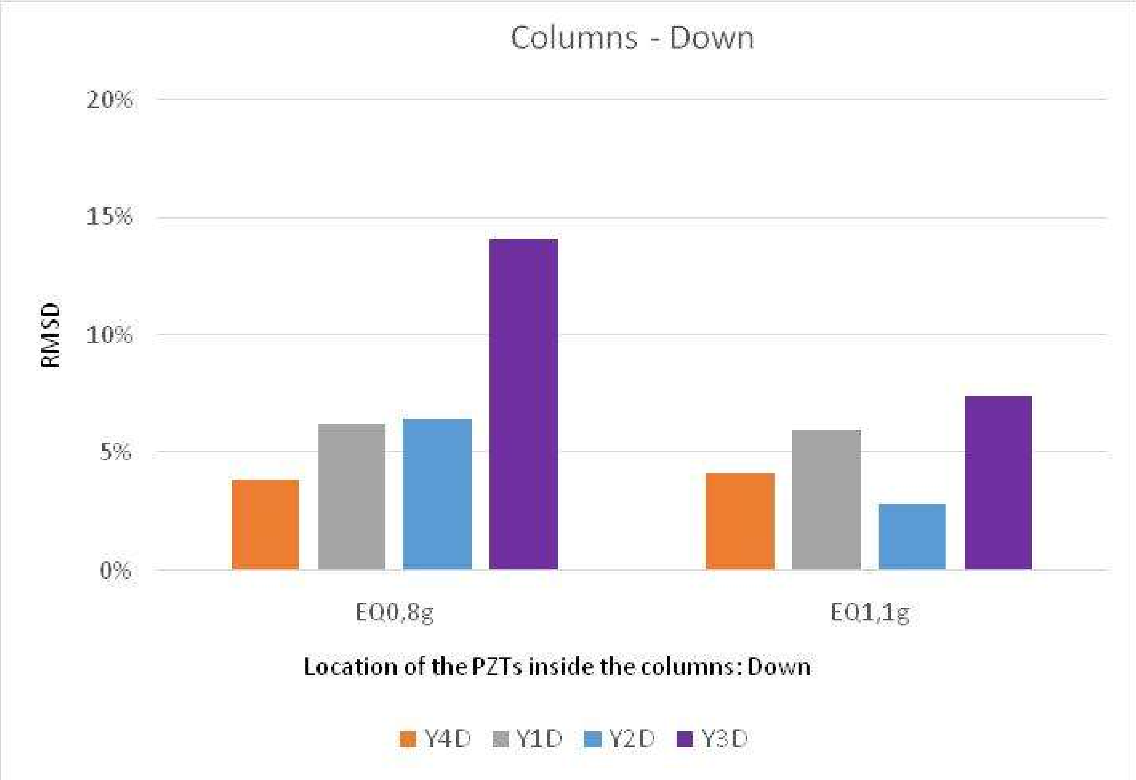

Figure 3.4.10 RMSD Damage Index Values of PZT sensors inside the columns: Down

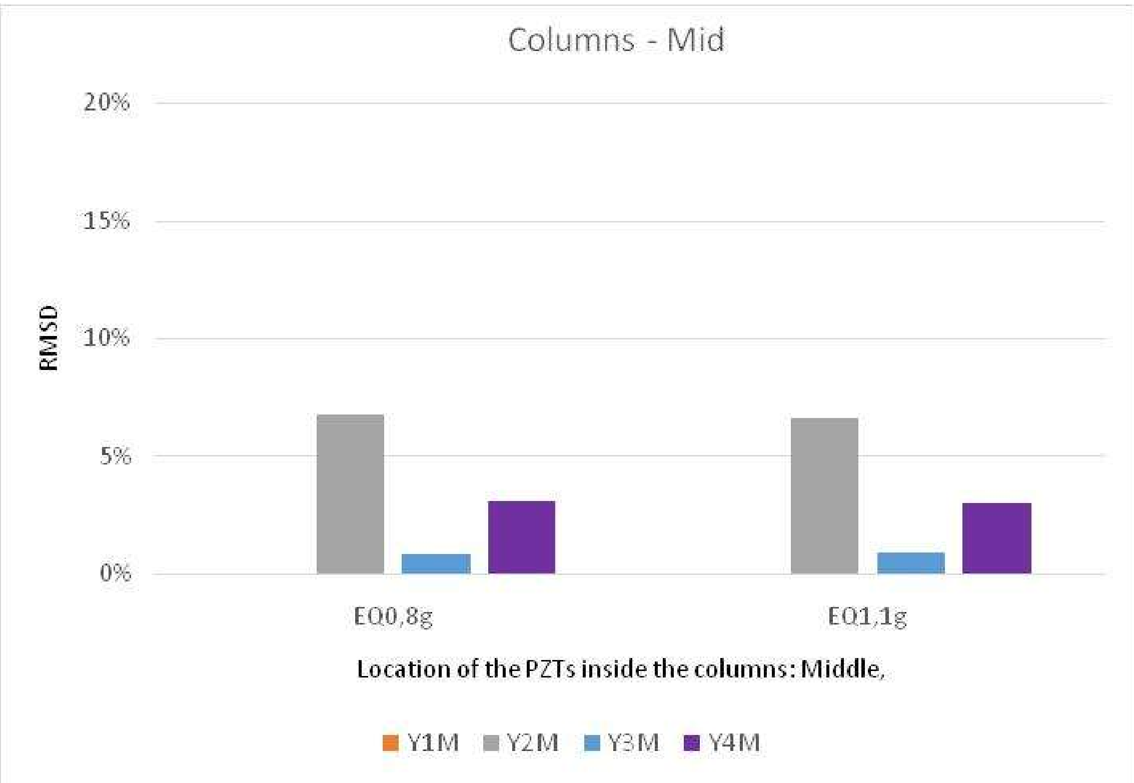

Figure 3.4.11 RMSD Damage Index Values of PZT sensors inside the columns: Middle

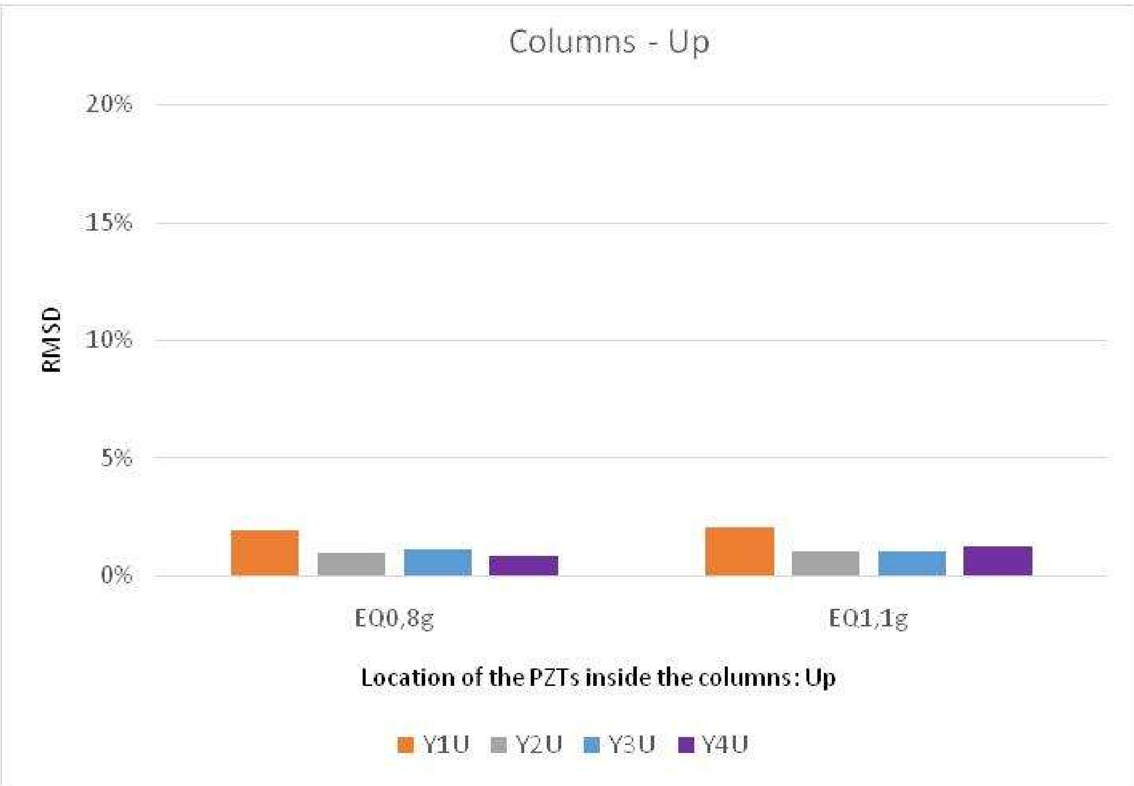

Figure 3.4.12 RMSD Damage Index Values of PZT sensors inside the columns: Up

Beams

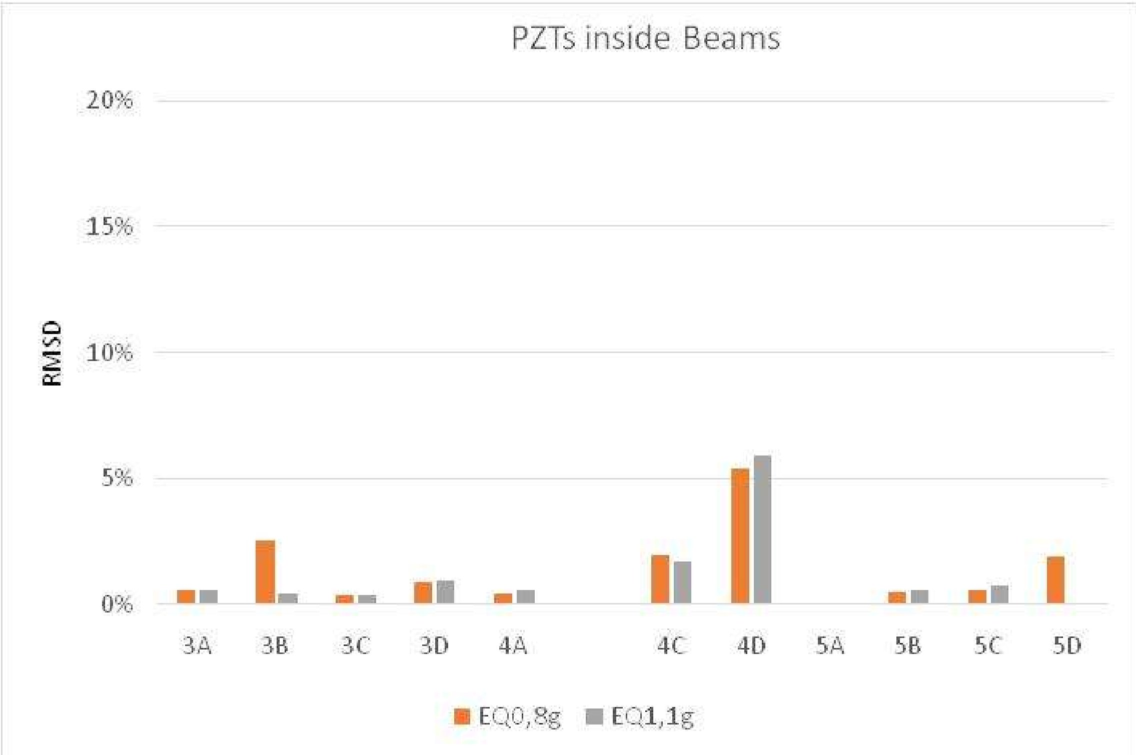

Figure 3.4.13 RMSD Damage Index Values of PZT sensors inside all beams

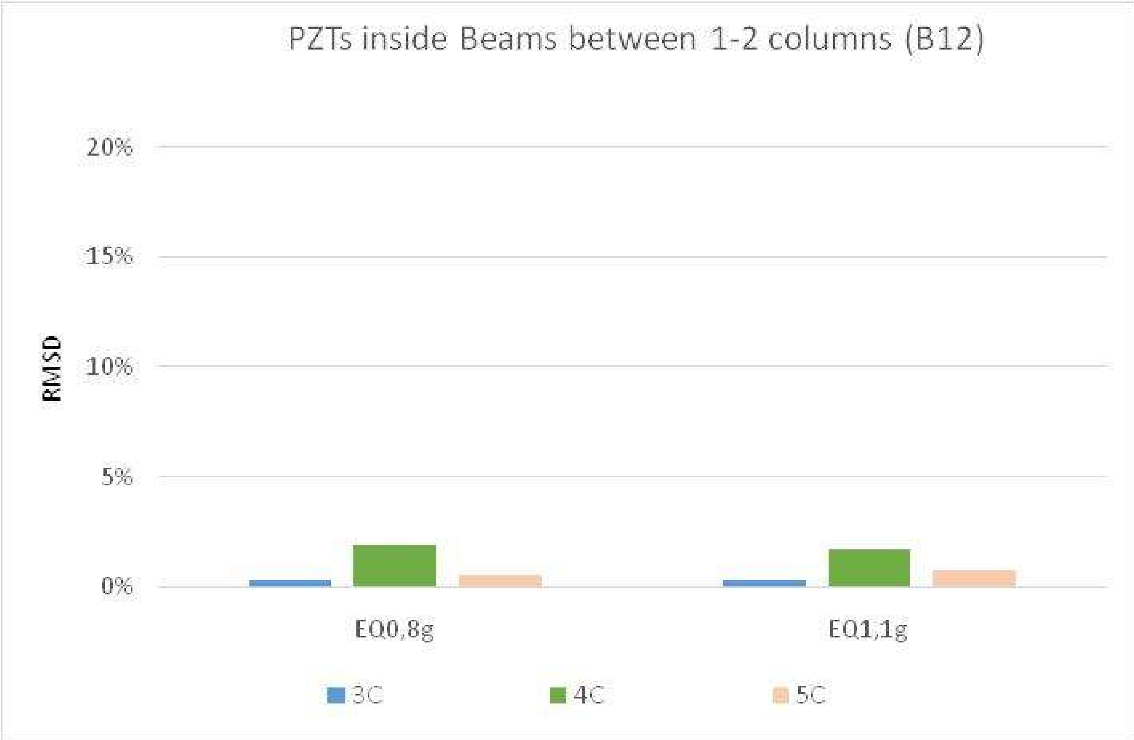

Figure 3.4.14 RMSD Damage Index Values of PZT sensors inside beam B12

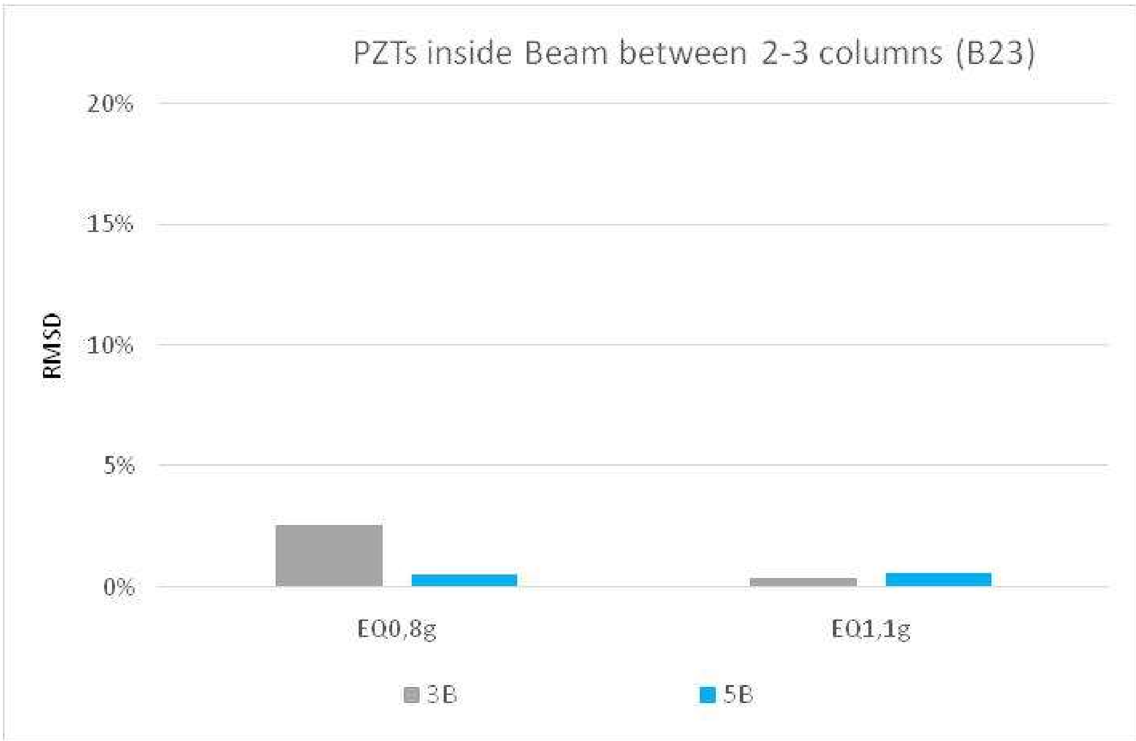

Figure 3.4.15 RMSD Damage Index Values of PZT sensors inside beam B23

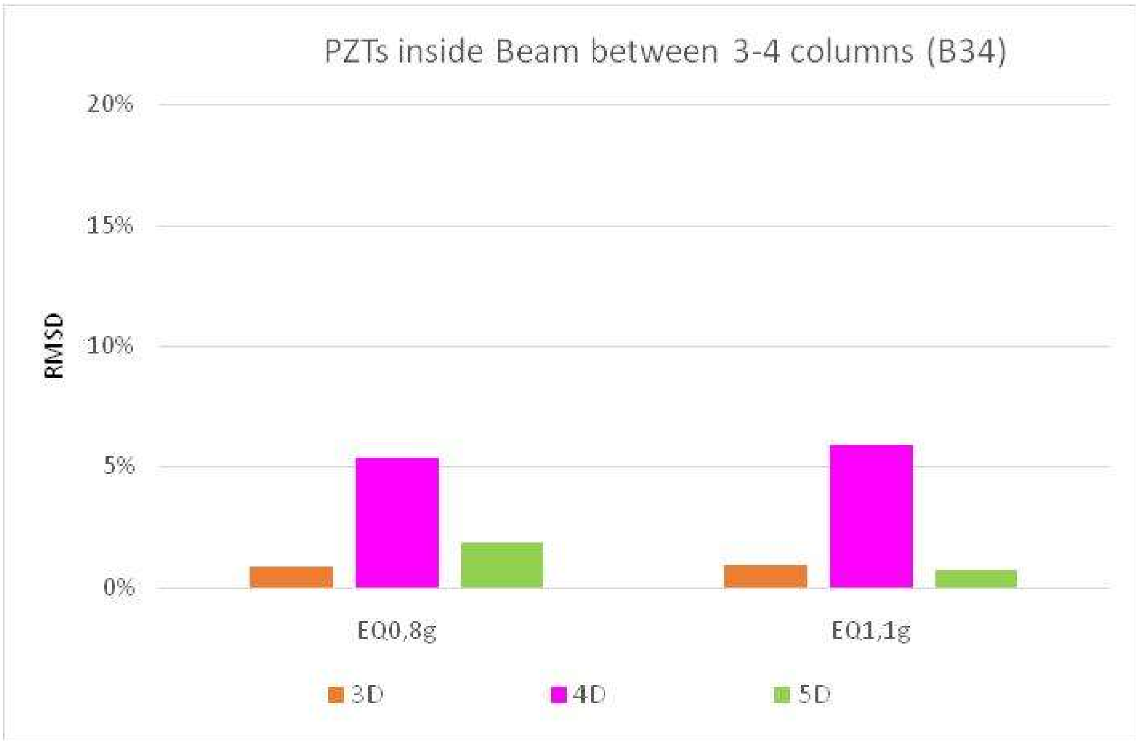

Figure 3.4.16 RMSD Damage Index Values of PZT sensors inside beam B34

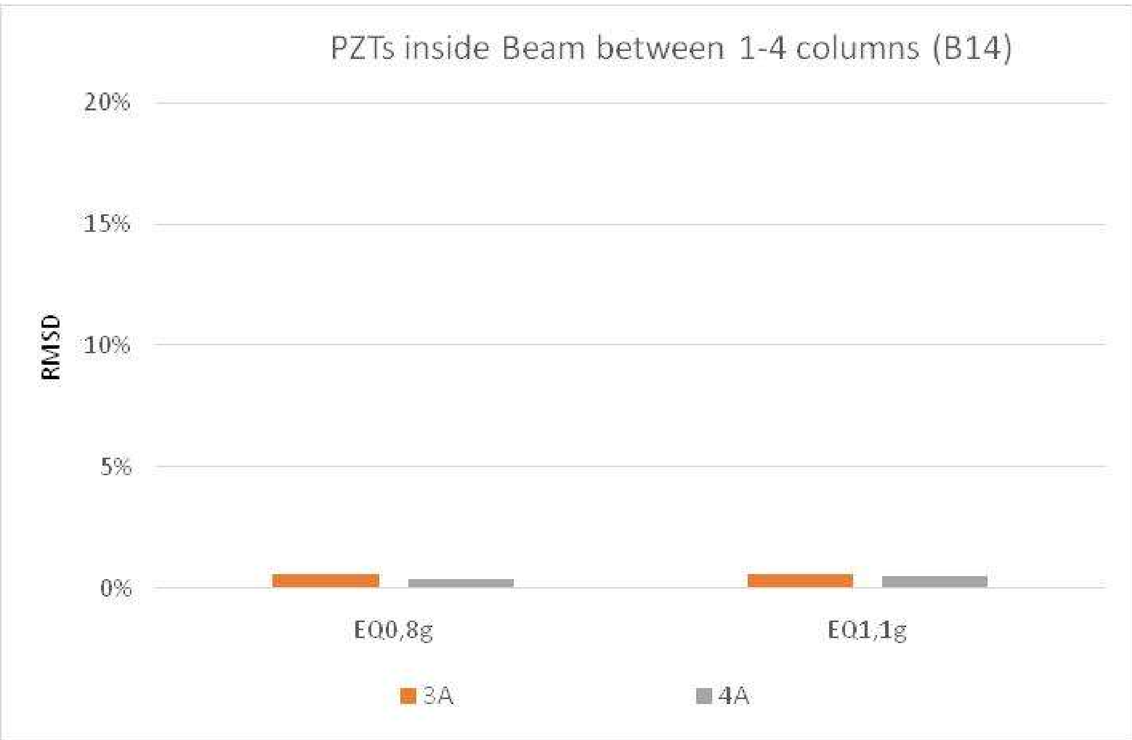

Figure 3.4.17 RMSD Damage Index Values of PZT sensors inside beam B14

Joints

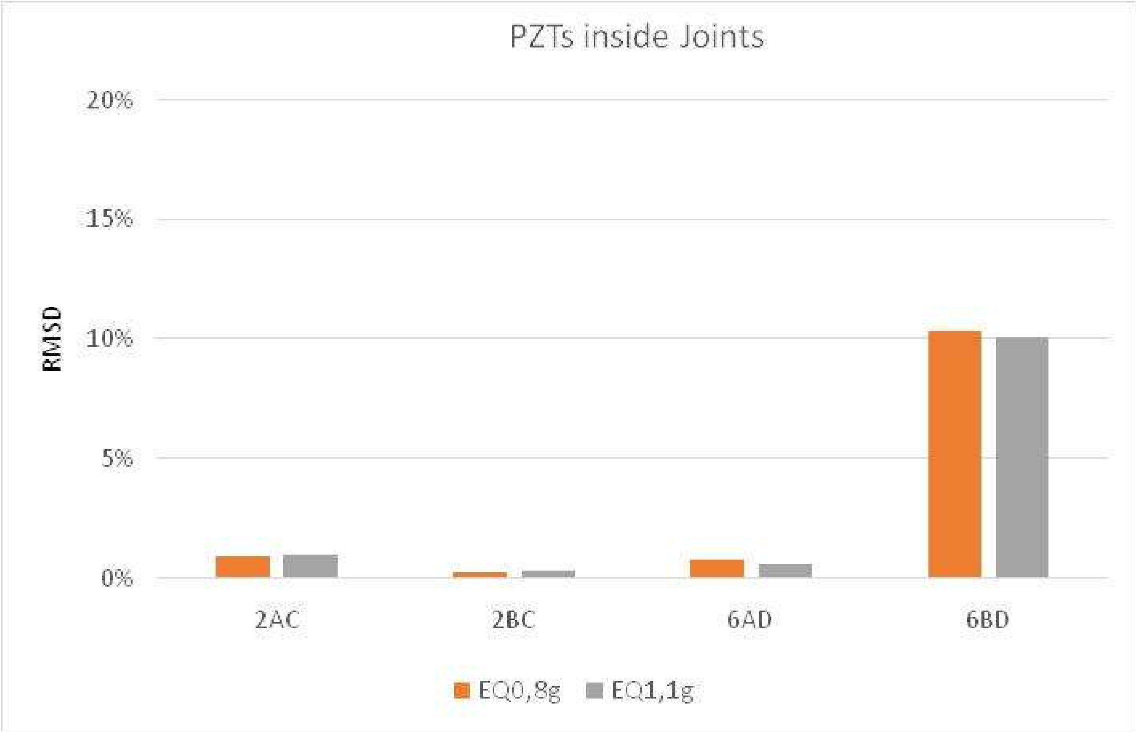

Figure 3.4.18 RMSD Damage Index Values of PZT sensors inside joints for every joint

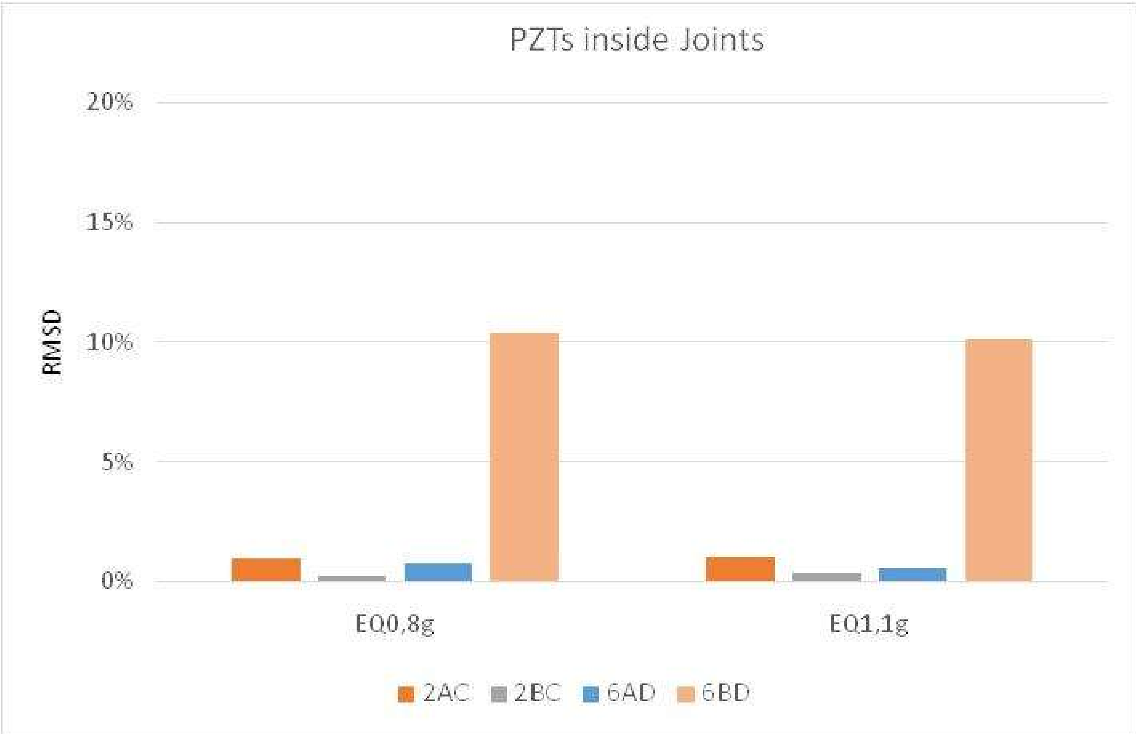

Figure 3.4.19 RMSD Damage Index Values of PZT sensors inside joints for performed tests EQ0,8g and EQ1,1g

Cantilevers

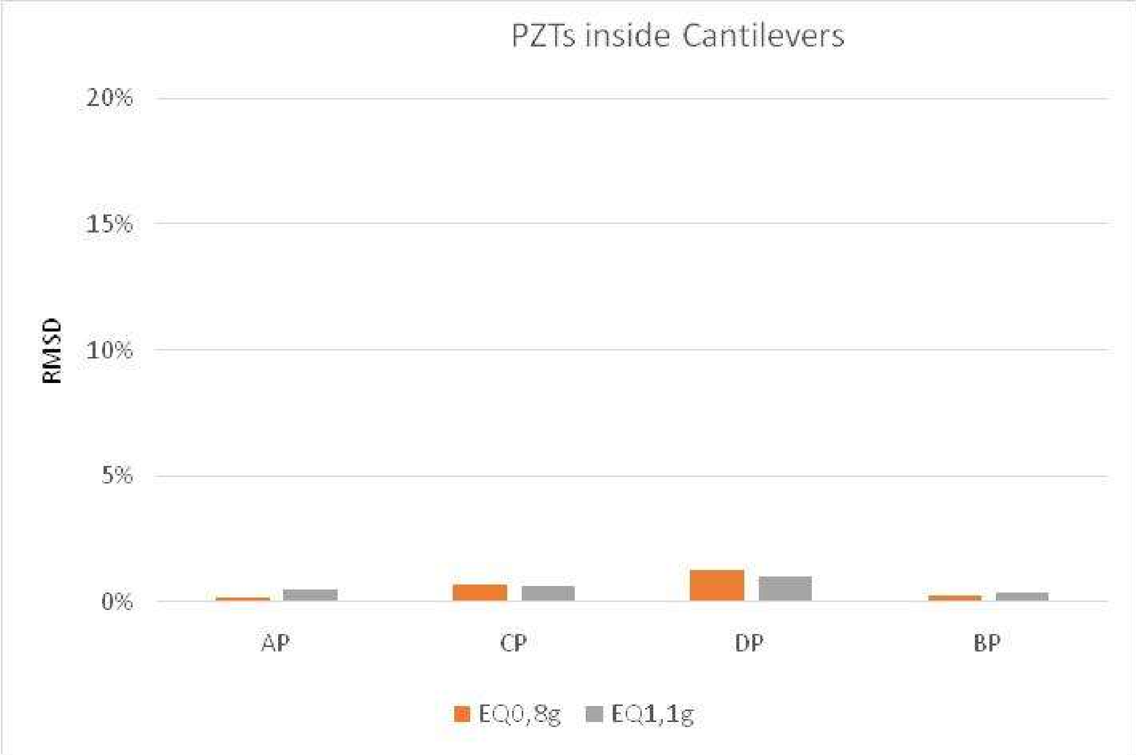

Figure 3.4.20 RMSD Damage Index Values of PZT sensors inside cantilevers for every cantilever

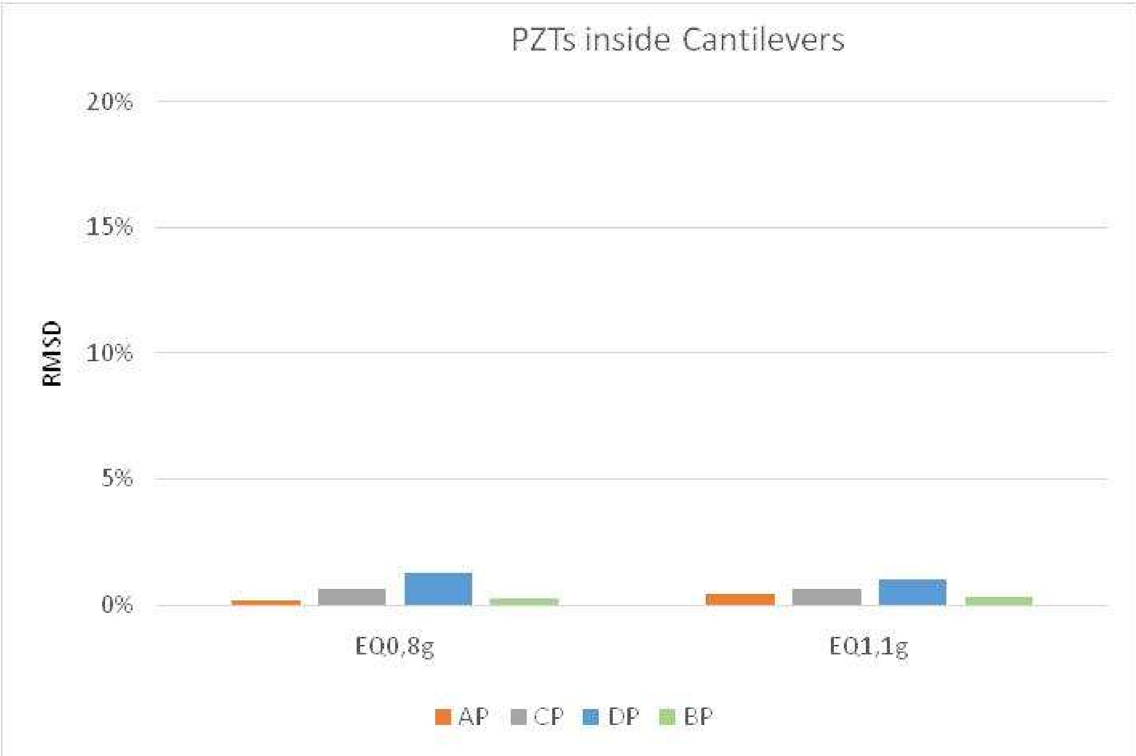

Figure 3.4.21 RMSD Damage Index Values of PZT sensors inside cantilevers for performed tests EQ0,8g and EQ1,1g

Infilled walls

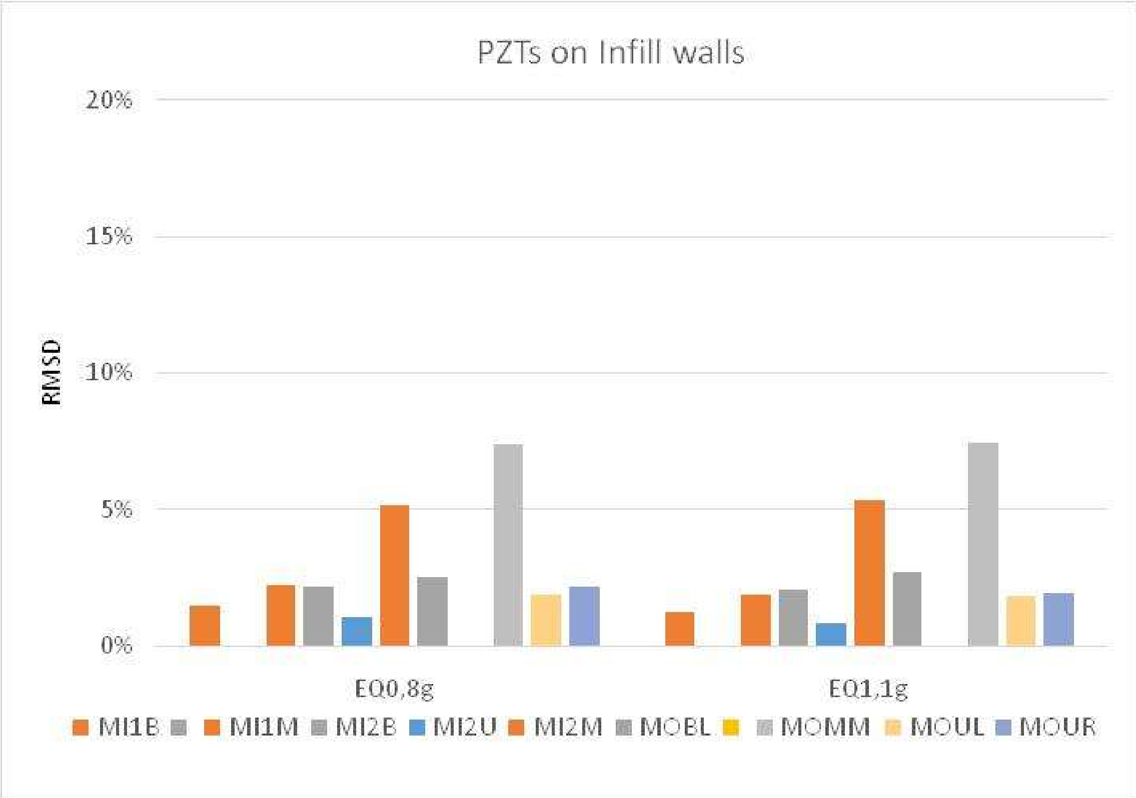

Figure 3.4.22 RMSD Damage Index Values of PZT sensors on all Infill walls

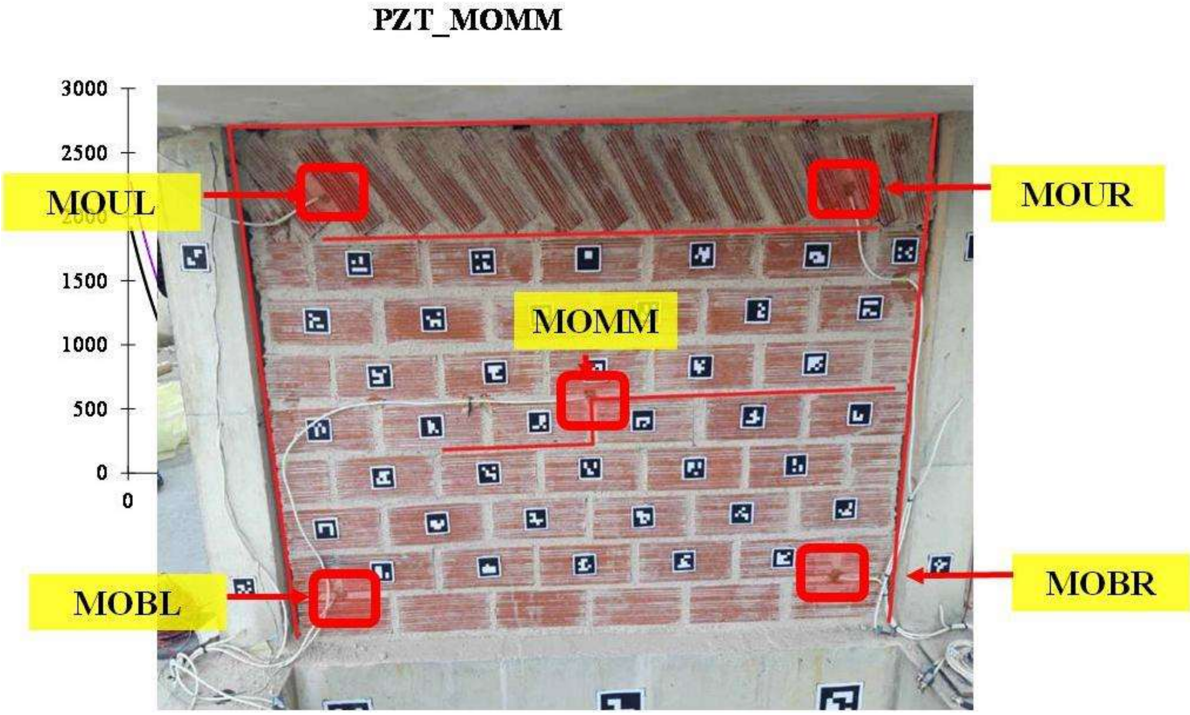

Figure 3.4.23 Observed damage after 1.1g test and location of PZT sensors on full Infill wall between columns 1-2

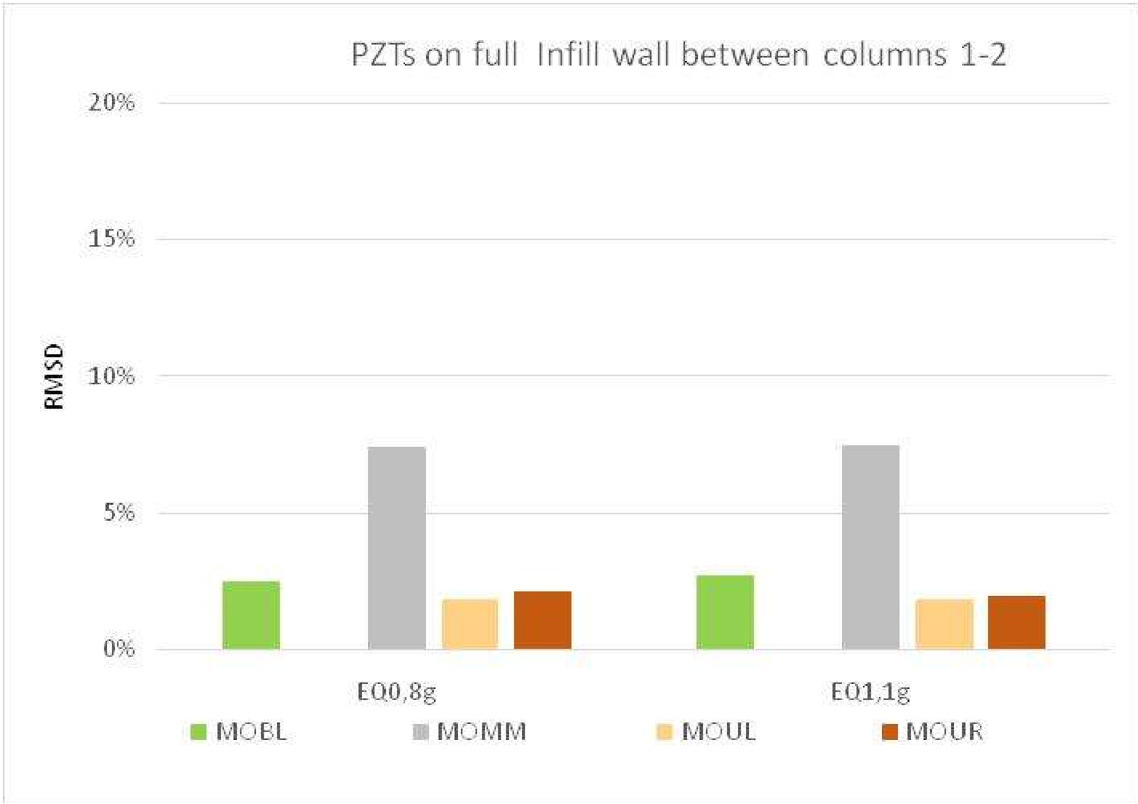

Figure 3.4.24 RMSD Damage Index Values of PZT sensors on full Infill wall between columns 1-2

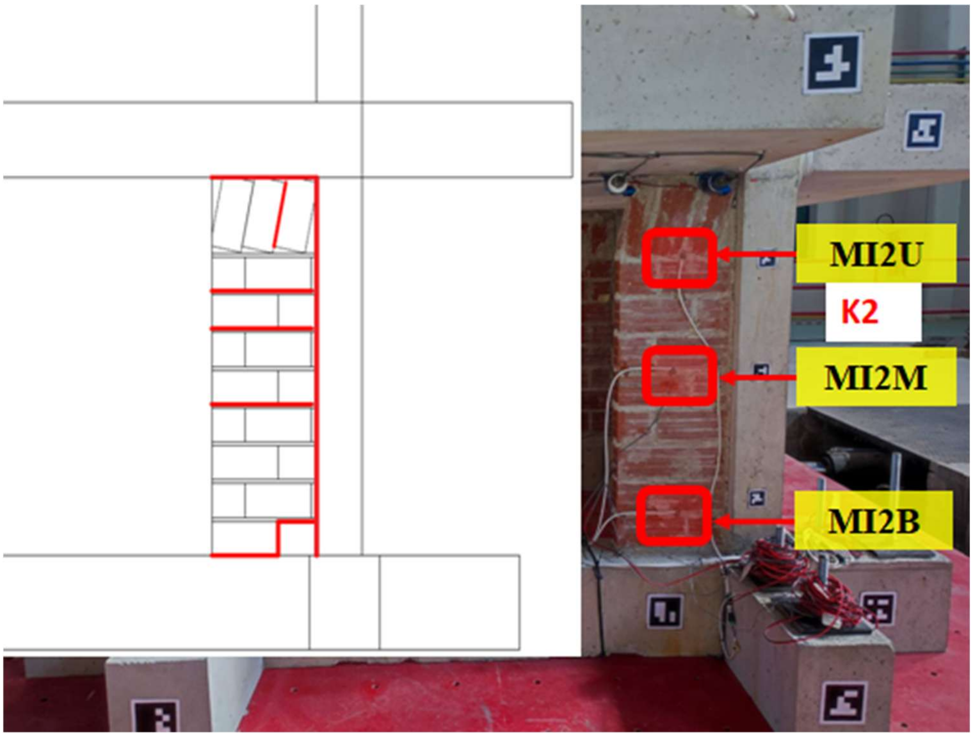

Figure 3.4.25 Observed damage after 1.1g test and location of PZT sensors on full Infill wall between columns 2-3

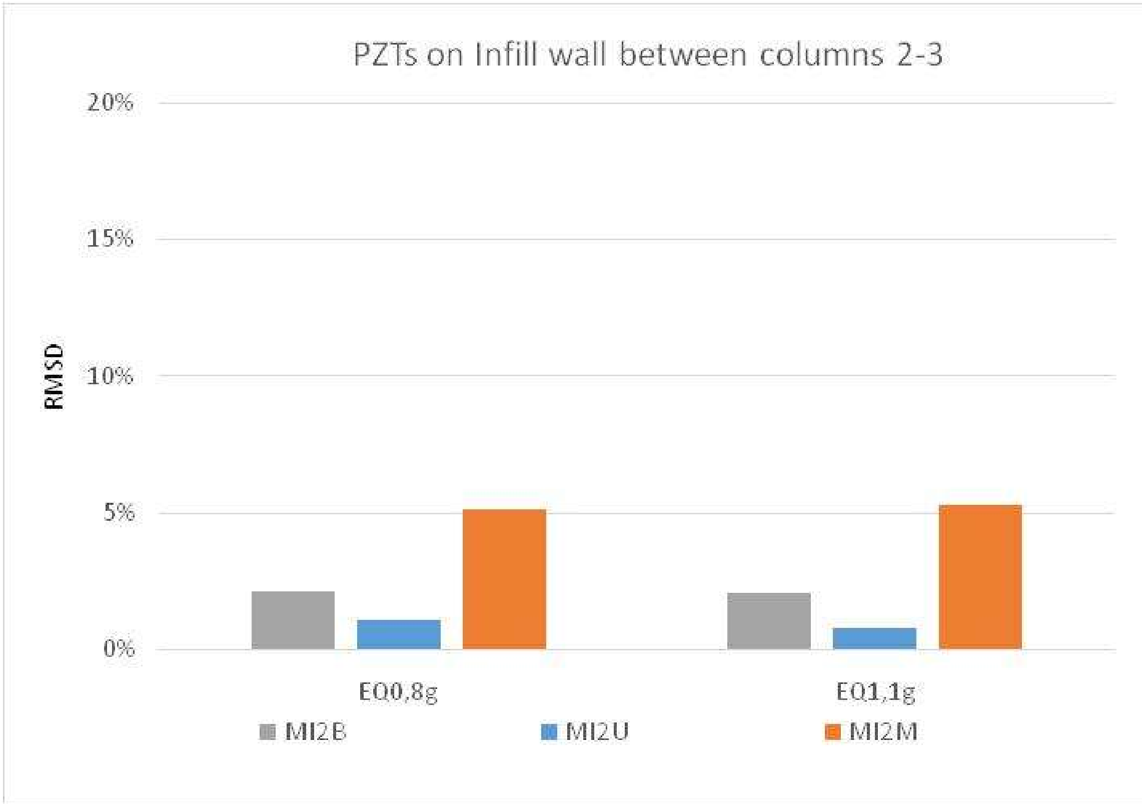

Figure 3.4.26 RMSD Damage Index Values of PZT sensors on Infill wall between columns 2-3

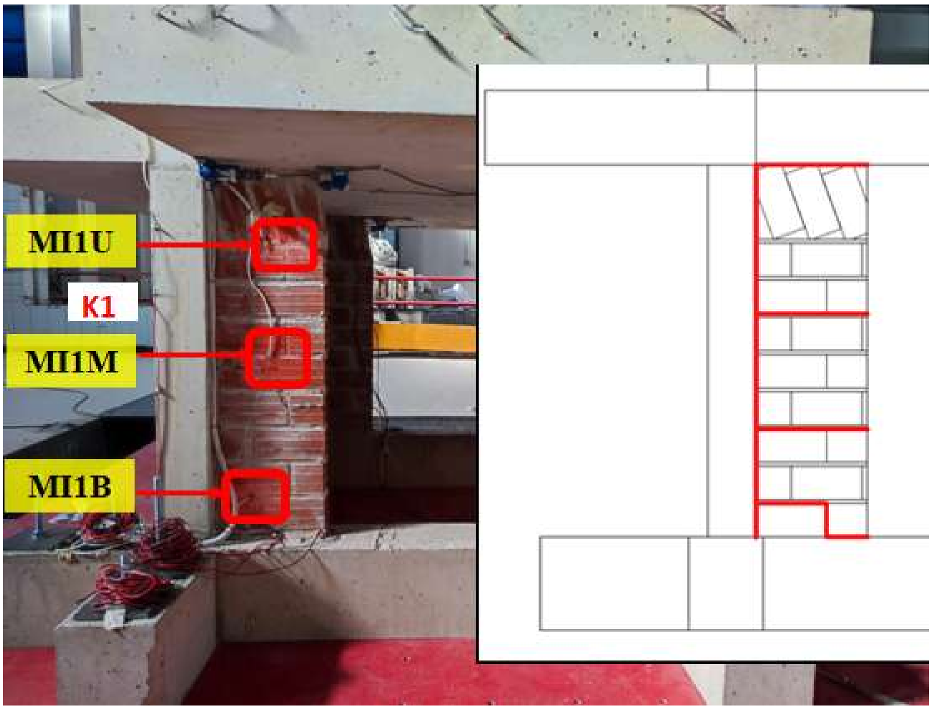

Figure 3.4.27 Observed damage after 1.1g test and location of PZT sensors on full Infill wall between columns 1-4

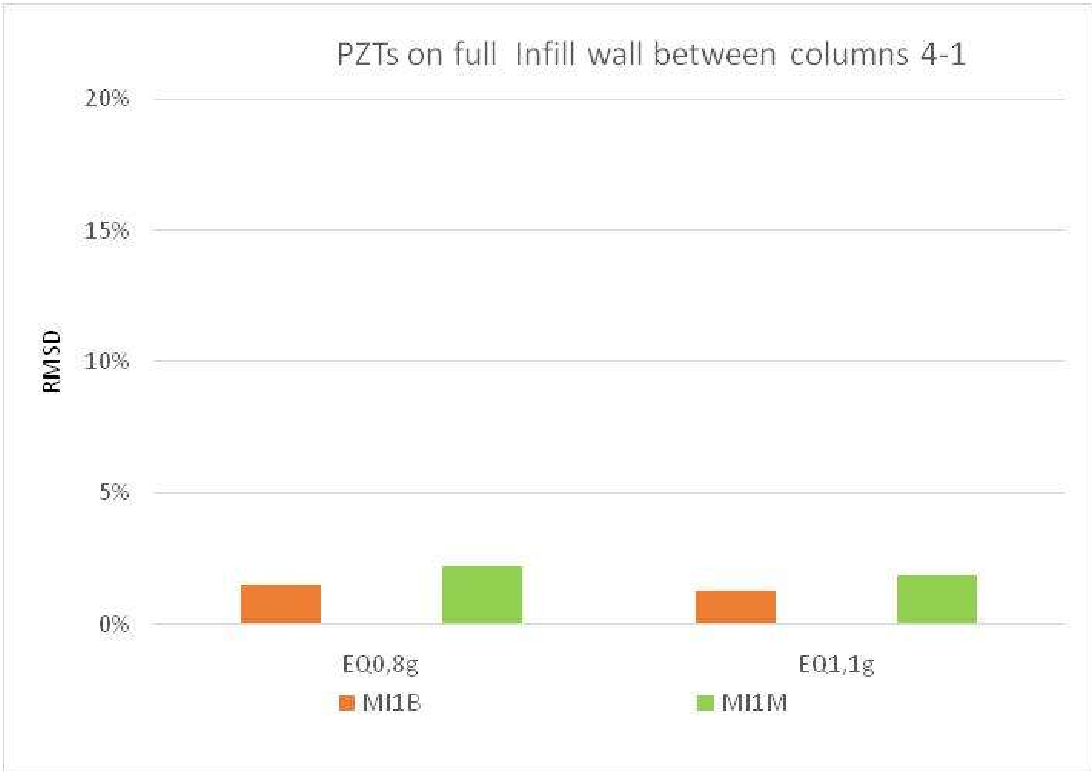

Figure 3.4.28 RMSD Damage Index Values of PZT sensors on Infill wall between columns 4-1

The assessment of the structural condition of the frame was conducted using the Root Mean Square Deviation (RMSD) values derived from the responses of the piezoelectric sensors (PZTs). Higher RMSD values suggest the presence of damage. It was observed that elevated RMSD values were not present in the PZTs situated in regions where no cracking was detected.

No significant values were observed in the RMSD indices for the PZT cases installed on the cantilevers and the slab, where no structural damage was detected. All columns show increased RMSD values at all areas (down, mid, up), indicating that damage has developed. The lower regions of all columns exhibited higher RMSD values compared to the upper areas.

PZT installed within Joint 6BD, situated on Column Y3, exhibits elevated RMSD values, attributable to accumulated damage within Column Y3. Elevated RMSD values were recorded at other beams, particularly those connected to Column Y3.

The PZTs installed on the infill walls recorded increased RMSD values, indicating debonding from the surrounding concrete frames. Notably, the PZT sensors installed in these infill walls' middle and upper areas displayed higher values. High RMSD values were observed across all PZT sensors in the full-infill wall. Specifically, a significantly elevated RMSD value was recorded in the central area, coinciding with a large horizontal crack where the PZT is installed.

These results support the effectiveness and reliability of the implemented instrumentation and the adopted EMI-based monitoring method for structural health assessment.

4 Conclusions

The report cites all critical results from the relative accelerations and displacement drifts of the structure during each test. Further, numerous strain gauge values and different positions of steel bars allow straight-foreword assessment of their axial strain level. Relative top to bottom accelerations reach a maximum of 1.59g, while maximum displacement drift reaches 11.37‰.

The detailed assessment of the as – built structure after the first phase of testing concludes that the infill walls suffer bed joint cracking and varying debonding from concrete columns and slab. The concrete columns suffer minor cracking around the construction joints. Longitudinal steel bars develop tensile axial strains lower than their yielding limit. The top slab shows no damage.

PZTs provide a solid framework for the assessment of health condition of the structure at different positions. The assessment utilizes the Root Mean Square Deviation (RMSD) values obtained from the piezoelectric sensors (PZTs) measurements. The assessment provides detailed correlation of the position and of the level of damage observed in situ and the measurements recorded by PZTs sensors. Histories of recorded accelerations on infill 3-4 as well as PZT measurements coincide with photographic validation and observations of cracking and debonding of brick infill walls. Finally, PZT measurements agree well with the observed minor cracks also in columns.

Therefore, the first phase of the seismic testing is completed successfully, based on the Serviceability Limit State (SLS) level damages of the as-built structure after the execution of 11 dynamic tests, including 5 levels of earthquake excitations.

References

Chalioris, C.E.; Karayannis, C.G.; Angeli, G.M.; Papadopoulos, N.A.; Favvata, M.J.; Providakis, C.P. Applications of Smart Piezoelectric Materials in a Wireless Admittance Monitoring System (WiAMS) to Structures-Tests in RC Elements. Case Stud. Constr. Mater. 2016, 5, 1-18, doi:10.1016/j.cscm.2016.03.003.

Chalioris, C.E.; Papadopoulos, N.A.; Angeli, G.M.; Karayannis, C.G.; Liolios, A.A.; Providakis, C.P. Damage Evaluation in Shear-Critical Reinforced Concrete Beam Using Piezoelectric Transducers as Smart Aggregates. Open Eng. 2015, 5, 373-384, doi:10.1515/eng-2015-0046.

Chalioris, C.E.; Voutetaki, M.E.; Liolios, A.A. Structural health monitoring of seismically vulnerable RC frames under lateral cyclic loading. Earthq. Struct. 2020, 19, 29-44.

Naoum, M.C.; Papadopoulos, N.A.; Sapidis, G.M.; Voutetaki, M.E. Efficacy of PZT Sensors Network Different Configurations in Damage Detection of Fiber-Reinforced Concrete Prisms under Repeated Loading. Sensors 2024, 24, 5660. https://doi.org/10.3390/s24175660 .

Naoum, M.C.; Papadopoulos, N.A.; Voutetaki, M.E.; Chalioris, C.E. Structural Health Monitoring of Fiber-Reinforced Concrete Prisms with Polyolefin Macro-Fibers Using a Piezoelectric Materials Network under Various Load-Induced Stress. Buildings 2023, 13, 2465. https://doi.org/10.3390/buildings13102465.

Rousakis T, Ilki A, Kwiecien A, Viskovic A, Gams M, Triller P, Ghiassi B, Benedetti A, Rakicevic Z,Colla C, Halici OF, Zając B, Hojdys Ł, Krajewski P, Rizzo F, Vanian V, Sapalidis A, Papadouli E, Bogdanovic A. Deformable Polyurethane Joints and Fibre Grids for Resilient Seismic Performance of Reinforced Concrete Frames with Orthoblock Brick Infills. Polymers 2020; 12(12). DOI: https://doi.org/10.3390/polym12122869.Thomoglou, A.K.; Falara, M.G.; Gkountakou, F.I.; Elenas, A.; Chalioris, C.E. Smart Cementitious Sensors with Nano-, Micro-, and Hybrid-Modified Reinforcement: Mechanical and Electrical Properties. Sensors 2023, 23, 2405. https://doi.org/10.3390/s23052405.

Rousakis, Theodoros, Vanian Vachan, Fanaradelli Theodora, and Anagnostou Evgenia. 3D FEA of Infilled RC Framed Structures Protected by Seismic Joints and FRP Jackets. Applied Sciences,2021, 11, no. 14: 6403. https://doi.org/10.3390/app11146403

Łukasz Hojdys, Piotr Krajewski, Arkadiusz Kwiecien, Theodoros Rousakis, Vachan Vanian, Marcin Tekieli, Alberto Viskovic, Alper Ilki, Matija Gams, Zoran Rakicevic, Bogusław Zajac, and Aleksandra Bogdanovic (2023). Quick Repair of Damaged Infill Walls with Externally Bonded FRPU Composites: Shake Table Tests, Journal of Composites for Construction ASCE, Volume 27, Issue 1 - February 2023. doi: 10.1061/(ASCE)CC.1943-5614.0001268

Sam-Daliri, O.; Faller, L.M.; Farahani M.; Roshanghias, A.; Araee, A.; Baniassadi, M.; Oberlercher, H.; Zangl, H., Impedance analysis for condition monitoring of single lap CNT-epoxy adhesive joint. International Journal of Adhesion and Adhesives, 88, 59-65, doi:10.1016/j.ijadhadh.2018.11.003.

Sam-Daliri, O.; Faller, L.M.; Farahani M.; Zangl, H., Structural health monitoring of adhesive joints under pure mode I loading using the electrical impedance measurement. Engineering Fracture Mechanics, 245, 107585, doi:10.1016/j.engfracmech.2021.107585.

Thomoglou, A.K.; Voutetaki, M.E.; Fantidis, J.G.; Chalioris, C.E. Novel Natural Bee Brick with a Low Energy Footprint for "Green" Masonry Walls: Mechanical Properties. Eng. Proc. 2024, 60, 9. https://doi.org/10.3390/engproc2024060009.

Voutetaki, M.E.; Papadopoulos, N.A.; Angeli, G.M.; Providakis, C.P. Investigation of a New Experimental Method for Damage Assessment of RC Beams Failing in Shear Using Piezoelectric Transducers. Eng. Struct. 2016, 114, 226-240, doi:10.1016/j.engstruct.2016.02.014

Voutetaki, M.E.; Naoum, M.C.; Papadopoulos, N.A.; Chalioris, C.E. Cracking Diagnosis in Fiber-Reinforced Concrete with Synthetic Fibers Using Piezoelectric Transducers. Fibers 2022, 10, 5. https://doi.org/10.3390/fib10010005.

Chalioris, C.E.; Kytinou, V.K.; Voutetaki, M.E.; Karayannis, C.G. Flexural damage diagnosis in reinforced concrete beams using a wireless admittance monitoring system—Tests and finite element analysis. *Sensors*2021,*21*,679. https://doi.org/10.3390/s21030679

Na, W.S.; Baek, J. A review of the piezoelectric electromechanical impedance based structural health monitoring technique for engineering structures. Sensors 2018, 18, 1307,https://doi.org/10.3390/s18051307